Time Series Modeling with Hidden Variables and Gradient-Based Algorithms

by

Piotr Mirowski

A dissertation submitted in partial fulfillment
of the requirements for the degree of
Doctor of Philosophy
Department of Computer Science
Courant Institute of Mathematical Sciences
New York University

January, 2011

Yann LeCun

In memory of Sam Roweis,

who laid the foundations

for this research

Acknowledgements

These past five and a half years of doctoral studies at New York University have constituted a personally transformative experience (and I am claiming this independently of the jazz clubs, concert halls and vibrant community populating the greater Greenwich Village area). During these years, I have benefited from countless contributions that are impossible to acknowledge in a few lines. I will limit myself to mentioning a few individuals who directly enabled this work, hoping to eventually have the opportunity to contribute to someone else's development in return.

I would like to immensely thank my adviser, Prof. Yann LeCun, for providing me with resources, guidance, and freedom to pursue my research. *Merci beaucoup pour avoir cru en moi, Yann.* Yann LeCun's lab is an intellectual hub with connections far beyond the field of Machine Learning, and therefore a very exciting research environment. Pursuing there my doctoral work has provided me with a constant source of instructive interactions. On a personal level, I admire Yann's wide range of musical, robotic, political, culinary and cultural interests as well as his ability to convert extremely complex mathematics and neuroscience into tangible and intuitive concepts in order to build things. I also greatly appreciate his "open door" policy that enabled us to discuss research for long hours and that sustained my motivation in the darkest hours of debugging.

The development of the techniques described in this doctoral work and the need for proofs of concept were only a pretext to start highly stimulating collaborations and to discover amazing researchers and specialists in fields I cannot comprehend. I will begin with Dr. Ruben Kuzniecky and Dr. Deepak Madhavan, who originated my research on the prediction of epileptic seizures from EEG and who provided me with three semesters and two summers of funding through NYU's FACES (Finding A

Cure for Epilepsy and Seizures) foundation. Thanks to them, I learned the patient's perspective on the statistical concepts of "false positive" and "false negative". Still in the field of epilepsy prediction, I would also like to acknowledge fruitful discussions with Profs Nandor Ludvig, Sertac Artan and Thomas Thesen.

Second, I am very grateful to Prof. Dennis Shasha, for providing me with a difficult and defining problem for my doctoral studies, with an application to Computational Biology. Dennis Shasha invested a lot of time and attention in my research, supporting my many endeavors and professional aspirations, and effectively making me a member of his lab and of the NYU Center for Genomics and Systems Biology. Along with Gabriel Krouk, who tried to teach me genetics, and with Jesse Lingeman, we made a fine team with whom I would like to maintain close ties.

Third, I would like to thank Craig Friedman from Standard & Poor's, who provided me with precious feedback, intellectual stimulation, statistical rigour and summer support for my work on sentiment analysis and text categorization, and who sparked my research interest in dynamic topic modeling.

And last but not least among the external collaborations, I am very grateful to Sumit Chopra, Suhrid Balakrishnan and Srinivas Bangalore for an extremely enjoyable summer at AT&T Labs Research and for an exciting and promising work on statistical language modeling.

During my doctoral years I enjoyed the company and friendship of talented fellow students and post-docs. While I extend my gratitude to everyone, I would like to especially thank Marc'Aurelio Ranzato for numerous collaborations (*Grazie mille, Marc'Aurelio: non ho rimpianti per aver iniziato questi studi*!), as well as Graham Taylor, Karol Gregor and Koray Kavukcuoglu, for their precious feedback on this research. Thank you all for contributing to a nurturing and supportive research environment. I would also like to acknowledge people who supported me on the ad-

ministrative side: Rosemary Amico, Robb Biffano, Profs Michael Overton, Margaret Wright and Denis Zorin.

I am grateful for the advice and guidance provided by the members of my thesis committee: Yann, Dennis and Srinivas, as well as Profs Vladimir Pavlovic and Chris Bregler. Their ideas and suggestions have given me the opportunity to considerably improve this dissertation. I would also like to thank Tin Kam Ho, from Bell Labs, for believing in me and my research.

Pursuing my doctoral research in machine learning has been possible in the first place thanks to my colleagues at Schlumberger: David McCormick, Claude Signer, Romain Prioul and Gilles Mathieu. I owe them having introduced me to rigorous applied research at an early stage of my career, having deeply stimulated my interest for statistical learning, and I am profoundly grateful to them for facilitating my transition from a comfortable engineer's life to that of a starving student.

I would like to acknowledge the support of Profs Alain Ayache and Vincent Charvillat, from ENSEEIHT in Toulouse, and of Gérard Aublet at Lycée Sainte Geneviève in Versailles. They represent two outstanding learning institutions that gave me a very competitive and thorough education in Math and Computer Science.

The butterfly effect originated with my parents, Teresa and Janusz Mirowski, as well as my brother Adam, who ignited my passion for science and engineering. They subsequently practiced reinforcement learning on me, while providing me with their unconditioned support, and thus enabled me to pursue my dreams. *Dziękuję wam najbardziej serdecznie za wszystko.*

But my decision to embark in doctoral studies comes from Alessia Pannese, who has continuously demonstrated the power of unsupervised learning and a passion for knowledge and discovery in any field. *Merci pour tout et pour être mon compagnon de voyage, Alessia.*

Abstract

We collect time series from real-world phenomena, such as gene interactions in biology or word frequencies in consecutive news articles. However, these data present us with an incomplete picture, as they result from complex dynamical processes involving unobserved state variables. Research on state-space models is motivated by simultaneously trying to infer hidden state variables from observations, as well as learning the associated dynamic and generative models.

To address this problem, I have developed tractable, gradient-based methods for training Dynamic Factor Graphs (DFG) with continuous latent variables. DFGs consist of (potentially highly nonlinear) factors modeling joint probabilities between hidden and observed variables. My hypothesis is that a principled inference of hidden variables is achievable in the energy-based framework, through gradient-based optimization to find the minimum-energy state sequence given observations. This enables higher-order nonlinearities than graphical models. Maximum likelihood learning is done by minimizing the expected energy over training sequences with respect to the factors' parameters. These alternated inference and parameter updates constitute a deterministic EM-like procedure.

Using nonlinear factors such as deep, convolutional networks, DFGs were shown to reconstruct chaotic attractors, to outperform a time series prediction benchmark, and to successfully impute motion capture data in presence of occlusions. In a joint work with the NYU Plant Systems Biology Lab, DFGs have been subsequently employed to the discovery of gene regulation networks by learning the dynamics of mRNA expression levels.

DFGs have also been extended into a deep auto-encoder architecture for time-stamped text documents, with word frequencies as inputs. I focused on collections of

documents exhibiting temporal structure. Working as dynamic topic models, DFGs could extract latent trajectories from consecutive political speeches; applied to news articles, they achieved state-of-the-art text categorization and retrieval performance.

Finally, I used DFGs to evaluate the likelihood of discrete sequences of words in text corpora, relying on dynamics on word embeddings. Collaborating with AT&T Labs Research on a project in speech recognition, we have improved on existing continuous statistical language models by enriching them with word features and long-range topic dependencies.

Abstract en Français

Modélisation de séries temporelles avec variables cachées et descente de gradient

Nous pouvons collecter des séries temporelles en mesurant toutes sortes de phénomènes tels que les interactions entres gènes, l'activité électro-physiologique du cerveau voire les fréquences de mots dans des articles de journaux. Ces données nous apportent cependant une vision partielle de la réalité, car elles dérivent de processus dynamiques complexes dont les variables aléatoires internes (variables ou vecteurs d'état) sont inconnues. La recherche sur la modélisation des représentation d'état est confrontée au double problème inverse de 1) reconstruire la séquence de variables cachées, et 2) d'apprendre les paramètres du modèle dynamique sous-jacent.

Pour répondre à ce problème, j'ai mis au point un nouvel algorithme d'apprentissage statistique pour entrainer des réseaux Bayésiens dynamiques ("Dynamic Factor Graphs", DFG; Graphes Dynamiques Factoriels, GFD) avec variables aléatoires cachées continues (réelles). Leur inférence repose sur une optimisation par descente de gradient. Chaque "facteur" correspond à un système d'équations non-linéaires, avec une composante aléatoire, et peut être exprimé comme une fonction de transfert avec des entrées et des sorties, suivies d'un terme d'erreur qui suit une loi de probabilité. Un GFD définit une loi de probabilité conjointe, aussi bien sur les variables aléatoires observées que sur les variables cachées; toutes ces variables sont échantillonnées dans le temps et les variables cachées constituent une chaîne de Markov. A chaque combinaison de variables aléatoire, est assignée une probabilité; l'objectif de l'algorithme d'inférence est de maximiser cette probabilité en trouvant la séquence de variables cachées qui explique au mieux les variables observées, pour un modèle dynamique donné. Je propose un algorithme d'inférence approximatif, lequel, au lieu

de calculer exactement la distribution des variables cachées, trouve seulement la configuration la plus probable des variables cachées (maximum a posteriori) à travers une minimisation par descente de gradient. Mon hypothèse est que les approximations de ma méthode d'inférence MAP sont largement contre-balancées par une plus grande versatilité fonctionnelle. Je prouve en effet que mon algorithme permet d'utiliser des fonctions d'évolution et d'observation bien plus complexes que celles permises par les réseaux Bayésiens traditionnels (tels que les modèles de Markov cachés ou les filtres de Kalman). Les paramètres du modèle sont appris par l'estimation du maximum de vraisemblance, en utilisant diverses optimisation telles que descente de gradient ou gradient conjugué. L'alternance entre inférence et optimisation par gradient peut être vue comme une version déterministe de l'algorithme d'espérance-maximisation (EM).

Les applications des GFDs sont multiples et aussi nombreuses que leurs architectures fonctionnelles. Par exemple, grâce à des fonctions de transfert consistant en réseaux de neurones convolutionnels, les GFDs ont ainsi prouvés pouvoir modéliser des séquences non-linéaires en reconstruisant des attracteurs chaotiques et surpasser en performance d'autres algorithmes sur des données d'une compétition de prédiction de séries temporelles. Appliqués aux données de capture de mouvement (coordonnées tri-dimensionnelles de marqueurs corporels), les GFDs ont pu reconstruire parfaitement la totalité des mouvement d'un squelette 3D en présence d'occlusions importantes (Mirowski & LeCun, ECML 2009). Les GFDs ont aussi été appliqués à la bio-informatique, en collaboration avec le centre de biologie moléculaire de New York University. En particulier, les GFDs ont été employés pour découvrir des réseaux de régulation génétique, en apprenant le modèle dynamique sous-jacent des niveaux d'expressions génétique des ARN messagers, mesurés au moyen de puces à ADN (Mirowski et al, Genome Biology 2010).

Un autre champ d'application des GFDs sont les documents texte structurés dans le temps, par exemple les articles de journaux, discours politiques ou publications scientifiques. Une architecture spécifique des GFDs, exprimés sous forme de réseaux de neurones auto-encodeurs, a ainsi pu être appliquée à ce type de séries temporelles, en utilisant la fréquence des mots en variable d'entrée du système. En utilisant des GFDs, j'ai ainsi pu étudier la dynamique des sujets cachés dans les discours politiques, prédire la volatilité des cours de marché à partir d'informations financières, ou obtenir une performance inégalée dans la classification de documents texte et dans le data-mining ("fouille de données"; Mirowski et al, NIPS Deep Learning Workshop 2010). Une extension possible de cette architecture GFD serait son application à mes recherches précédentes sur la prédiction des crises d'épilepsie à partir d'enregistrements d'électro-encéphalogrammes (Mirowski et al, IEEE MLSP 2008; Clinical Neurophysiology 2009; dépot de brevet industriel en cours).

Pour finir, j'ai utilisé les GFDs pour évaluer la vraisemblance de séquences de nombres entiers (suites de mots dans un corpus de documents écrits ou oraux), en inférant la dynamique cachée des représentations vectorielles de ces mots, et en augmentant ces représentations avec des informations syntactiques et avec des dépendances sémantiques au niveau de plusieurs phrases consécutives. Au cours d'un projet sur la reconnaissance de la parole, en collaboration avec AT&T Labs Research, nous avons ainsi pu améliorer la performance des modèles statistiques du langage, utiliser ces modèles en conjonction avec un modèle acoustique pour réduire le taux d'erreur par mots lors de la reconnaissance vocale, et atteindre l'état de l'art dans ce domaine (Mirowski et al, IEEE SLT 2010; dépôt de brevet industriel en cours).

Contents

List of Figures

List of Tables

Chapter 1

Introduction

The future ain't what it used to be.

Yogi Berra

Time series are ordered sequences of data points. They typically correspond to measurements taken from real-world natural or man-made phenomena, but could as well be the outputs of numerical simulation. Examples of time series that I investigated during my doctoral studies include mRNA expression levels, spatial positions of markers used in motion capture, electro-encephalographic recordings of brain activity, financial stock market volatility, word frequencies in streams of news articles, written or spoken language, as well as, on the purely artificial side, chaotic data.

This introductory chapter gives an overview of the time series problem that can be addressed (and for a large part, that have been touched in this work), as well as a glimpse of the state-of-the-art associated techniques. Most importantly, it provides the rationale for modeling time series with additional, *hidden variables*.

1.1 Time Series Problems

Although traditional time series problems are *univariate* (typically when one is interested in the "history" of successive values taken by one variable, or in its statistical distribution), additional insight about the real-world phenomenon can be gained from *multivariate* time series, exhibiting the interaction of several variables.

In their common definition, time series are implicitly *continuously-valued*. In this thesis, we have however encompassed specific cases where we could apply to *discrete sequences* methods that were actually designed for continuously-valued time series. Those two cases correspond to "bag-of-words" representations of word counts in consecutive documents, and to sub-sequences of words. The crucial difference between a sequence of discrete events and a one-dimensional time series is that continuous (real) numbers have a natural metric that discrete events lack: e.g. 0.1 can be quantified as being closer to 0 than to 3, while it would be more difficult (or more arbitrary) to establish which word among "sat" or "cat" is closer to "mat". For this reason, real-valued time series problems on one hand and discrete sequence problems on the other hand often resort to different mathematical tools (e.g. linear models vs. count-based n-gram models). Of course, one can always convert a "one-dimensional" string of discrete events (where each event is chosen out of a vocabulary of N possible items) into an N-dimensional time series of event counts or frequencies, and thereby consider it as a sequence of multivariate real-valued numbers.

Time series modeling is motivated by a wealth of interesting problems:

- **forecasting**, i.e. predicting future time points from previous ones. In subsequent chapters, I will evoke time series prediction on chaotic data (Chapter 3), as well as predictive modeling on biological mRNA levels (Chapter 4). Fore-

casting can be conducted at various time horizons, and can consist in iterating a time series model to produce successive time point predictions.

- **imputation**, i.e. the recovery of missing time points. This problem is slightly different from forecasting, as both past and future data points, as well as non-missing values (in the case of multivariate time series) can be used for prediction. I will explain an application to the reconstruction of motion capture data in Chapter 3.

- **inference of a hidden representation**: I will introduce in this chapter the concept of hidden explanatory variables for time series. Two examples of hidden variables inference that I have worked on include the reconstruction of a chaotic attractor and the separation of an oscillatory signal into components (in Chapter 3), as well as the projection (compression) of word counts taken from consecutive State-of-the-Union presidential addresses onto a two-dimensional space which could symbolize a "political" (if not lexical) trajectory (see Chapter 5).

- **learning a dynamical system**, i.e. understanding how a time series is generated and how the measured variables interact. A key application is the reverse-engineering of gene regulation networks described in Chapter 4.

- **classification** and **regression** of sub-sequences. Regression of stock-market log-volatility from streams of online financial news, as well as the text categorization of documents, are two examples of such tasks, detailed in Chapter 5. One problem that I tackled during my studies but that I did not cover in this thesis is the prediction of epileptic seizures from electro-encephalograms by classifying short patterns of EEG as "pre-ictal" or "interictal" (Mirowski et al., 2008,

2009a,b).

- as a corollary to classification, the estimation of the **likelihood of a sequence**. This problem has been addressed for discrete sequences of words and applied to statistical language modeling in Chapter 6.

1.1.1 Imprecise Sampling, Incompleteness and Time-Variance

A key limitation of time series is that they are an incomplete observation of reality, for three different reasons (upon which I stumbled during my research).

First, one observes data only at specific **sampling** points (generally regularly spaced), whereas the process which generated them exists beyond those infinitesimal sampling instants. This limitation makes the learning of a dynamical system inherently approximate.

Second, only a **subset of the variables** that would be required to understand the process is available. This problem is particularly striking in the case of genetic data, where the process (transcription of mRNA by proteins) involves more biological actors than are measured with current instrumentation, or with EEG recordings, where each electrode measures electrophysiological signals (post-synaptic potentials) averaged over millions of neuronal cells. Those two biological examples of incomplete observed data, are among the justifications for introducing additional, hidden variables to the time series, under appropriate models and constraints on those unknown variables.

Third, the time series might derive from a process that is **not time-invariant**[1]. In that case, the time series model has an explicit dependency on the time variable. More precisely, given input $x(t)$ at time t, the model predicts $y(t)$, but an identical input $x(t + \Delta t)$ at a later time $t + \Delta t$ would be associated to a different prediction

[1] We could also say that the time series is **non-stationary**, which means that the joint distribution of the random variables changes over time.

$y(t + \Delta t) \neq y(t)$. In some specific cases, the *time-variance* of the process can be recovered solely from the available data $\mathbf{X}$ and $\mathbf{Y}$, using a model with *long-range dependencies*, such as a model with "switching dynamics" or with a "memory" (both of which can be enabled by hidden variables). In other cases, the process generating the time series is unfortunately different between the (historical) training set and the (future) test set, and therefore any statistical model fitted to historical data would become useless for predicting future data points[2].

As a side note, I shall point out that this thesis focuses on time series analysis from a time-domain point of view (i.e. by studying the explicit relationships between consecutive data points)[3]. Another approach would have consisted in looking at the frequency domain of time series (Box and Jenkins, 1976; Weigend and Gershenfeld, 1994), using spectral or wavelet (Mallat, 1999) analyses.

1.2 Time Series Modeling Without Hidden Variables

1.2.1 Time-Delay Embedding and Markov Property

Throughout the thesis, I note $y(t)$ or y_t the instance of the univariate time series observed at time t, $\mathbf{y}(t)$ or $\mathbf{y}_t$ for multivariate time series, and $\mathbf{Y}$ for the entire sequence. Using the simplification that the time sampling interval is $\Delta t = 1$, I note the *time-delay embedding* of past p time-points before t as $\mathbf{y}_{t-p}^{t-1}$. The time-delay embedding operation is here merely a concatenation of the vectors corresponding to

[2]In the specific case of econometrics and sociology, where human actors interact in complex networks, within an open system, this "inability to predict" from historical data has been vehemently exhibited in (Taleb, 2007). The author laid the blame on our obstination to fit statistical models with Gaussian distributions to historical data, while the distributions of those time series are both time-dependent and fat-tailed.

[3]With one exception: in the chapter devoted to statistical language modeling, we do exploit the structured interaction of word "variables" in a sentence, in order to derive rich word features such as part-of-speech tags or supertags.

successive time points of the time series. One often refers to this as the *state-space* representation of the time series (Weigend and Gershenfeld, 1994).

The most common assumption when designing continuous models for time series is that the model should follow the Markov property, which states that any current value $\mathbf{y}(t)$ of the time series at time t depends only on its short history[4] (Durrett, 1996), namely on past p values $\mathbf{y}_{t-p}^{t-1}$. Such a model is by consequence time-invariant, for a specific value of Markov order p.

Another way of rephrasing the Markov property is that the time series forms a Markov chain where each data point $\mathbf{y}(t)$ is *conditionally independent* of its long-term history $\mathbf{y}_1^{t-p-1}$ *given* its immediate history $\mathbf{y}_{t-p}^{t-1}$.

As a result of the time-delay embedding, the training dataset consists of $T-p$ couples $\left\{(\mathbf{y}_1^p, \mathbf{y}_{p+1}), (\mathbf{y}_2^{p+1}, \mathbf{y}_{p+2}), \ldots, (\mathbf{y}_{T-p}^{T-1}, \mathbf{y}_T)\right\}$.

Time-delay embedding raises the issue of choosing the order p of the embedding, and specific models address that question in different ways. For example, linear or probabilistic models rely on the Bayesian Information Criterion (Box and Jenkins, 1976) or the Akaike Information Criterion (Akaike, 1973), which essentially place a penalty on large values of the order p (or on the number of model parameters) relative to the sequence length T.

The Markov property can also be extended to highly nonlinear time series with chaotic dynamics (whose definition we remind in Section 1.2.7). It often is the case that univariate chaotic time series are produced by a multivariate system of nonlinear equations, like for instance the 3-variate Lorenz model (Lorenz, 1963). The Takens theorem (Takens, 1981) establishes, for these univariate chaotic time series, that one can reconstruct the original multivariate state-space attractor by time-delay embed-

[4]The original definition by Russian mathematician Andryi Markov applies to stochastic processes in continuous time and on a single "time-step" dependency. Multi-step histories can be recovered by time-delay embedding and a state-space representation.

ding; various techniques for the estimation of the state-space dimension of the chaotic attractor have been summarized in (Abarbanel et al., 1993).

1.2.2 Probabilistic Models: n-grams on Discrete Sequences

In the case of discrete sequences, one can express the Markov property in terms of n-grams[5]. $\mathbf{y}_{t-n+1}^{t}$. n-grams can be computed as absolute counts on the data, or estimated from the sequence as conditional probabilities $P\left(y_t|\mathbf{y}_{t-n+1}^{t-1}\right)$. The latter results in the joint likelihood of the full sequence $\mathbf{Y}$ of length T being equal to:

$$P\left(\mathbf{y}_1^T\right) = P\left(\mathbf{y}_1^{n-1}\right)\prod_{t=n}^{T} P\left(y_t|\mathbf{y}_{t-n+1}^{t-1}\right) \tag{1.1}$$

The strength of n-grams is that, unlike their continuously-valued counterpart, they can define any conditional distribution, including multi-modal ones. Their major limitation is that as the size of the *context* (i.e. the embedding dimension) n increases, the size of the corpus needed to reliably estimate the probabilities grows exponentially with n. Because the language corpora are generally limited in size, they do not cover all the possible n-grams. In order to overcome this sparsity, back-off mechanisms (Katz, 1987) are used to approximate n^{th} order statistics with lower-order ones, and missing probabilities may be further approximated by probability smoothing (Chen and Goodman, 1996), which essentially amounts to giving a low-probability prior to unseen n-grams.

We will keep the Markov chain likelihood formulation (Eq. 1.1) in what follows.

[5] n-grams can be attributed to Claude Shannon's work in information theory, illustrated on conditional probabilities of a letter given the previous $n-1$ letters (Wikipedia).

1.2.3 Maximum Likelihood Formulation: Gaussian Regression

The first approach to continuously-valued time series modeling considers observations $\mathbf{Y}$ as the result of a purely auto-regressive linear or non-linear process. In other words, one hypothesizes that there exists a deterministic mapping[6] f from the time-delay embedding of $\mathbf{y}_{t-p}^{t-1}$ to $\mathbf{y}_t$. That mapping f, which generates a prediction $\bar{\mathbf{y}}_t$ from a linear sum or a nonlinear function over $\mathbf{y}_{t-p}^{t-1}$, is perturbed by an additional noise term $\eta(t)$ that stems from a unimodal, zero-mean, distribution:

$$\mathbf{y}(t) = f\left(\mathbf{y}_{t-p}^{t-1}\right) + \eta(t) \tag{1.2}$$

Equation (1.2) expresses the 1-step inference and can be iterated to generate the continuation of $\mathbf{y}(t)$ for long-term prediction.

By restating problem (Eq. 1.2) as a probability $P\left(\mathbf{y}(t) = f\left(\mathbf{y}_{t-p}^{t-1}\right) | \mathbf{y}_{t-p}^{t-1}\right)$ under the distribution of residual noise $\eta(t)$, and using the conditionally independent Markov chain of (Eq. 1.1), one can solve for the mapping f by maximizing the likelihood of $P\left(\mathbf{Y}\right)$. Numerical optimization is usually conducted by expressing the product $P\left(\mathbf{Y}\right)$ as a sum in logarithmic domain.

Theoretically, the statistical learning techniques used for solving for f would require the data points $\left\{(\mathbf{y}_1^p, \mathbf{y}_{p+1}), (\mathbf{y}_2^{p+1}, \mathbf{y}_{p+2}), \ldots, (\mathbf{y}_{T-p}^{T-1}, \mathbf{y}_T)\right\}$ to be *independently and identically distributed*. Clearly, the time series $\mathbf{Y}$ itself is not i.i.d., since there are serial correlation between consecutive samples $\mathbf{y}_{t-1}, \mathbf{y}_t, \mathbf{y}_{t+1}, \ldots$. But the Markov property ensures the conditional independence of outputs/targets $\mathbf{y}(t)$ given their associated inputs/features $\mathbf{y}_{t-p}^{t-1}$, and thus enables the likelihood $P(\mathbf{Y})$ to be expressed as a product (Eq. 1.1).

Regarding the identical distribution requirement, it means that the residual noise

[6] This mapping can be seen as a discrete version of a continuous system of differential equations.

$\eta(t)$ has to be stationary, i.e. that the joint distribution of $\{\dots, \eta_{t-1}, \eta_t, \eta_{t+1}, \eta_{t+2}, \dots\}$ needs to have the same zero mean and same variance, regardless of time localization t (Box and Jenkins, 1976). Another way of rephrasing this requirement is that residual noise should not exhibit visible structure when plotting it across time or against the data (Weigend and Gershenfeld, 1994). This assumption, generally tested by statisticians during exploratory data analysis, is however often ignored by the machine learning community.

Luckily, there are recipes to cope with non-stationarity. For instance, when a time series displays a local variance of $\mathbf{y}(t)$ that is clearly a function of the amplitude of $\mathbf{y}(t)$ (e.g. the variance of the noise is large for large values of $\mathbf{y}(t)$, and small for small values of $\mathbf{y}(t)$), then it might be sufficient to apply exponentiation or the logarithm to all time points $\mathbf{y}(t)$, in order to correct for that obvious non-stationarity. Other transformations on time series consist in *de-trending* (removing obvious linear trends) or correcting for *seasonality* (e.g. removing a periodic oscillation from the data points[7]).

Using the normal distribution for $\eta(t)$, the Gaussian regression problem corresponds in logarithmic domain to "sum of least squares" (LS) optimization:

$$-\log P\left(\mathbf{Y}|\mathbf{\Theta}\right) \propto \sum_{t=p+1}^{T} \parallel \mathbf{y}(t) - f\left(\mathbf{y}_{t-p}^{t-1}\right) \parallel_2^2 + const \tag{1.3}$$

In the above equation, $\mathbf{\Theta}$ corresponds to model parameters. Gaussian regression is the Maximum Likelihood (ML) formulation used in most chapters of this thesis. Other ML formulations include Laplace regression (sum of absolute values) in Chapter 5, multinomial (Softmax) regression in Chapters 5 and 6 and logistic (binomial) regression in Chapter 5.

[7]The concept of seasonality often arises in data collected over the time course of a year, where one can distinguish the effect of "seasons".

Learning time series models under the ML formulation consists in finding the optima of $-\log P(\mathbf{Y})$ w.r.t. model parameters $\mathbf{\Theta}$. This is achieved by differentiating $-\log P(\mathbf{Y})$ w.r.t. each parameter variable, and finding zero-crossings:

$$\forall k,\ \frac{\partial\left(-\log P\left(\mathbf{Y}|\mathbf{\Theta}\right)\right)}{\partial\theta_k} = 0 \tag{1.4}$$

1.2.4 Predicting One Time Series from Another

Some multivariate time series problems fall into the more usual setting (predict some output $\mathbf{y}(t)$ from corresponding inputs $\mathbf{x}(t)$ lying in a different data space). They consist in learning to predict one part of the variables at time t (so-called "targets" or "outputs") from the other part of the data point (so-called "features" or "inputs"), and can be expressed by the following equation:

$$\mathbf{y}_t = h\left(\mathbf{x}_t\right) + \epsilon(t) \tag{1.5}$$

The mapping h, which generates a prediction $\bar{\mathbf{y}}_t$ from a linear sum or a nonlinear function over $\mathbf{x}_t$, is perturbed by an additional noise term $\epsilon(t)$ that stems from a unimodal, zero-mean, distribution. Although the usual maximum likelihood-based methods can be applied to fit function h, the remarks made in the previous section about the non i.i.d. nature of $\mathbf{X}$ and $\mathbf{Y}$ are still valid.

Examples of such problems include the categorization of consecutive news articles (Joachims, 1998; Kolenda and Kai Hansen, 2000), the regression of stock market volatility from word counts in consecutive financial news articles (Gidofalvi and Elkan, 2003; Robertson et al., 2007) (see Chapter 5) or the prediction of power transformers' time-to-failure from dated chemical measurements of dissolved gases in transformer

oil[8] (Mirowski et al., manuscript in preparation). In those cases, although the basic predictive model uses only data from a single time point, the temporal structure in the data could probably benefit the model learning.

One solution is time-delay embedding on the inputs $\mathbf{x}_t$, which can be concatenated into $\mathbf{x}_{t-p}^{t}$, although this might prove expensive in the case of high-dimensional vectors $\mathbf{x}_t$. Another potential approach is based on the use of hidden variables and "memory" from sample $(\mathbf{x}_{t-1}, \mathbf{y}_{t-1})$ at time $t-1$ to sample $(\mathbf{x}_t, \mathbf{y}_t)$ at time t.

1.2.5 Limitation of *Memoryless* Time Series Models

The drawback of time-embedding-based models is indeed that they do not have any "memory" of the full time series and of long-term dependencies (Bengio et al., 1994): during the learning procedure, each training sample is considered independently of its time location t, and, at time t, the system's memory of $\mathbf{Y}$ (and optionally, of $\mathbf{X}$) goes only as far back in time as its time-delay embedding dimension p permits. As such, "memoryless" architectures yield satisfactory results on time series with simple stationary dynamics but may have difficulties with long-term prediction or with capturing long-range dynamics.

Let us nevertheless enunciate the most popular approaches to solve for (Eq. 1.2) and (Eq. 1.5) without the use of hidden variables. Most of these methods are indeed the building blocks for memory-enabled models.

[8] This work, which was not included in this thesis, was conducted in collaboration with NYU Poly and Consolidated Edison.

1.2.6 Linear time series models

Auto-Regressive $AR(p)$ Models

We start with a simple one, the univariate p-th order linear Auto-Regressive model:

$$y_t = \sum_{k=1}^{p} \phi_k y_{t-1} + \eta_t \tag{1.6}$$

The driving noise η_t in equation 1.6, also called *innovation*, makes the time series "interesting". We notice that $AR(1)$ models where $\phi_1 = 1$ correspond to random walks. Without noise, if one iterated $AR(1)$ models ($\phi_1 \neq 1$) for multi-step prediction, then the resulting time series would either decay exponentially (if $\phi_1 < 1$) or diverge (grow) exponentially (if $\phi_1 > 1$). $AR(p)$ models with $p > 1$ introduce oscillations. Again, without innovation noise, they would either decay or diverge exponentially and in an oscillatory way, depending on the values of their coefficients $\mathbf{\Phi}$. $AR(p)$ models that decay exponentially are called *mean-reverting* and are stationary (Tsay, 2005).

Although the coefficients $\mathbf{\Phi}$ can be fitted by linear regression, the tool of choice is the auto-correlation function defined by l-lag autocorrelation coefficients. Auto-correlation coefficients (Eq. 1.7) describe how much, on average, two values of a time series that are l time steps apart co-vary with each other (Weigend and Gershenfeld, 1994).

$$\forall l,\ \rho_l = \rho_{-l} = \frac{\mathrm{Cov}\left(y_t, y_{t-l}\right)}{\mathrm{Var}\left(y_t\right)} \tag{1.7}$$

These autocorrelation coefficients (Eq. 1.7) can be used to define a system of p Yule-Walker equations (Eq. 1.8) in order to solve for $\mathbf{\Phi}$ (Weigend and Gershenfeld, 1994; Tsay, 2005).

$$\forall k \in \{1, \ldots, p\},\ \rho_k = \phi_1 \rho_{1-k} + \phi_2 \rho_{2-k} + \cdots + \phi_{p-1} \rho_{p-1-k} + \phi_p \rho_{p-k} \tag{1.8}$$

Vector Auto-Regressive $VAR(p)$ Models

The multivariate equivalent to $AR(p)$ are the Vector Auto-Regressive models $VAR(p)$, driven by multivariate, zero-mean uncorrelated noise η_t with covariance matrix $\mathbf{\Sigma}$:

$$\mathbf{y}_t = \sum_{k=1}^{p} \mathbf{\Phi}_k \mathbf{y}_{t-1} + \eta_t \tag{1.9}$$

$VAR(p)$ models behave like $AR(p)$ models, but instead of scalar coefficients ϕ_k, they have square matrix coefficients $\mathbf{\Phi}_k$, and first order $VAR(1)$ already exhibit an oscillatory behavior. In the specific case of $VAR(1)$, it can also be shown (Tsay, 2005) that the condition for stationarity (i.e. mean reversion of the iterated prediction) is for the coefficient matrix $\mathbf{\Phi}_1$ to have eigenvalues smaller than 1.

$VAR(p)$ and even $VAR(1)$ models are relatively powerful: it is for instance a commonly used benchmark for the inference of gene regulation networks, by learning to model the linear dynamics between consecutive micro-array-based measures $\mathbf{y}_t$ of mRNA expression levels during the time course of a biological experiment (Alvarez-Buylla et al., 2007; Bonneau et al., 2006, 2007; Efron et al., 2004; Lozano et al., 2009; Shimamura et al., 2009; Wahde and Hertz, 2001; Wang et al., 2006b; Zou and Hastie, 2005) (see Chapter 4).

In order to solve for the parameters $\mathbf{\Phi}_k$, one can rely on maximum likelihood based methods, such as performing a linear regression for each dimension of $\mathbf{y}_t$. Alternatively, by introducing l-lag cross-correlation matrices $\mathbf{\Gamma}_l$, one can resort to the matrix equivalent of the Yule-Walker equations (Tsay, 2005).

Moving Average $MA(q)$ Models

$AR(p)$ models can be described as convolutions and in terms of Infinite Impulse Response (IIR) filters (Weigend and Gershenfeld, 1994), which *grosso modo* means that input y_t can be felt beyond time point $t + p$. The other type of filters are Finite Impulse Response (FIR) filters, where, in absence of input, the output y_{t+q} is guaranteed to go to zero after q time steps. To design such a filter/model, one simply needs to separate the input time series $\mathbf{X}$ from the output time series $\mathbf{Y}$. Hence the definition for univariate q-th order Moving Average models:

$$y_t = \sum_{k=1}^{q} \psi_k x_{t-k} + \eta_t \tag{1.10}$$

$MA(q)$ coefficients $\mathbf{\Psi}$ are estimated using maximum likelihood techniques. Their auto-correlation coefficients ρ_l vanish after lag l.

Auto-Regressive Moving Average $ARMA(p, q)$ Models

The final linear model that we mention[9] are Auto-Regressive Moving Average models:

$$y_t = \sum_{k=1}^{p} \phi_k y_{t-k} - \sum_{k=1}^{q} \psi_k x_{t-k} + \eta_t \tag{1.11}$$

Various techniques have been derived over years to identify $ARMA(p, q)$, i.e. to select model orders p and q before fitting the coefficients (Tsay, 2005). This procedure is a bit more complicated, but the general idea is that after fitting a good model with correct order, the residual noise should become structureless (Weigend and Gershen-

[9]Since the focus of this thesis is not specifically on financial time series, we will skip further description of *Heteroscedastic* models (ARCH, GARCH, etc...), which essentially focus on modeling the variance of the innovation noise η_t in non-stationary linear models (Tsay, 2005). In the case of time series measuring the financial returns $\mathbf{Y}$ of stock market prices, the main application of such heteroscedastic models is modeling the time-dependent structure of stock volatility. We will simply use in Chapter 5 the observation that volatility depends on external factors (such as news).

feld, 1994). One notion that can be introduced at that point is the number of degrees of freedom of the model, which corresponds both to the number of parameters to estimate, and to the number of previous "states" that the time series can retain (Weigend and Gershenfeld, 1994).

There are however many time series datasets where linear models "break down", as one cannot choose between a linear model driven by stochastic noisy input, or a deterministic nonlinear model with a small number of degrees of freedom (Weigend and Gershenfeld, 1994). Before dwelling into nonlinear models, we shall make the observation that, after all, commonly used random number generators (which provide the seemingly independently and identically distributed noise in computer simulations), are essentially the iterated prediction of a chaotic (highly nonlinear) time series model (Herring and Palmore, 1995).

1.2.7 Chaotic Time Series

As we introduced in the previous subsections, nonlinear mappings can generate chaotic dynamics. The general definition of chaos is "aperiodic long-term behavior in a deterministic system that exhibits sensitive dependence on initial conditions" (Strogatz, 1994).

This means that if one iterates function f over $\mathbf{y}_{t-p}^{t-1}$ to make successive predictions, then an initial perturbation in the time series grows exponentially in time (which causes the forecasting problem to remain difficult (Casdagli, 1989)). Let us note $\mathbf{y}_1$ and $\mathbf{y}'_1$ two initial values, and $\Delta\mathbf{y}_1$ their initial separation. After n iterations of f, we obtain respectively $\mathbf{y}_n = f^n(\mathbf{y}_0)$ and $\mathbf{y}'_n = f^n(\mathbf{y}'_0)$. We can quantify the rate of this separation using Lyapunov exponents[10]. λ defined as following:

[10] As one can obtain different values of λ depending on the direction of the initial perturbation, there actually exist a full spectrum of Lyapunov exponents, for which we can extract the maximum

$$\| \Delta \mathbf{y}_n \| \approx e^{\lambda t} \| \Delta \mathbf{y}_1 \| \tag{1.12}$$

It is important to distinguish between diverging systems and chaotic systems: chaotic time series have aperiodic behavior and the values of $\mathbf{y}(t)$ lie on a manifold that is also called *strange attractor* (Strogatz, 1994).

1.2.8 Nonlinear Models: Time-Delay Neural Networks

Neural networks (Rumelhart et al., 1986) are a multi-layer, nonlinear architectures[11], that are capable, theoretically at least, to learn a "universal approximation" to any nonlinear function h (Cybenko, 1989). Neural networks can be likened to a stack of D multivariate linear regressions (i.e. a matrix-vector multiplication with matrix $\mathbf{W}^{(l)}$, where $l \in \{1, \ldots, D\}$), each followed by a nonlinearity such as the hyperbolic tangent sigmoid $tanh(x)$ or the logistic sigmoid $1/(1+e^{-x})$. In our case, the input to the first layer is vector $\mathbf{x}_t$ or $\mathbf{y}_{t-p}^{t-1}$, and there are intermediary (hidden) variable vectors $\mathbf{z}_t^{(l)}$ (where $l \in \{1, D-1\}$) that are generated between each layer. Note however that the traditional maximum likelihood-based learning algorithm (Rumelhart et al., 1986) for neural networks does not optimize *explicitly* for that hidden representation (with a few early exceptions suggested in (Krogh et al., 1990; Rohwer, 1989)).

Trained neural networks can be iterated on time series $\mathbf{y}(t)$, modeling nonlinear dynamical equations f; as a matter of fact, they can exhibit chaotic behavior (Strogatz, 1994). Time-Delay Neural Networks (TDNN) (Lang and Hinton, 1988; Waibel et al., 1989) are a specialization of neural nets, which exploit the time structure of the input by performing convolutions on overlapping windows. Similarly to the two-

Lyapunov exponent.

[11] I will spare the enlightened reader with reminders about the neural network architecture and about gradient-based learning; a good reference is Chris Bishop's comprehensive textbook (Bishop, 2006).

dimensional convolutional networks applied to image recognition problems (LeCun et al., 1998a), TDNN are not fully connected and share weights across the time dimension, performing de facto convolutional FIR filtering on the time series. Although it is easier to design TDNNs using 3D arrays, one can view their 2D matrix parameters $\{\mathbf{W}^{(l)}\}_{l\in\{1,D\}}$ as very sparse and with replicated columns.

In previous doctoral work (Mirowski et al., 2007), I modeled the dynamics of EEG at the onset of an epileptic seizure using a TDNN architecture. As another example, TDNNs managed to obtain very good prediction results on the Lorenz-like laser chaotic dataset (Wan, 1993), where they successfully predicted the first 100 time-step continuation of a time series. As detailed in (Weigend and Gershenfeld, 1994), TDNN however performed poorly on longer prediction horizons on that same dataset, and the predicted time series did not "look" like the original chaotic attractor anymore.

In its basic version, the open-loop training algorithm of TDNN minimizes the one-step prediction error (i.e. tries to maximize the likelihood of Eq. 1.2) instead of multi-step prediction errors, which are necessary for good long-term prediction performance. Further research in that field (Kuo and Principe, 1994; Bakker et al., 2000) attempted better long-term (iterated) predictions using Back-Propagation Through Time (BPTT) and closed-loop training.

1.2.9 Nonlinear Models: Kernel Methods

The philosophy behind Kernel-based methods can be seen as being at the opposite of parametric models such as $VAR(p)$ or TDNNs, and they are often qualified as non-parametric (even if they do need a few hyper-parameters). They require the evaluation

of a $T \times T$ Gram matrix[12] $\mathbf{K}$ on the learning dataset $\{(\mathbf{x}_1, \mathbf{y}_1), (\mathbf{x}_2, \mathbf{y}_2), \ldots, (\mathbf{x}_T, \mathbf{y}_T)\}$ (general case) or on $\left\{(\mathbf{y}_1^p, \mathbf{y}_{p+1}), (\mathbf{y}_2^{p+1}, \mathbf{y}_{p+2}), \ldots, (\mathbf{y}_T^{T+p-1}, \mathbf{y}_{T+p})\right\}$ (in the case of auto-regressive models).

The Gram matrix $\mathbf{K} = \{k_{i,j}\}_{i \in \{1,\ldots,T\}, j \in \{1,\ldots,T\}}$ is called the *kernel matrix* [13], and one can also define a kernel function $k(\mathbf{x}, \mathbf{x}')$ between any two datapoints $\mathbf{x}$ and $\mathbf{x}'$. The two types of kernel matrices that were used during the experiments conducted in this thesis were the popular linear kernel $k(\mathbf{x}, \mathbf{x}') = \mathbf{x}^T\mathbf{x}'$, and the Gaussian kernel $k(\mathbf{x}, \mathbf{x}') = \exp\left(- \parallel \mathbf{x} - \mathbf{x}' \parallel_2^2 / 2\sigma^2\right)$, the latter depending on the bandwidth parameter σ (Bishop, 2006). For auto-regressive models, one simply needs to replace the $\mathbf{x}_t$ by $\mathbf{y}_{t-p}^{t-1}$.

Weighted Kernel Regression

The simple Weighted Kernel Regression (WKR), also called the Nadaraya-Watson regression (Bishop, 2006), proposes to predict the value $y_{t'}$ of a new datapoint $\mathbf{y}_{t'-p}^{t'-1}$ as a locally-based average of the entire support $S = \{1, \ldots, T\}$ of the training dataset (Eq. 1.13), using the Gaussian kernel function. WKR make univariate predictions, and correspond to Radial Basis Functions with a basis function at every training set datapoint.

$$y_{t'} = \frac{\sum_{t \in S} k\left(\mathbf{y}_{t'-p}^{t'-1}, \mathbf{y}_{t-p}^{t-1}\right) y_t}{\sum_{t \in S} k\left(\mathbf{y}_{t'-p}^{t'-1}, \mathbf{y}_{t-p}^{t-1}\right)} \tag{1.13}$$

[12] Gram matrices define a Hermitian inner product between T vectors, such as for instance the dot product in Euclidian space.

[13] Gram matrix $\mathbf{K}$ is symmetric, semi-definite positive, which means that for any non-zero vector $\lambda \in \mathcal{R}^T$, $\mathbf{K}$ has the following hermitian property: $\lambda^T\mathbf{K}\lambda \geq 0$ (Bishop, 2006).

Support Vector Regression

Support Vector Regression (SVR) (Muller et al., 1999) with Gaussian kernels can be viewed as a specialization of WKR, with a sparse support $S \subset \{1, \ldots, T\}$. Without going into the specifics of Support Vector Machines (Cortes and Vapnik, 1995)[14], we can say that SVR provides with predictions $\bar{y}'_t = \sum_{t \in S} \lambda_t k \left(\mathbf{y}_{t'-p}^{t'-1}, \mathbf{y}_{t-p}^{t-1} \right) + b$, where b is a bias term, λ_t are positive Lagrange coefficients, and where the subset S of training samples is chosen so that the predictions $\bar{y}_t$ on the training datapoints $t \in \{1, \ldots, T\}$, satisfy the following constraint: $|y_t - \bar{y}_t| \leq \epsilon$, for a fixed ϵ. There can be a few exceptions, which are outlier datapoints that cannot be fitted. The datapoints where $|y_t - \bar{y}_t| = \epsilon$ are called the *margin support vectors*. Datapoints where $|y_t - \bar{y}_t| < \epsilon$ are not part of the set of support vector S (their Lagrange coefficient is $\lambda_t = 0$).

When Gaussian kernels are used, the solution to SVR can be seen as a manifold in an $N+1$ dimensional space (where N is the number of dimensions in inputs $\mathbf{y}_{t-p}^{t-1}$ and the last dimension is covered by targets y_t and predictions $\bar{y}_t$); that manifold tries to keep within a distance of ϵ of all the training datapoints. Its smoothness, as well as the number of outliers, depend on the bandwidth parameter σ.

SVR has been very successfully applied to time series prediction. In (Mattera and Haykin, 1999; Mukherjee et al., 1997; Muller et al., 1999), SVR made long-term iterated predictions on the Lorenz (Lorenz, 1963) and Mackay-Glass chaotic datasets. In particular, SVR was capable of staying within the chaotic attractor's orbit, unlike most neural networks-based predictors. On the downside, SVR theoretically requires the training data to be i.i.d., an assumption which is clearly violated (Mattera and Haykin, 1999), and it does not explicitly model dynamical equations (i.e. the interaction of variables) on the time series.

[14] Note that SVM and SVR are optimized using a different formulation than maximum likelihood.

Gaussian Processes

Gaussian Processes (GP) (Williams and Rasmussen, 1996) are particular kernel-based method. GPs assume that the time series $\{y_1, y_2, \ldots, y_T\}$ is jointly Gaussian, and express the covariance between any two training samples t and t' as a Gaussian kernel function on $\mathbf{x}_t$ and $\mathbf{x}_{t'}$:

$$\mathrm{Cov}\left(y_t, y_{t'}\right) = k\left(\mathbf{x}_t, \mathbf{x}_{t'}\right) = \theta_0 \exp\left(-\frac{\theta_1}{2} \parallel \mathbf{x}_t - \mathbf{x}_{t'} \parallel_2^2\right) + \theta_2 + \theta_3 \mathbf{x}_t^T \mathbf{x}_{t'} \tag{1.14}$$

In order to regress $y_{t'}$ given $\mathbf{x}_{t'}$ and the training dataset $\{(\mathbf{x}_t, y_t)\}$, GPs compute the Gaussian conditional probability $P(y_{t'}|\mathbf{Y})$. As such, GPs do not approximate (non)linear dynamical systems on the observed variables, but compute the pairwise similarity between the inputs of training samples. To learn a GP model means to compute the kernel matrix and to fit the hyperparameters $\mathbf{\Theta}$, which is achieved using maximum likelihood.

GPs have been applied to iterated time series prediction (Girard et al., 2003), using time-delay embedding $\mathbf{y}_{t-p}^{t-1}$ in lieu of $\mathbf{x}_t$.

1.2.10 Regularization

When learning a time series model, it is important not to overfit the training dataset, which would preclude the generalization faculty of the model to unseen time points. This can be achieved by *regularization*, which is the addition of a prior on the model parameters $\mathbf{\Theta}$ to the likelihood $P(\mathbf{Y})$ of the time series (Bishop, 2006). That prior says that the values of the weights should be small or sparse, as this is a simple way not to overfit the data. The two most common regularizations are the L_2-norm

Tikhonov regularization[15] (zero-mean Gaussian distribution prior on $\mathbf{\Theta}$) and the L_1-norm regularization (or the so-called parameter shrinkage, with a zero-mean fat-tail Laplace distribution prior on $\mathbf{\Theta}$), formulated by Tibshirani (Tibshirani, 1996)[16]. For a model parameterized by $\mathbf{\Theta}$, the Gaussian regression from (Eq. 1.3) can be expressed as respectively (Eq. 1.15) and (Eq. 1.16), with regularization coefficient λ:

$$-\log P\left(\mathbf{Y}|\mathbf{\Theta}\right) \quad \propto \quad \sum_{t=p+1}^{T} \parallel \mathbf{y}(t) - f\left(\mathbf{y}_{t-p}^{t-1}\right) \parallel_2^2 + \lambda \parallel \mathbf{\Theta} \parallel_2^2 + const \tag{1.15}$$

$$-\log P\left(\mathbf{Y}|\mathbf{\Theta}\right) \quad \propto \quad \sum_{t=p+1}^{T} \parallel \mathbf{y}(t) - f\left(\mathbf{y}_{t-p}^{t-1}\right) \parallel_2^2 + \lambda \sum_{k} |\theta_k| + const \tag{1.16}$$

In summary, we have seen several "memoryless" time series models that model the interaction between time-embedded variables, or the similarity between the time embeddings, but do not incorporate dynamics between hidden variables that represent long term memory. For every time step t, their dynamical model uses information only from the previous p time steps, and ignores longer-range dependencies.

Such models can be perfectly appropriate for learning simple dynamical systems, for time series forecasting, for the classification or regression of subsequences, and for evaluating the likelihood of a sequence. They cannot however be used for imputing missing values, and of course, do not provide with hidden sequence representation, neither do they incorporate unobserved data that might be useful for dynamical modeling (such as unknown protein levels in the case of genetic mRNA microarray data).

[15] Also called ridge regression for linear models.

[16] Note that SVM and SVR express their L_2-norm regularization in different terms of *maximum margins* (Cortes and Vapnik, 1995).

1.3 Time Series Modeling with Hidden Variables

The previously mentioned "memory", also called state information, consists of additional variables $\mathbf{Z}$ that interact with the observed multivariate time series $\mathbf{Y}$ (in the case when we separate output time series $\mathbf{Y}$ from input time series $\mathbf{X}$, the hidden variables $\mathbf{Z}$ interact also with $\mathbf{X}$). Most importantly, the notion of memory is entertained by a dynamical relationship between consecutive values $\ldots, \mathbf{z}_{t-1}, \mathbf{z}_t, \mathbf{z}_{t+1}, \ldots$.

What each hidden variable $\mathbf{z}_t$ represents is a summary of the time series $\mathbf{Y}$ and $\mathbf{X}$ up to time-point t. We can exploit this "summary" while learning the time series model, by "inferring" the hidden representation corresponding to the observed time series. Let us for instance ignore $\mathbf{X}$ and only consider the following standard system of observation (1.17) and dynamical (1.17) equations, also called first Markov order *state-space* model:

$$\mathbf{y}_t = g\left(\mathbf{z}_t\right) \tag{1.17}$$

$$\mathbf{z}_t = f\left(\mathbf{z}_{t-1}\right) \tag{1.18}$$

One can recursively express the above system as $\mathbf{y}_t = g\left(f^{(p)}(\mathbf{z}_{t-p})\right)$, for any order p (up to $p \to \infty$), and not involving the observed variables $\mathbf{y}_{t-p}^{t-1}$. Because, in this generative model, each $\mathbf{y}_t$ is generated from $\mathbf{z}_t$, the recursive formulation implicitly establishes a p-order dependency on the past observed values of the time series, while maintaining a simple first-order Markov system of equations.

1.3.1 Recurrent Neural Networks and Vanishing Gradients

Let us illustrate this notion of memory using the Time-Delay Neural Network architecture. TDNNs work by outputting a prediction $\mathbf{y}_t$ to an input $\mathbf{y}_{t-p}^{t-1}$ or $\mathbf{x}_t$, and use temporary inter-layer variables $\mathbf{z}_t^{\{l\}}$ at each layer l; their output $\mathbf{y}_t$ and variables $\mathbf{z}_t^{\{l\}}$ depend solely on that input. Their difference with Recurrent Neural Networks (RNN) is that RNN keep the values of intermediary layers' activations $\mathbf{z}_t^{\{l\}}$ in memory, and for a new sample $t+1$, compute the values of the new activations $\mathbf{z}_{t+1}^{\{l\}}$ by adding the result of nonlinear operations on the new input to existing values of $\mathbf{z}_t^{\{l\}}$ at each hidden layer l. One speaks about recurrent connections modeling temporal dependencies between hidden states. Figure 1.1 illustrates the difference between a TDNN and a RNN on two toy architectures.

Unfortunately, RNNs require special learning procedures, and ML algorithms based on exact gradient descent (Rumelhart et al., 1986) such as Backpropagation Through Time (BPTT) or Real-Time Recurrent Learning (RTRL) (Williams and Zipser, 1995), fail. The well-known problem of vanishing gradients is responsible for RNN to forget, during training, outputs or activations that are more than a dozen time steps back in time (Bengio et al., 1994). Several alternative training algorithms have been proposed to avoid the vanishing gradient problem in RNN. One of them consists in using Kalman Filtering as a second-order method to optimize the weights of the RNN (Puskorius and Feldkamp, 1994). Another one, called Long Short-Term Memory (LSTM) consists in designing a new type of units with gates that prevent these nodes from forgetting information (Hochreiter and Schmidhuber, 1995; Wierstra et al., 2005).

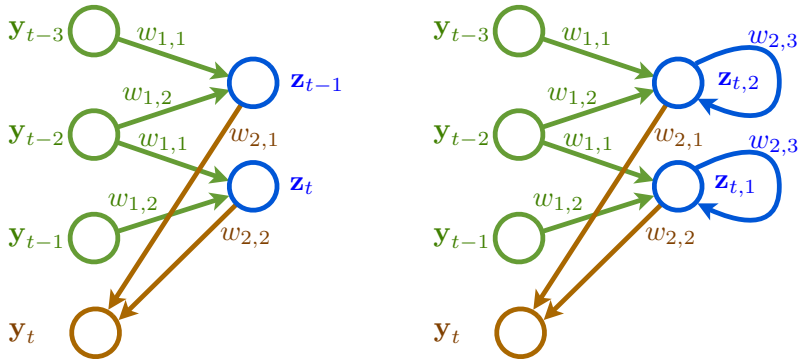

Figure 1.1: Example of an elementary Time-Delay Neural Network architecture (left), and of an associated Recurrent Neural Network (right). The TDNN defines a 3^{rd}-order Markov dependency on the input data $\mathbf{Y}$, predicting y_t from $\mathbf{y}_{t-3}^{t-1}$. It relies on temporary "inter-layer" variables $\mathbf{z}_{t-1}^{t}$, which are connected to the inputs $\mathbf{y}_{t-3}^{t-1}$ and which share two weights $w_{1,1}$ and $w_{1,2}$ (each hidden variable is predicted by the same convolutional kernel of size 2, parameterized by $[w_{1,1}, w_{1,2}]$; notice how we have called the two hidden nodes). In closed-loop training and at time point $t+1$, node $\mathbf{z}_{t-1}$ takes the same value as node $\mathbf{z}_t$ at time point t, which is a consequence of deterministic prediction from consecutive segments of $\mathbf{Y}$ and of weight sharing. The two hidden variables $\mathbf{z}_{t-1}^{t}$ predict in turn y_t (through connection weights $w_{2,1}$ and $w_{2,2}$). In the elementary RNN architecture, those hidden variables are dynamically connected, from one time step to the next one (here, through a single connection of weight $w_{2,3}$). Because they feel the effects of their activations from previous time steps (so-called "memory"), those two hidden nodes may have different values (we use a different notation $\mathbf{z}_{t,1}$ and $\mathbf{z}_{t,2}$ to stress the fact that those two hidden nodes acquire a different behavior).

1.3.2 Models Capable of Inferring Latent Variables

We notice that contrary to procedures evoked in the next sections, gradient descent-based BPTT and RTRL in RNN do not try to optimize the values of hidden variables $\mathbf{z}_t^{\{l\}}$ with respect to the model likelihood.

Let us now introduce methods that explicitly optimize the distribution of the latent variables. All of the methods below try to represent the modeled time series $\mathbf{Y}$ and the hidden sequence $\mathbf{Z}$ in terms of probabilities.

With a few exceptions, most of the models presented subsequently use maximum likelihood for model learning (introduced in Section 1.2.3), and require an iterative learning procedure based on Expectation Maximization (EM) (Dempster et al., 1977), which will be explained in further details in Chapter 2.

There are several differences between these models, which lie in the inference procedure (finding the distribution of the latent variables $\mathbf{Z}$ conditional on the model), in the linear or nonlinear nature of the model, and in the discrete or continuous nature of the sequences.

1.3.3 Discrete Sequence Hidden Variable Models

Hidden Markov Models

Perhaps the most commonly used hidden variable model, introduced for speech recognition, is the Hidden Markov Model (Rabiner, 1989), which consists of a sequence of discrete *state* observations $\mathbf{z}_1^T$ that are governed by a probabilistic transition table and a prior distribution on the M states. At each time point t, a state x_t can emit a multivariate observation $\mathbf{y}_t$ that has a Gaussian distribution. HMMs are therefore a *generative* model.

Assuming a trained HMM, the full inference of the distribution of each $\mathbf{z}_1^T$ can be done using the message-passing *forward-backward* algorithm; alternatively the most likely sequence $\bar{\mathbf{z}}_1^T$ can be found using the Viterbi decoding, which is essentially a dynamic programming algorithm. Because of the Gaussian, finite nature of the HMMs, learning and inference are tractable and can be done in an EM framework, recapitulated in Chapter 2.

Input-Output Hidden Markov Models (IOHMM) (Bengio and Frasconi, 1995) extend HMMs by conditioning the latent variables on additional input time series $\mathbf{X}$.

Conditional Random Fields

Conditional Random Fields (CRF) are a more recent model (Lafferty et al., 2001) that is specific to discrete sequences $\mathbf{Y}$, and which does away with the i.i.d. assumption taken by HMMs. Instead of being a generative model, CRFs can be viewed as undirected graphs that condition the distribution of the latent variables on $\mathbf{Y}$, with a Markov assumption on the graph of $\mathbf{Y}$ (not necessarily a chain). The value of interest is $P(\mathbf{Z}|\mathbf{Y})$. CRFs are typically used for labeling and segmentation problems.

1.3.4 Linear Dynamical Systems

HMMs and CRFs, though powerful, do not fit most of our continuous domain time series. Let us therefore introduce their continuously-valued counterparts.

State-Space Models (SSM) are a general category of models for time series that incorporate a continuously-valued hidden variable $\mathbf{z}_t$, also called *state variable*, which follows a first-order Markov dynamic and generates the observed vector $\mathbf{y}_t$ (Ghahramani, 1998).

$$\mathbf{z}_t = f(\mathbf{z}_{t-1}) + \eta_t \tag{1.19}$$

$$\mathbf{y}_t = h(\mathbf{z}_t) + \epsilon_t \tag{1.20}$$

Linear Dynamical Systems (LDS) are a linear embodiment of SSMs, which means that functions f and h are linear operation (respectively matrix $\mathbf{F}$ and $\mathbf{H}$). Sometimes, function f can also depend on additional time series inputs $\mathbf{x}_t$, which means that $\mathbf{z}_t = \mathbf{F}\mathbf{z}_{t-1} + \mathbf{C}\mathbf{x}_t + \eta_t$. The dynamic and observation noises are distributed as

multivariate Gaussians[17]. LDS were introduced as Kalman Filters (Kalman, 1960).

Both the State-Space Models and the Hidden Markov Models fall into the category of Dynamic Bayesian Networks (DBN), which are directed graphical models for sequences and time series (Ghahramani, 1998). Similar to HMM, and because of their linear nature and of the Gaussian distributions, LDS benefit from a tractable forward-backward inference and tractable ML learning, in the EM framework. One makes the difference between Kalman Smoothing, which is a bidirectional forward-backward inference of the distribution of the latent variables, and which takes advantage of "future" values of $\mathbf{Y}$, $\mathbf{X}$ and $\mathbf{Z}$, and the forward-only Kalman Filtering. During forward and backward recursion, the distribution of $\mathbf{Z}$ is computed by forward- or backward-propagating the noise covariances.

Parameter Learning as a Dual Filtering Problem

A simplified learning procedure for finding some or all the parameters of a Kalman Filter-based dynamical systems is "dual filtering", when the parameters are "filtered" (estimated) simultaneously with the latent states (Nelson and Stear, 1976; Wan and Nelson, 1996). Dual filtering consists of adding the parameters $\mathbf{\Theta}$ of the model as additional dimensions to the state variable $\mathbf{Z}$, and in applying the forward Kalman filtering inference to update θ_t w.r.t. observations $\mathbf{x}_t$ and $\mathbf{y}_t$ as well as "observations" coming from the latent variables $\mathbf{z}_t$. The dynamics on θ_t are assumed to be a random walk.

Of course, LDS have inherent limitations, which is that they cannot model non-linear dynamics, which are the object of next section.

[17]Note that all these matrices and Gaussian covariance matrices could be non-stationary, and depend on t, but in practice the models are time-invariant.

Conditional State Space Models

Similar to CRF, one can define linear SSM in terms of undirected graphs, and condition the continuously-valued latent variable $\mathbf{Z}$ on the observed variables $\mathbf{Y}$, instead of a generative model from $\mathbf{Z}$ to $\mathbf{Y}$. This approach, with linear first-order Markov dynamics on $\mathbf{Z}$, was adopted by (Kim and Pavlovic, 2007). Latent variable inference was done using a Kalman filter, and ML learning was done using gradient descent on the parameters[18].

1.3.5 Nonlinear Dynamical Systems

Suppose now that we replace linear functions f and h in Equations (1.19) and (1.20) by any nonlinear relationship.

Because the inference in DBN is probabilistic, a closed-form solution might not exist, and that inference might become difficult or even intractable in the case of highly nonlinear dynamics and observation models, as is illustrated with the difficulties encountered by so-called Extended Kalman Filters/Smoothers. The root of the problem is in the propagation of the covariance matrices: the nonlinearity that predicts $\mathbf{z}_{t+1}$ from $\mathbf{z}_t$ makes the distribution of $\mathbf{z}_{t+1}$ no longer Gaussian. Because of the issues with latent variable inference, and because of the partition function problem explained in Section 2.2.2, the learning of the parameters is made all the more difficult, as it cannot easily be expressed in closed form and is not tractable.

Several workarounds have been devised in the past decade, which we enumerate below. Beforehand, we shall only mention that, keeping the imperfect Extended Kalman Filter/Smoother architecture, (Wan and Nelson, 1996) devised a dual fil-

[18]Interestingly, because the latent variables (consisting in human poses, associated to observed silhouettes from videos) in the training dataset were known, the hidden variable model was actually trained discriminatively.

tering/smoothing approach for joint state and parameter estimation, which at least greatly simplified the learning procedure.

Unscented and Particle Filtering for Inference

A popular algorithm for latent variable inference in nonlinear models is the Unscented Kalman Filter/Smoother (Wan and Van Der Merwe, 2000). Instead of propagating the mean and covariance matrix of $\mathbf{z}_t$ through the nonlinearity, the UKF propagates the mode and $2M$ "particles", 2 particles per dimension of $\mathbf{z}_t$, on each side of the peak of the distribution and in each dimension. This works very well for unimodal distributions. For more complex distributions, one can use the Particle Filter (PF), with a cloud of (thousands of) particles $\{\mathbf{z}_t\}$ propagated at each time step, out of which one can sample the distribution of $\mathbf{z}_t$. UKF and PF resort to joint filtering for parameter estimation, though.

Making the Learning Tractable

The main issue with learning Nonlinear Dynamic Systems, and hidden variable models in general, will be explicited in Section 2.2.2, and is linked to the fact that one cannot properly compute the probability distribution over $\mathbf{Z}$, because of the intractable *partition function* (in short, one would need to sum over all the possible values of $\mathbf{Z}$, which can be done easily only for a limited number of distributions such as the Gaussian). As a consequence, DBNs that are more complex than LDS and HMMs break out once certain nonlinear architectures are designed (Ghahramani, 1998).

Several approaches have been designed to overcome the issue of the partition function, including the expensive sampling techniques, and the sometimes complicated Variational Bayes derivations to the EM learning procedure. Those approximate techniques enable approximate inference of the full distribution of the hidden

variables[19].

On one hand, (Ghahramani and Roweis, 1999) introduced an NDS where the dynamic function f consisted of Radial Basis Functions, i.e. a mixture of Gaussians. This enabled an exact inference and learning steps in the EM algorithm, but required the RBF centers to be properly initialized.

On the other hand, (Ilin et al., 2004) simplified the NDS to first-order Markov dynamics (it was effectively an SSM), where the nonlinearities were represented by Multi-Layer Perceptrons (MLP) with one hidden layer with *tanh* nonlinearity. This enabled to devise a variational Bayes approximation for approximating the distribution of $\mathbf{Z}$. Their algorithm was applied to model chaotic attractors and to detect changes in nonlinear dynamics.

Both the RBF and MLP nonlinearities employed in NDS were relatively simple compared to the kind of nonlinearities (convolutional networks) used in Chapter 3 of this doctoral work.

NDS with Approximate Inference of Hidden Variables

An early model of nonlinear dynamical system with inferred hidden variables is the Hidden Control Neural Network (Levin, 1993), where a latent variable $\mathbf{z}(t)$ is added as an additional input to mapping (1.2). Although the dynamical model remains unchanged (thus stationary) across the whole time series, the latent variable $\mathbf{z}(t)$ modulates the dynamics of (1.2), enabling a behavior more complex than in pure autoregressive systems. The training algorithm iteratively optimizes the sequence $\mathbf{Z}$ of latent variables (1.21) and the weights $\mathbf{W}$ of the Time-Delay Neural Network

[19] As explained in the next chapter, I used in my doctoral work a different approach to the inference of hidden variables, performing maximum a-posteriori inference of the most likely configuration of the hidden variables. By "cutting corners" in the inference process, my technique is able to handle a much richer class of nonlinearities (essentially, any kind of nonlinear function that is differentiable) than traditional graphical models.

(TDNN) (equation 1.22):

$$\mathbf{Z} = \arg\min_{\mathbf{Z}'} E\left(Y(t), \mathbf{W}, \mathbf{Z}'\right) = \arg\min_{\mathbf{Z}'} \sum_{t} \parallel \mathbf{y}_t - f\left(\mathbf{y}_{t-1}, \mathbf{Z}'; \mathbf{W}\right) \parallel_2^2 \quad (1.21)$$

$$\mathbf{W} = \arg\min_{\mathbf{W}'} E\left(\mathbf{Y}, \mathbf{Z}; \mathbf{W}'\right) \quad (1.22)$$

The latter algorithm, which is likened to approximate maximum likelihood training, is the starting point for my own method, which relies on the same iterative learning, but instead of finding a sequence of dynamic-modulating latent variables, finds the latent variables $\mathbf{Z}$ that generate the observations $\mathbf{Y}$, as in DBNs. Moreover, I propose to consider non-Markovian (or higher-order Markovian) dynamics where hidden states $\mathbf{z}_t$ depend on a time-delay embedding of $\mathbf{z}_{t-p}^{t-1}$.

A more recent model of DBN with deterministic dynamics and explicit inference of latent variables was introduced in (Barber, 2003). However, the inference of the hidden variables was done by message passing in the forward direction only, and the dynamics were first-order Markov only. Both these algorithms were successfully applied to short-sequence speech recognition problems.

1.3.6 Mixed Models for Switching Dynamics

A large area of research has been focusing on mixed state-space models that model switching dynamics and cope with nonstationarity. For instance (Kohlmorgen et al., 1994, 1998) employ a mixture of HMMs and Neural Networks experts (such as Radial Basis Functions RBF) for identification of wake/sleep in physiological recordings, whereas (Pavlovic et al., 1999) employs a mixture of HMMs and LDS for modeling and classifying time series corresponding to different motions.

1.3.7 Recurrent Boltzman Machines

An alternative nonlinear generative model with explicit inference of latent variables is the Restricted Boltzman Machine (RBM). RBMs contain stochastic binary latent variables and real-valued observations (Hinton et al., 1995) with an EM-like inference and learning procedure. Multilayer RBM architectures (Hinton et al., 2006) enable non-linear dynamics, and (Sutskever and Hinton, 2006) enables p^{th} order temporal dependencies on the latent and visible units. Although difficult and long to train, RBMs have been successfully applied to difficult time series, such as motion reconstruction and even long-term prediction (Taylor et al., 2006). Their stochastic nature enables them to create more interesting but still realistic trajectories and to "jump" out of fixed attractors.

1.3.8 Gaussian Processes with Latent Variables

It is possible to incorporate lower-dimension latent variables into Gaussian Processes Latent Variable Models (GPLVM). In that case, one expresses the probability of the observed variables $\mathbf{Y}$ conditional on $\mathbf{X}$ by using a covariance matrix based on a Gaussian kernel on $\mathbf{X}$, and in the ML formulation, tries to maximize the log-likelihood not only w.r.t. the hyperparameters of the kernel function, but also w.r.t. the kernel matrix itself. Because of computational complexity involved in that learning process, a special kernel algorithm is required (Lawrence, 2004). The GPLVM can be extended by adding dynamics to $\mathbf{X}$ (Wang et al., 2006a), notably by expressing $\mathbf{x}_t$ as a Gaussian Process on $\mathbf{x}_{t-1}$. The Gaussian Process Dynamical Model (GPDM) thus comprises a low-dimensional latent space with associated dynamics, and a map from the latent space to an observation space, with a closed-form marginalization of the model parameters for both the dynamics and the observation mappings.

A further embodiment of the GPLVM can be achieved by adding a third GP on input variables $\mathbf{X}$, with an architecture similar to IOHMM or illustrated on Figure 2.2. When both the data $\mathbf{X}$ and $\mathbf{Y}$ are known (e.g. images features and pose, respectively), the model can be trained discriminatively to infer a hidden representation that matches both the inputs and the outputs. On new data $\mathbf{X}$, one can infer the latent variables $\mathbf{Z}$ then the predictions $\bar{\mathbf{Y}}$ (Moon and Pavlovic, 2008).

GPLVM/GPDM have been applied to modeling dynamics on motion capture data, and more recently, to the inference of latent protein transcription factors (Zhang et al., 2010). It seems however that the kernel nature of the algorithm precludes long sequences.

1.3.9 Limitations of Existing Hidden Variable Models

Let us conclude this introductory section by Table 1.1, which recapitulates the strengths of all the common methods for time series modeling with hidden variables. As I suggest in the last line of that table, I introduce in this thesis a new algorithm, Dynamic Factor Graphs (DFG) that is more versatile than the state-of-the-art.

Table 1.1: Summary of existing hidden variable time series models and of their limitations. The table recapitulates the following algorithms: Recurrent Neural Networks (RNN), Long Short-Term Memory (LSTM), Hidden Markov Models (HMM), Conditional Random Fields (CRF), Linear Dynamical Systems (LDS) and Kalman Filters (KF), Nonlinear Dynamical Systems (NDS) and Extended Kalman Filters (EKF), Unscented Kalman Filters (UKF) and Particle Filters (PF), Conditional Restricted Boltzmann Machines (RBM), Gaussian Process Latent Variable Models (GPLVM), and finally, the method developed in this thesis, Dynamic Factor Graphs (DFG). For each method, we listed whether the method performs a proper inference of hidden representations, whether the model is trainable, whether that representation is continuously-valued (real), whether it enables complex nonlinearities and whether it handles long sequences in linear time.

Method	Infers hidden variables	Trainable	Real-Valued	Complex Nonlinearity	Long Sequences
RNN		✓	✓	✓	✓
LSTM		✓	✓	✓	✓
HMM	✓	✓	discrete		✓
CRF	✓	✓	discrete	✓	✓
LDS	✓	✓	✓		✓
NDS	✓	✓	✓	1^{st} order Markov	✓
UKF, PF	✓	joint infer.	✓	1^{st} order Markov	✓
CRBM	✓	✓	binary	✓	✓
GPLVM	✓	✓	✓	1^{st} order Markov	
DFG	✓	✓	✓	✓	✓

Chapter 2

Common Framework: Dynamical Factor Graphs

Let's do the time warp again!

Richard O'Brien

In this chapter, I explain how we define a new inference and training algorithm for modeling time series with Recurrent Neural Networks, using approximate iterative inference and learning algorithms derived from state-space model such as Dynamic Bayesian Networks, and using the Factor Graphs formalism. I will stress the importance on the most important contribution of this doctoral thesis, which is to perform Maximum A Posteriori inference of continuously-valued hidden variables, while maintaining the partition function constant by construction, thereby enabling to model any kind of differentiable nonlinear dynamics and observation functions (in particular, any Markov order p), and thus achieving a much stronger representative power than usual Graphical Models.

2.1 Our Factor Graph formalism

2.1.1 Factor Graphs

According to their definition (Kschischang et al., 2001; Bishop, 2006), a *factor graph* is a bipartite graph with two types of nodes, *variables* $\mathbf{y}_t$ and *factors* g_i (which are functions of variables). Each variable node can be connected only to factor nodes, and each factor node can be connected only to variables nodes. Factor graphs express a global function g of all variables as a product of functions on the subset of variables to which they are directly connected. It means that function g_i takes as arguments only variables $\{\mathbf{y}_t\}_{t\in S_i}$ to which it is directly connected in the graph. For T variables and P functions, we have the following factorization:

$$g\left(\mathbf{y}_1, \mathbf{y}_2, \ldots, \mathbf{y}_T\right) = \prod_{i=1}^{P} g_i\left(\{\mathbf{y}_t\}_{t\in S_i}\right) \tag{2.1}$$

Because of their factorial nature, factor graphs can represent, among others, bayesian models (such as Hidden Markov Models), modeling the joint probability of the full model as a product of conditional probabilities at each factor. Even if ones does not use probabilities but hard constraints (one constraint per factor), the conjunction of all the hard constraints in the model can be expressed as a product of boolean indicators, one per factor (Kschischang et al., 2001).

When the graph structure is a tree, one can directly compute the marginal function $g\left(\mathbf{y}_t\right)$ for any variable $\mathbf{y}_t$ using the *sum-product* algorithm for factor graphs, which is based on message passing between the variable nodes. The sum-product algorithm is the factor graph equivalent of both the forward-backward algorithm for hidden sequence inference and of the Viterbi algorithm in HMMs, and for linear dynamical

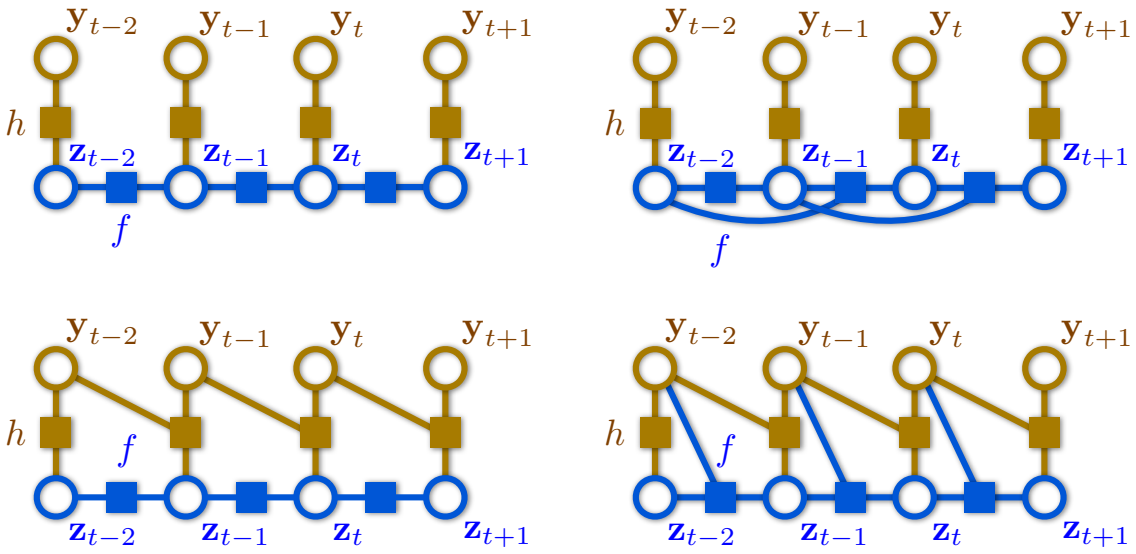

Figure 2.1: Several Dynamic Factor Graphs that admit observed variables $\mathbf{Y}$ and latent variables $\mathbf{Z}$, which are factorized by observation (h) and dynamic (f) factors.

systems, corresponds to Kalman filtering (Kschischang et al., 2001). Figure 2.1 (top left) illustrates the factor graph representation that is common to HMM and to one embodiment of the algorithms discussed in the next chapters (specifically, the one we used for learning the gene regulation network of the *Arabidopsis* in Chapter 4).

Several state-space models consist in Directed Acyclic Graphs (DAG), but an undirected factor graph representation cannot be represented by a tree. The sum-product algorithm nevertheless works for undirected factor graphs with cycles, it simply needs to be repeated and has no guarantees of convergence (in the general case). Figure 2.1 illustrates other factor graphs architectures that I will use. Among others I investigated n-th order Markov dependencies (top right of the figure) for modeling chaotic dynamics in Chapter 3. For the inference of protein transcription factors in Chapter 4, I used observation and dynamic models that expressed the rates of change of $\mathbf{y}_t$ and of $\mathbf{z}_t$ (bottom part of the figure). Finally, Figure 2.2 shows

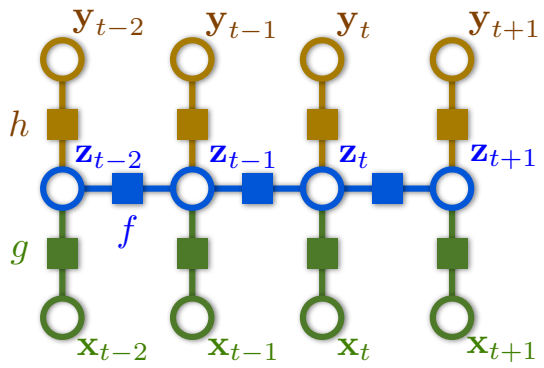

Figure 2.2: Dynamic Factor Graph that admits two types of observed variables: inputs $\mathbf{X}$ and outputs $\mathbf{Y}$, as well as latent variables $\mathbf{Z}$, which are all factorized by observation (h), dynamic (f) and input (g) factors.

an input-output architecture that separates observed sequences into $\mathbf{X}$ and $\mathbf{Y}$; this architecture corresponds to supervised auto-encoders with dynamical dependencies between hidden variables in Chapter 5. Since all the aforementioned factor graphs are specialized for sequence modeling, I call them *Dynamic Factor Graphs*.

The Factor Graph formalism has already been applied to model data where the latent variable had a spatial structure, notably for modeling house prices. In that case, the price y_i of the i-th house in the dataset was considered as depending both on associated input variables $\mathbf{x}_i$ and on a latent desirability factor z_i that was geographically smooth (Chopra et al., 2007).

2.1.2 Maximum Likelihood and Factor Graphs

As I suggested in the first chapter, model learning and the inference of hidden representations in this thesis is done using a maximum likelihood framework[1]. For numerical reasons, this is performed in logarithmic space, using the negative log-likelihood

[1]We cannot apply discriminative learning of the hidden representations because we cannot evaluate the partition function of our nonlinear model with continuous hidden variables.

instead. For the case of a Dynamical Bayesian Network such as an Input-Output HMM (Bengio and Frasconi, 1995) (which can be described by the factor graph of Figure 2.2), the joint likelihood (Eq. 2.2) and negative log-likelihood (Eq. 2.4) are expressed as:

$$P(\mathbf{X}, \mathbf{Y}, \mathbf{Z}) = \prod_t P(\mathbf{z}_t|\mathbf{z}_{t-1}) P(\mathbf{z}_t|\mathbf{x}_t) P(\mathbf{y}_t|\mathbf{z}_t) P(\mathbf{x}_t) \quad (2.2)$$

$$NLL = -\log P(\mathbf{X}, \mathbf{Y}, \mathbf{Z}) \quad (2.3)$$

$$NLL = const + \sum_t -\log P(\mathbf{z}_t|\mathbf{z}_{t-1}) - \log P(\mathbf{z}_t|\mathbf{x}_t) - \log P(\mathbf{y}_t|\mathbf{z}_t) \quad (2.4)$$

Consistently with DBNs, we keep the factor graph formalism while operating in the logarithmic space, which simply means that we add each factor's contributions instead of multiplying them.

2.1.3 Factors Used in This Work

Different factors will be detailed in subsequent chapters, but we can express now their common properties. Our factors contain two modules. The first one consists in a deterministic function (let us call it g) that takes argument variables $\mathbf{a}_t$ and generates prediction variables $\bar{\mathbf{o}}_t$. Those predictions are then compared to the actual target variable $\mathbf{o}_t$ and an error term is computed. The function that evaluates the error constitutes the second module of the factor. Function g is parameterized by parameters $\mathbf{W}$, which we shall learn in order to minimize the prediction error of the factor. Figure 2.3 recapitulates these concepts.

We notice that factor graphs are undirected; one can see them as "springs" between variables. The main idea in our algorithm is that even if the functions are directed

(from arguments to predictions), the error term is not. Therefore, during inference of latent variables, one can try to minimize the error by acting both on the latent variable arguments of the function and on the latent variable that are targets of that same function. This principle is similar to Kalman smoothing, which is bidirectional, as opposed to Kalman filtering (Kalman, 1960), which is forward only.

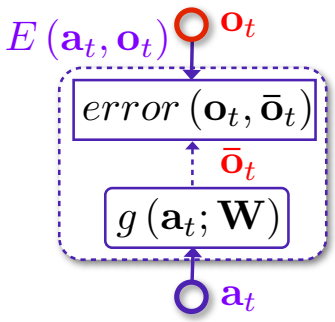

Figure 2.3: General description of a factor linking variables $\mathbf{a}_t$ and $\mathbf{o}_t$ through function g, with energy term $E(\mathbf{a}_t, \mathbf{o}_t)$.

We considered several types of functions g in this work, enumerated below:

- *identity* function, for instance for modeling random walk dynamics on latent variables, or latent variables that are a de-noised version of observed variables: $\bar{\mathbf{o}}_t = \mathbf{a}_t$
- *linear matrix* operations: $\bar{\mathbf{o}}_t = \mathbf{W}\mathbf{a}_t$,
- *linear matrix* operations followed by a nonlinearity such as the hyperbolic tangent *tanh*: $\bar{\mathbf{o}}_t = tanh(\mathbf{W}\mathbf{a}_t)$,
- *linear matrix* operations followed by a *softmax* function, to produce probability distributions over the output dimension space: $\forall k, \bar{o}_{k,t} = \frac{e^{\mathbf{w}_k \mathbf{a}_t}}{\sum_j e^{\mathbf{w}_j \mathbf{a}_t}}$,

- a highly nonlinear *TDNN* or convolutional network, typically for modeling chaotic dynamics on the latent variables. Note that contrary to (LeCun et al., 1998a), we did not resort to 2D convolutions, as we used only convolutions across time, not across channels.

Similarly, we considered different types of errors, which would all correspond to negative log-likelihoods: most commonly the sum of squares (Gaussian distribution) and sum of absolute values (Laplace), but also the logistic error (Binomial) and the cross-entropy error (Multinomial) for classification. The latter two errors are reminded in Chapters 5.

2.2 Maximum Likelihood Energy-Based Inference

Now that we have defined the building blocks of our architecture, involving latent and hidden variables, we would like to be able to infer the sequence of hidden variables $\mathbf{Z}$ that optimally represents the observed sequence $\mathbf{Y}$ (and $\mathbf{X}$, if relevant) under the model. This is a simpler problem than that of inferring a full distribution over $\mathbf{Z}$, which is normally done for Dynamic Bayesian Networks and (Non)-Linear Dynamical Systems (Ghahramani, 1998; Ghahramani and Roweis, 1999).

2.2.1 Energy as Negative Log-Likelihood

Let us introduce the notion of *energy*, which is among others reviewed in (LeCun et al., 2006). Using the notation from Figure 2.3, our energy term $E(\mathbf{a}_t, \mathbf{o}_t)$ at each factor merely corresponds to the error that results from predicting $\bar{\mathbf{o}}_t$ instead of $\mathbf{o}_t$. Using the factor graph formalism in the logarithmic domain, the energy of the whole sequence of observed and hidden variables is a sum of energies at all the factors,

and is noted $E(\mathbf{Y}, \mathbf{Z})$ or $E(\mathbf{X}, \mathbf{Y}, \mathbf{Z})$. Without loss of generality, let us focus on models without inputs $\mathbf{X}$, and also include the model parameters $\mathbf{W}$ into the energy term: $E(\mathbf{Y}, \mathbf{Z}; \mathbf{W})$. As we mentioned earlier, we make our energy proportional to the negative log-likelihood of joint variables $\mathbf{Y}$ and $\mathbf{Z}$:

$$E(\mathbf{Y}, \mathbf{Z}; \mathbf{W}) \propto -\log P(\mathbf{Y}, \mathbf{Z}|\mathbf{W}) + const \tag{2.5}$$

2.2.2 Intractable Partition Functions

Note that energy in Equation (2.5) does not define by itself a probability distribution, because the normalization terms are unknown. For a proper normalization and to obtain the actual value of $P(\mathbf{Y}, \mathbf{Z}|\mathbf{W})$, one would need to resort to the so-called Boltzmann distribution (LeCun et al., 2006) with an additional "temperature" coefficient $1/\beta$ (Eq. 2.6). The Boltzmann distribution, used in statistical mechanics, provides with the maximum entropy distribution[2] that is still compatible with the observations.

$$P(\mathbf{Y}, \mathbf{Z}|\mathbf{W}) = \frac{e^{-\beta E(\mathbf{Y}, \mathbf{Z}; \mathbf{W})}}{\int_{\mathbf{Y}'} \int_{\mathbf{Z}'} e^{-\beta E(\mathbf{Y}', \mathbf{Z}'; \mathbf{W})} d\mathbf{Y}' d\mathbf{Z}'} \tag{2.6}$$

$$= \frac{e^{-\beta E(\mathbf{Y}, \mathbf{Z}; \mathbf{W})}}{\Gamma_{Y,Z}} \tag{2.7}$$

The normalization constant $\Gamma_{Y,Z}$ is called the partition function.

For a given configuration of energies $E(\mathbf{Y}, \mathbf{Z}|\mathbf{W})$, the lower the temperature $1/\beta$, the more peaked the associated Boltzmann distribution (conversely, the higher the temperature, the more uniform the distribution). At sufficiently low temperatures, in

[2] i.e. most uniformly random

the limit of $\beta \to \infty$, the associated distribution would become unimodal, even if the energy surface admitted local minima; therefore, the joint configuration of observed and hidden variables given the model would seem simpler than it actually is.

In order to evaluate the likelihood of observed sequence $\mathbf{Y}$, one needs to marginalize $P(\mathbf{Y}, \mathbf{Z}|\mathbf{W})$ and (Eq. 2.6) over all the values that hidden sequence $\mathbf{Z}$ can take:

$$P(\mathbf{Y}|\mathbf{W}) = \int_{\mathbf{Z}'} P(\mathbf{Y}, \mathbf{Z}'|\mathbf{W})\, d\mathbf{Z}' \tag{2.8}$$

$$= \int_{\mathbf{Z}'} \frac{e^{-\beta E(\mathbf{Y}, \mathbf{Z}'; \mathbf{W})}}{\int_{\mathbf{Y}'} \int_{\mathbf{Z}''} e^{-\beta E(\mathbf{Y}', \mathbf{Z}''; \mathbf{W})} d\mathbf{Y}' d\mathbf{Z}''} d\mathbf{Z}' \tag{2.9}$$

Evaluating the integrals of (Eq. 2.6) and (Eq. 2.9) over all observed and hidden sequences is intractable for continuous variables under non-Gaussian distributions. It is similarly difficult when the distributions are Gaussian but the factors are nonlinear. As we detailed in the first chapter, DBN, LDS and NDS algorithms have resorted to various approximations involving sampling and variational Bayes approximations.

2.2.3 Maximum A Posteriori Approximation

Similarly to previous work in that field conducted in Prof. LeCun's lab (LeCun et al., 2006; Chopra et al., 2007; Ranzato et al., 2007), we propose to use a maximum a posteriori (MAP) approximation, which foregoes the full distribution in favor of its mode. What follows is an analogy to the proofs derived in (Ranzato, 2009).

Let us first define the "marginal" energy of the observed sequence $\mathbf{Y}$, after having *integrated away* the latent variables. This definition is arbitrary but fits nicely into previous equation (2.9):

$$E(\mathbf{Y};\mathbf{W}) = -\frac{1}{\beta}\log\int_{\mathbf{Z}'} e^{-\beta E(\mathbf{Y},\mathbf{Z}';\mathbf{W})}d\mathbf{Z}' \tag{2.10}$$

$$e^{-\beta E(\mathbf{Y};\mathbf{W})} = \int_{\mathbf{Z}'} e^{-\beta E(\mathbf{Y},\mathbf{Z}';\mathbf{W})}d\mathbf{Z}' \tag{2.11}$$

$$P(\mathbf{Y}|\mathbf{W}) = \frac{e^{-\beta E(\mathbf{Y};\mathbf{W})}}{\int_{\mathbf{Y}'} e^{-\beta E(\mathbf{Y}';\mathbf{W})}d\mathbf{Y}'} \tag{2.12}$$

We will show that a) $E(\mathbf{Y};\mathbf{W})$ can be approximated by $\arg\min_{\mathbf{Z}} E(\mathbf{Y},\mathbf{Z};\mathbf{W})$, and that b) $\arg\min_{\mathbf{Z}} E(\mathbf{Y},\mathbf{Z};\mathbf{W}) = \arg\max_{\mathbf{Z}} P(\mathbf{Z}|\mathbf{Y},\mathbf{W})$. Let us begin with the second statement.

By the Bayes rule $P(\mathbf{Y},\mathbf{Z}|\mathbf{W}) = P(\mathbf{Z}|\mathbf{Y},\mathbf{W})\,P(\mathbf{Y}|\mathbf{W})$, maximizing $P(\mathbf{Y},\mathbf{Z}|\mathbf{W})$ w.r.t. $\mathbf{Z}$ is akin to maximizing $P(\mathbf{Z}|\mathbf{Y},\mathbf{W})$ w.r.t. $\mathbf{Z}$ since $P(\mathbf{Y}|\mathbf{W})$ does not depend on $\mathbf{Z}$. Then, using Equation (2.6), $\arg\max_{\mathbf{Z}} P(\mathbf{Z}|\mathbf{Y},\mathbf{W}) = \arg\max_{\mathbf{Z}} e^{-\beta E(\mathbf{Y},\mathbf{Z};\mathbf{W})}$ because the partition function is independent of the variables. Hence:

$$\arg\min_{\mathbf{Z}} E(\mathbf{Y},\mathbf{Z};\mathbf{W}) = \arg\max_{\mathbf{Z}} P(\mathbf{Z}|\mathbf{Y},\mathbf{W}) \tag{2.13}$$

Now, to prove that $E(\mathbf{Y};\mathbf{W})$ can be approximated by $\arg\min_{\mathbf{Z}} E(\mathbf{Y},\mathbf{Z};\mathbf{W})$, we take Equation (2.10) to the limit in β. Assuming that the energy $E(\mathbf{Y},\mathbf{Z};\mathbf{W})$ is positive and admits a zero minimum in $\mathbf{Z}_0$ (which is the case for instance for quadratic errors):

$$\lim_{\beta\to\infty} -\frac{1}{\beta}\log\int_{\mathbf{Z}'} e^{-\beta E(\mathbf{Y},\mathbf{Z}';\mathbf{W})}d\mathbf{Z}' = \lim_{\beta\to\infty} -\frac{1}{\beta}\log\int_{\mathbf{Z}'} \delta_{\mathbf{Z}'=\mathbf{Z}_0} e^{-\beta E(\mathbf{Y},\mathbf{Z}';\mathbf{W})}d\mathbf{Z}' \tag{2.14}$$

$$= \lim_{\beta\to\infty} -\frac{1}{\beta}\log\left(e^{-\beta E(\mathbf{Y},\mathbf{Z}_0;\mathbf{W})}\right) \tag{2.15}$$

$$= E(\mathbf{Y},\mathbf{Z}_0;\mathbf{W}) \tag{2.16}$$

In the rest of this work, we subsequently note that, for an observed sequence $\mathbf{Y}$ and given a model parameterized by $\mathbf{W}$, the result of the latent variable inference is the minimum energy state of the model for that sequence:

$$E(\mathbf{Y};\mathbf{W}) = \arg\min_{\mathbf{Z}} E(\mathbf{Y},\mathbf{Z};\mathbf{W}) \tag{2.17}$$

2.2.4 Summing Energies from Diverse Factors

As illustrated on Figures 2.1 and 2.2, our factor graphs contain several types of factors replicated over the time dimension of the sequences. We therefore need to sum up, for all time points, energies from various factors.

We design our factor graph and energy functions under the assumption that all time series including the latent variables $\mathbf{Z}$ are identically distributed, with conditional independencies beyond the reach of each factor (see section 1.2.3). This means that for a given type of factor, the *additive* normalization term (due to the partition function) $-\log \Gamma_{Z,Y}(t)$ remains constant across time samples $t \in \{1,\ldots,T\}$. This also means that, for exponential distributions (such as Laplace and Gaussian), the *multiplicative* scale coefficients for each data point are constant across time. Recall that for the Gaussian distribution, these scale coefficients are linked to the inverse of the covariance matrix $\mathbf{\Sigma}$. As many latent variable techniques in the machine learning literature do, we will claim[3] that the covariance matrix is diagonal with identical terms across the diagonal: $\mathbf{\Sigma} = \sigma I$.

However, because we did not properly normalize the energies of our factors, we are left with "guessing" the relative weight of the scales σ for each type of factors. For a clearer picture, let us focus for instance on a DFG composed of observation h and

[3]We can of course design latent variables such that their covariance is diagonal, and we can always standardize the observed time series $\mathbf{Y}$ to zero-mean and unit variance for each dimension, and then apply a principal component analysis to de-correlate the rows of $\mathbf{Y}$.

dynamic f factors (as in Chapters 3 and 4), with associated energies $E_h(\mathbf{y}_t, \mathbf{z}_t; \mathbf{W})$ and $E_f\left(\mathbf{z}_{t-p}^{t-1}, \mathbf{z}_t; \mathbf{W}\right)$. Let us assume (as is the case in those chapters) that their underlying distributions are Gaussian, which also means that their error terms are Gaussian:

$$\forall t,\ P\left(\mathbf{y}_t - h\left(\mathbf{z}_t; \mathbf{W}\right) | \mathbf{z}_t\right) \sim \mathcal{N}\left(0, \mathbf{\Sigma}_h\right) = \mathcal{N}\left(0, \sigma_h I_N\right) \tag{2.18}$$

$$\forall t,\ P\left(\mathbf{z}_t - f\left(\mathbf{z}_{t-p}^{t-1}; \mathbf{W}\right)\right) \sim \mathcal{N}\left(0, \mathbf{\Sigma}_f\right) = \mathcal{N}\left(0, \sigma_f I_M\right) \tag{2.19}$$

In our energy-based framework, we simply replace the scales σ_h and σ_f by their relative weight coefficient γ (e.g. coefficient of the dynamic factor). The total energy of a sequence of observed $\mathbf{Y}$ and hidden variables $\mathbf{Z}$ is written as (Eq. 2.20), and the inference problem becomes (Eq. 2.21).

$$E\left(\mathbf{Y}, \mathbf{Z}; \mathbf{W}\right) = \sum_t E_h\left(\mathbf{y}_t, \mathbf{z}_t; \mathbf{W}\right) + \gamma \sum_t E_f\left(\mathbf{z}_{t-p}^{t-1}, \mathbf{z}_t; \mathbf{W}\right) \tag{2.20}$$

$$E\left(\mathbf{Y}; \mathbf{W}\right) = \arg\min_{\mathbf{Z}'} \left\{ \sum_t E_h\left(\mathbf{y}_t, \mathbf{z}_t; \mathbf{W}\right) + \gamma \sum_t E_f\left(\mathbf{z}_{t-p}^{t-1}, \mathbf{z}_t; \mathbf{W}\right) \right\} \tag{2.21}$$

We can use a few tricks to make the guessing of γ easier. First of all, if there are several factors with similar types of energies (e.g. Gaussian sum of square errors), then we can normalize the energies by the number of dimensions of the variables involved. Secondly, varying the relative contributions of each factor type can be treated like adjusting additional hyper-parameters with an intuitive explanation: the coefficient γ is related to the "weight" or "importance" we want to give to the dynamic factor; the larger the γ, the tighter the scale or bandwidth of that factor. Finally, γ can be

adjusted with the usual arsenal of techniques such as cross-validation.

2.2.5 Interpretation in Terms of Lagrange Multipliers

Another explanation of the γ can be provided from the Lagrange multipliers technique, developed by French mathematician Joseph Louis Lagrange. Let us consider indeed the energy minimization problem (Eq. 2.17) with two factors[4], one for the observation (h) and one for the dynamics (f), as a constrained optimization problem with an objective (Eq. 2.22) and a constraint (Eq. 2.23):

$$\min_{\mathbf{Z}} E_h\left(\mathbf{Y}, \mathbf{Z}; \mathbf{W}\right) \tag{2.22}$$

$$\text{subject to: } \forall t,\ \mathbf{z}_t = f\left(\mathbf{z}_{t-1}; \mathbf{W}\right) \tag{2.23}$$

The Lagrange multiplier technique proposes to integrate those constraints into one Lagrange function $\Lambda\left(\mathbf{Z}, \lambda\right)$, after multiplying each constraint (over all time points and for all M dimensions of $\mathbf{Z}$) by a corresponding Lagrange coefficient $\lambda_{k,t}$:

$$\Lambda\left(\mathbf{Z}, \lambda\right) = E_h\left(\mathbf{Y}, \mathbf{Z}; \mathbf{W}\right) + \sum_{t=2}^{T}\sum_{k=1}^{M} \lambda_{k,t}\left(z_{k,t} - f_k\left(\mathbf{z}_{t-1}; \mathbf{W}\right)\right) \tag{2.24}$$

The Lagrange function enables to define the notion of a Lagrangien $\Lambda\left(\lambda\right)$, which is a lower bound on Λ for a specific configuration of the Lagrange multipliers (Eq. 2.25). We can set equal constraints on all time points (conditional i.i.d. assumption) and on all dimensions of $\mathbf{Z}$ (not favoring one hidden dimension over another), to obtain a simplified Lagrangien depending on a single variable (Eq. 2.26).

[4]For simplicity, but without loss of generality, we assumed that the Markov order p was one in constrain (Eq. 2.23).

$$\Lambda(\lambda) = \min_{\mathbf{Z}} \left\{ E_h(\mathbf{Y}, \mathbf{Z}; \mathbf{W}) + \sum_{t=2}^{T} \sum_{k=1}^{M} \lambda_{k,t} \left(z_{k,t} - f_k(\mathbf{z}_{t-1}; \mathbf{W}) \right) \right\} \quad (2.25)$$

$$= \min_{\mathbf{Z}} \left\{ E_h(\mathbf{Y}, \mathbf{Z}; \mathbf{W}) + \lambda \left(\sum_{t=2}^{T} \sum_{k=1}^{M} \left(z_{k,t} - f_k(\mathbf{z}_{t-1}; \mathbf{W}) \right) \right) \right\} \quad (2.26)$$

The last equation (Eq. 2.26) shows the analogy to the energy-based inference (Eq. 2.21). Note however that in numerical optimization, the solution $(\mathbf{Z}, \lambda)$ to the Lagrange optimization does not correspond to the optimum of $\Lambda(\mathbf{Z}, \lambda)$, but rather to a so-called *saddle-point* or critical point, which is at the same time a minimum w.r.t. $\mathbf{Z}$ and a maximum w.r.t. the Lagrange coefficients λ.

2.2.6 Inference of Latent Variables

As we will illustrate in the next chapters, inference of latent variables in an MAP setting becomes extremely simple. For a given configuration of the pseudo-Lagrange coefficients, one simply needs to find the optimum of $E(\mathbf{Y}, \mathbf{Z}; \mathbf{W})$, i.e. to differentiate the total sequence energy (Eq. 2.20) w.r.t. the latent variables, and therefore to solve for:

$$\frac{\partial E(\mathbf{Y}, \mathbf{Z}; \mathbf{W})}{\partial \mathbf{Z}} = 0 \quad (2.27)$$

This can be achieved using the well-known gradient descent algorithm. As evoked earlier, we back-propagate (Rumelhart et al., 1986) the gradients from the energy modules in *both* directions, and update each $\mathbf{z}_t$ by summing up the contributions coming from all the factors it is connected to. We repeat the gradient step using a

small learning rate, until a convergence criterion.

2.2.7 What DFGs Can Do That Graphical Models Cannot

The most important contribution of this doctoral thesis can be summarized in a single sentence: *Thanks to our Maximum A Posteriori approximation during the inference of continuously-valued hidden representations of time series, and because we maintain the partition function constant by construction, we are able to model any kind of differentiable nonlinear dynamics and observation functions, with any dependencies between the variables (in particular, any Markov order p), achieving a much stronger representative power than usual Graphical Models.*

2.2.8 On the Difference Between *Hidden* and *Latent* Variables

I would like to highlight at this point the difference between *hidden* and *latent* variables $\mathbf{Z}$. Both are variables that are not observed and that need to be extracted from observed data. However only the latent variables correspond to a maximum likelihood solution that is obtained through inference. The maximum likelihood solution corresponds to the mode of the distribution of $\mathbf{Z}$ for DBNs, and to the minimum energy sequence w.r.t. $\mathbf{Z}$ for our DFGs. If we think in terms of message passing through the factor graph, a hidden representation is obtained through a simple "forward" message passing (e.g. direct prediction by an encoder), whereas the latent representation is obtained after an iteration of "forward" and "backward" message passings, in a so-called relaxation procedure, until the hidden representation converges to a stable fixed point.

As such, the hidden variables in the language modeling task from Chapter 6 are not properly latent, since they are obtained through a deterministic look-up table

from a discrete observed sequence $\mathbf{y}_1^T$, without a relaxation step w.r.t. the dynamic energy linking the hidden variables. We abstained from full relaxation on the hidden variables because of the computational complexity of the language model on large vocabularies and large text corpora.

2.3 Expectation Maximization-Like Learning of DFG

2.3.1 Expectation Maximization Algorithm

In its original form, Expectation Maximization (EM) (Dempster et al., 1977) is an iterative and probabilistic maximum likelihood algorithm for estimating missing data and learning the parameters of the joint distribution of observed and missing data. EM alternates between parameter estimation/learning (**M-step**) and latent variables inference (**E-step**), and can be referred to as *coordinate ascent* of the likelihood. The main limitation of EM is that it converges to a local maximum likelihood.

In a nutshell, EM strives at maximizing the joint likelihood $P(\mathbf{Y}, \mathbf{Z}|\mathbf{\Theta})$ of complete data (observed and hidden) that one could obtain given a model parameterized by $\mathbf{\Theta}$. In other words, it tries to find the optimal $\mathbf{\Theta}$ such that $P(\mathbf{Y}, \mathbf{Z}|\mathbf{\Theta})$ is maximal. Because $\mathbf{Z}$ is unknown, it tries instead to maximize the expectation of the log-likelihood of the complete data under the model. The first step (E-step) consists in evaluating $\mathbb{E}\left[\log P\left(\mathbf{Y}, \mathbf{Z}|\mathbf{\Theta}^{(k)}\right)\right]$ given the current estimate $\mathbf{\Theta}^{(k)}$of the parameters. The second step (M-step) consists in maximizing that quantity with respect to the parameters $\mathbf{\Theta}$, i.e. assigning $\mathbf{\Theta}^{(k+1)} = \arg\max_{\mathbf{\Theta}} \mathbb{E}\left[\log P\left(\mathbf{Y}, \mathbf{Z}|\mathbf{\Theta}^{(k)}\right)\right]$.

As one can guess, the quantities enunciated above can be evaluated in closed form if one can compute the full distribution $P(\mathbf{Y}, \mathbf{Z}|\mathbf{\Theta})$, for instance in HMM or LDS. It is however more difficult in the case of intractable partition functions and

distributions. An alternative explanation of EM, in terms of free energy and entropy is given in (Ghahramani, 1998). In particular, the distribution $P(\mathbf{Y}, \mathbf{Z}|\mathbf{\Theta})$, which is unknown, is replaced by an approximate distribution $Q(\mathbf{Y}, \mathbf{Z}|\mathbf{\Theta})$ that is known, and during the E-step, instead of maximizing the expectation of $P(\mathbf{Y}, \mathbf{Z}|\mathbf{\Theta})$, one maximizes the log-likelihood of $Q(\mathbf{Y}, \mathbf{Z}|\mathbf{\Theta})$, which is proved to be a lower bound on the log-likelihood of $P(\mathbf{Y}, \mathbf{Z}|\mathbf{\Theta})$[5].

Since its inception, EM has found a wealth of applications in many fields, for instance in various fields of signal processing (Moon, 1996). Generalized EM (GEM) is a version of EM with truncated M-step that only partially improves the likelihood of the parameters given the latent variables inferred in the E-step. Stochastic and incremental (Neal and Hinton, 1998) variants of the EM are also possible.

2.3.2 Our Simplification and Approximation

The link between EM and our work is very simple, albeit simplistic. As we said earlier, instead of evaluating the full distribution $P(\mathbf{Y}, \mathbf{Z}|\mathbf{\Theta})$ (or $P(\mathbf{Z}|\mathbf{Y}, \mathbf{\Theta})$, for that matter) we replace it by its MAP approximation (its argmax). Then, maximizing the conditional likelihood of the hidden variables is equivalent to minimizing the energy, according to Equation (2.13). Since we are treating the "inferred" distribution of $\mathbf{Z}$ as its *mode*, or more plainly, as a fixed quantity (just like $\mathbf{Y}$), we can solve the M-step learning in a quantity of ways.

2.3.3 Alternated E-Step and M-Step Procedure

In summary, learning in an DFG consists in adjusting the parameters $\mathbf{W}$ in order to minimize the sum of energies at each factor. Because we introduce a regularization

[5]Such a formulation is useful for Variational Bayes inferrence (MacKay, 2003).

term $R(\mathbf{W})$ on the parameters (see Section 1.2.10) as well as another regularization term $R_z(\mathbf{Z})$ on the latent representation (see Section 2.4.2), we speak instead of a loss function $\mathcal{L}(\mathbf{Y}, \mathbf{Z}; \mathbf{W})$, defined in Equation (2.28). That loss function contains a crucial additional term, the log partition function $-\log \Gamma_{Y,Z}$, which is constant by construction in our case and can by consequence be ignored during minimization. Coming back to the example exhibited in the last section, the iterative procedure can be written as:

$$\mathcal{L}(\mathbf{Y}, \mathbf{Z}; \mathbf{W}) = \sum_t (E_h(t) + \gamma E_f(t)) + R_z(\mathbf{Z}) + R(\mathbf{W}) - \log \Gamma_{Y,Z} \quad (2.28)$$

$$\text{E-step: } \mathbf{Z} = \arg\min_{\mathbf{Z}'} L(\mathbf{Y}, \mathbf{Z}'; \mathbf{W}) \quad (2.29)$$

$$\text{M-step: } \mathbf{W} = \arg\min_{\mathbf{W}'} L(\mathbf{Y}, \mathbf{Z}; \mathbf{W}') \quad (2.30)$$

Minimization of the loss is done iteratively in an Expectation-Maximization-like fashion in which the states $\mathbf{Z}$ play the role of auxiliary variables. The inference described in part and equation (2.29) can be considered as the **E-step** (state update) of a deterministic gradient-based version of the EM algorithm. During the parameter-adjusting **M-step** (weight update) described by (2.30), the latent variables are frozen. This means that we are back into the non-hidden variable framework, and that we perform any kind of optimization[6] to adjust $\mathbf{W}$.

The E-step inference can be done either on the full sequence, or on **mini-batches** (we used sequence length ranging from 20 to 1000 samples) with an M-step parameter update after each mini-batch inference. In the latter case, during one epoch of training, the batches should be selected randomly, similar to regular stochastic gradient

[6]In the next chapters, we show that we investigated several ways to perform the M-step parameter learning.

with no latent variables (LeCun et al., 1998b; Bottou, 2004), in order to speed up the learning of the weight parameters.

2.4 Discussion

Hidden/latent models are not without certain limitations, which need to be handled. This section recapitulates the three most important ones.

2.4.1 Avoiding Flat Energy Surfaces During Inference

Hidden representations may raise the issue of flat energy surfaces. This means, that no matter what observed sequence $\mathbf{Y}$ is supplied to the hidden-variable model, the model can infer a good representation $\mathbf{Z}$ of $\mathbf{Y}$, where "good" means that its energy $E(\mathbf{Y})$ is very low (e.g. $E(\mathbf{Y}) = 0$). If the model can infer the same $E(\mathbf{Y}) = 0$ no matter what $\mathbf{Y}$, then it is not able to discriminate between sequences, and is not very informative. This could typically be acute in over-complete representations, where the dimension of the latent variables is greater than the dimension of the observed variables (Olshausen and Field, 1997; Ranzato et al., 2007).

In his thesis on that subject (Ranzato, 2009), Marc'Aurelio Ranzato provided two theorems and proofs that flat energy surfaces can be avoided, under some conditions. The first condition is that the dimension M of latent variables is smaller than the dimenion N of observed variables: this is the case for instance for all the models in Chapter 5 and some models in Chapter 4. The second condition, when $M \geq N$, is to have a sparse prior on the latent representation $\mathbf{Z}$, which corresponds to limiting the information content of the representation.

In Chapter 3, we introduce latent variables with $M > N$, while in Chapter 4, we have some models with $M = N$. Let us now prove, in a simple way, that our

dynamical constraint/model still prevents flat energy surfaces.

Without loss of generality, let us assume that the observation model h and the dynamical model f are linear (matrices $\mathbf{H} \in \mathcal{R}^{N \times M}$ and $\mathbf{F} \in \mathcal{R}^{N \times N}$), that we have the HMM-like DFG architecture from Figure 2.1 (top-left), and that the Markov order is $p = 1$, with a time series $\mathbf{Y} \in \mathcal{R}^{N \times T}$ of length T. Then, for each time-point and for each dimension of $\mathbf{Y}$, we have a linear combination of hidden variables $\mathbf{Z}$:

$$\forall t \in \{1, \ldots, T\},\ \forall k \in \{1, \ldots, N\},\ y_k(t) = \sum_{i=1}^{M} h_{k,i} z_i(t) \tag{2.31}$$

This yields $N \times T$ equations of $M \times T$ unknowns (elements of $\mathbf{Z}$), and we have $N \times T \leq M \times T$. However, the dynamical equations bring additional $M \times (T-1)$ equations, keeping the same $M \times T$ unknowns:

$$\forall t \in \{2, \ldots, T\},\ \forall i \in \{1, \ldots, M\},\ z_i(t) = \sum_{j=1}^{M} f_{i,j} z_j(t-1) \tag{2.32}$$

Trivially, provided that $N \times T \leq M$, the system is overdetermined. Hence we might not find, for any $\mathbf{Y}$, a solution $\mathbf{Z}$ that fits $\mathbf{Y}$ perfectly. Moreover, our energies (typically Gaussian) are not flat, but convex. Therefore, for sufficiently long sequences, flat energy surfaces can be avoided.

The specific case of sequence likelihood estimation in Chapter 6 does not fall into the flat energy trap, because the observation factor is a look-up table (which means that the latent representation of a discrete sequence $\mathbf{Y}$ is produced deterministically), and because the dynamical energy on sequences of hidden vectors $\mathbf{Z}$ integrates the partition function, which means that for each input $\mathbf{z}_{t-p}^{t-1}$ to the dynamical function f, there is only one possible output $\mathbf{z}_t$ that achieves minimal energy, and that output might be in contradiction with the embedding of y_t. Hence the energy surface of all possible sequences $\mathbf{Y}$ is certainly not flat: actually, we use that model to discriminate

between more or less "valid" sequences $\mathbf{Y}$.

2.4.2 Bounding the Hidden Representation

Although the learning and inference algorithms for DFGs turn out to be simple and flexible, and the energy surface of $E(\mathbf{Y}; \mathbf{W})$ cannot be flat, the hidden state inference might however still be under-constrained, particularly so when the number M of dimensions in latent variables $\mathbf{Z}$ is higher than the number N of dimensions of the observed variables $\mathbf{Y}$.

On one hand, there is for instance a risk that latent variables take extremely large or extremely low values, which we would like to avoid. On the other hand, we might want the latent variables to have a reproducible "appearance" from one learning procedure to another, or we would like to inject a prior on that appearance.

For this reason, we propose to (in)directly constrain and regularize the hidden variables in several ways.

Constraining the Observation Model

We could set some or all the parameters of the observation model to a fixed value. For instance, when the latent variable represents a hidden phenomenon (e.g. a protein transcription factor) and we want to know the influence of that phenomenon $\mathbf{Z}$ on the observed time series $\mathbf{Y}$, we could set the interaction between $\mathbf{Z}$ and one observed variable $\mathbf{y}_k$ to a certain value, and measure the interactions between $\mathbf{Z}$ and the other observed variables $\mathbf{y}_j$ relatively to $\mathbf{y}_k$ (see Chapter 4).

Alternatively, when there are more hidden variables than observed variables ($M > N$), we could even fix the observation model, and keep degrees of freedom of the system only on the dynamics (see Chapter 3). Models that contain more hidden variables

than observed variables can indeed be useful for modeling nonlinear dynamics.

Finally, even if the observation model retains most degrees of freedom, it can be constrained to have a fixed norm (e.g. a vector norm equal to 1). For instance if the observation model h is a linear matrix operation, we have $\bar{\mathbf{y}}_t = \mathbf{W}_h \mathbf{z}_t$, and because the norm of the observed variables $\mathbf{y}_t$ is fixed, the norm of $\mathbf{z}_t$ is fixed as well. This solution is typically used in sparse coding (Olshausen and Field, 1997).

Regularization of the Hidden Variables

The obvious way to bound the magnitude of latent variables is to add a regularization penalty to the inference gradient descent (E-step). An L_2-norm regularization limits their overall magnitude, while an L_1-norm enforces their sparsity both in time and across dimensions (Tibshirani, 1996).

In the case when the hidden variables are not latent but produced directly from a look-up table, without inference, the regularization shall be applied during parameter learning.

A third type of constraints on the latent variables is the smoothness penalty. This penalty is somewhat contradictory with the dynamical model f, since it forces two consecutive variables $\mathbf{z}_t$ and $\mathbf{z}_{t+1}$ to be similar. We can however view this penalty as an attempt at inferring slowly varying hidden states and at reducing noisy oscillations in the latent variables (which is particularly relevant when observations $\mathbf{Y}$ are sampled at a high frequency)[7]. By consequence, the dynamics of the latent states become smoother and perhaps simpler to learn:

$$R_z\left(\mathbf{z}_t^{t+1}\right) = ||\mathbf{z}_t - \mathbf{z}_{t+1}||_2^2 = \sum_{i=1}^{M} (z_i(t) - z_i(t+1))^2 \tag{2.33}$$

[7]Note that we are not merely modeling Brownian motion dynamics, because this regularization penalty on the hidden variables comes in addition to the other dynamics modeled by function f.

2.4.3 Avoiding Local Minima When Learning the Model

The author wishes he could write an extensive section on the matter of local minima avoidance. Unfortunately, Expectation Maximization (Dempster et al., 1977) and all derived algorithms and approximations (Neal and Hinton, 1998; Baldi and Rosen-Zvi, 2005; Chopra et al., 2007; Ranzato et al., 2007) are prone to local minima, which means here that depending on the initial guess of latent variables' values or distributions, one can end up with suboptimal solutions for the model.

Solution 1: Stochastic Learning

There are luckily a few workarounds to this problem. One of them is the inclusion of randomness into the learning procedure, by performing alternated E-steps and M-steps on short subsequences of the total sequence, and by selecting those subsequences in a random order, according to the stochastic learning principle (Bottou, 2004). This technique is used in Chapters 3 and 6.

Solution 2: Initializing Low-Dimensional Z Optimally w.r.t. Observations

Another workaround, specialized to models with a linear observation factor and where the latent variables have fewer dimensions than the observed variables, is to initialize the latent variables with a standard dimensionality reduction technique, such as Singular Value Decomposition, followed by Independent Component Analysis, consisting in rotating the latent variables' space in order to make them as independent as possible. This way, we start the optimization process with a latent variable configuration that is already very good w.r.t. the linear observation factor, and the learning is dedicated mostly to incorporate the dynamical factor's (and other potential factors') constraints into the latent representation. This technique was utilized in Chapters 4

and 5.

Solution 3: Bootstrapping

Finally, when the time series to be modeled is desperately short (such as mRNA level micro-arrays for gene regulation experiments, in Chapter 4), one can repeat the full learning procedure multiple times, and in a bootstrapping approach, draw statistics from all the models and inferred latent sequences.

The following four chapters all consist in various embodiments of Dynamic Factor Graphs. In particular, Chapters 3, 5 and 6 exhibit the advantage of using a simple, efficient MAP inference of hidden representations, that enables highly-nonlinear factors.

Chapter 3

Application to Time Series Modeling and to Dynamical Systems

> Prediction is very difficult,
> especially about the future
>
> Niels Bohr

This chapter presents the first application of Dynamic Factor Graphs (DFG) to the modeling of linear or chaotic time series by learning a dynamical system on the hidden continuously-valued representation. It has been published in (Mirowski and LeCun, 2009) and presented at the ECML 2009 conference.

In summary, our DFG includes factors modeling joint probabilities between hidden and observed variables, and factors modeling dynamical constraints on hidden variables. The DFG assigns a scalar energy to each configuration of hidden and observed variables. A gradient-based inference procedure finds the minimum-energy state sequence for a given observation sequence. Because the factors are designed to ensure a constant partition function, they can be trained by minimizing the expected energy over training sequences with respect to the factors' parameters. These alternated inference and parameter updates can thus be seen as a deterministic EM-like

procedure.

Using smoothing regularizers, DFGs are shown to reconstruct chaotic attractors and to separate a mixture of independent oscillatory sources perfectly. DFGs outperform the best known algorithm on the CATS competition benchmark for time series prediction. Finally, we illustrate an application of DFGs to the reconstruction of missing motion capture data.

3.1 Introduction

3.1.1 Background

Time series collected from real-world phenomena are often an incomplete picture of a complex underlying dynamical process with a high-dimensional state that cannot be directly observed. For example, human motion capture data gives the positions of a few markers that are the reflection of a large number of joint angles with complex kinematic and dynamical constraints. The aim of this chapter is to deal with situations in which the hidden state is continuous and high-dimensional, and the underlying dynamical process is highly non-linear, but essentially deterministic. It also deals with situations in which the observations have lower dimension than the state, and the relationship between states and observations may be non-linear. The situation occurs in numerous problems in speech and audio processing, financial data, and instrumentation data, for such tasks as prediction and source separation. It applies in particular to univariate chaotic time series which are often the projection of a multidimensional attractor generated by a multivariate system of nonlinear equations.

The simplest approach to modeling time series relies on time-delay embedding: the model learns to predict one sample from a number of past samples with a lim-

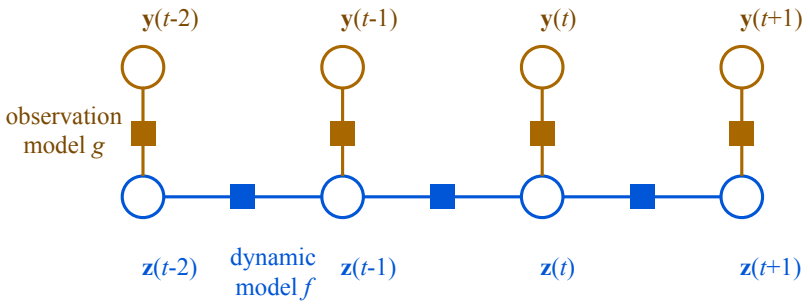

Figure 3.1: A simple Dynamical Factor Graph with a 1^{st} order Markovian property, as used in HMMs and state-space models such as Kalman Filters.

ited temporal span. This method can use linear auto-regressive models, as well as non-linear ones based on kernel methods (e.g. support-vector regression (Mattera and Haykin, 1999; Muller et al., 1999)), neural networks (including convolutional networks such as time delay neural networks (Lang and Hinton, 1988; Wan, 1993)), and other non-linear regression models. By Takens' theorem (Takens, 1981) the original multivariate chaotic attractor can indeed be theoretically reconstructed by using time-delay embedding of the observed sequence, but the forecasting problem (Casdagli, 1989) nevertheless remains difficult. The weakness of the above time-delay embedding approaches is that they have a hard time capturing hidden dynamics with long-term dependency because the state information is only accessible indirectly (if at all) through a (possibly very long) sequence of observations (Bengio et al., 1994).

One approach for time series prediction or modeling is to learn the temporal dependency between consecutive samples of the observed time series. In this chapter, we propose to address this problem by simultaneously inferring the unobserved variables and learning their dynamics. For instance, instead of learning to predict chaotic time series, we infer an underlying latent multivariate attractor, constrained by nonlinear dynamics.

To capture long-term dynamical dependencies, the model must have an internal

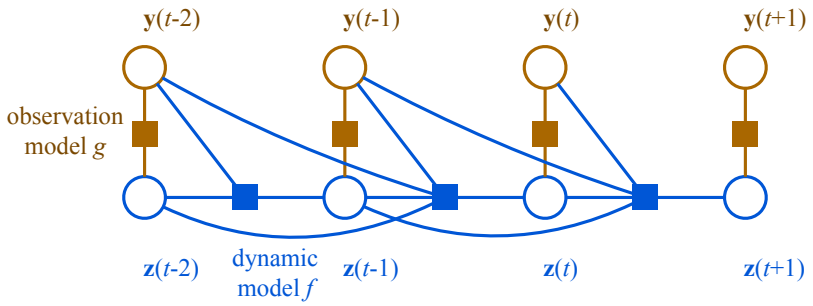

Figure 3.2: A Dynamic Factor Graph where dynamics depend on the past two values of both latent state $\mathbf{Z}$ and observed variables $\mathbf{Y}$.

state with dynamical constraints that predict the state at a given time from the states and observations at previous times (e.g. a state-space model). In general, the dependencies between state and observation variables can be expressed in the form of a *Factor Graph* (Kschischang et al., 2001) for sequential data, in which a graph motif is replicated at every time step. An example of such a representation of a state-space model is shown in Figure 3.1. Groups of variables (circles) are connected to a factor (square) if a dependency exists between them. The factor can be expressed in the negative log domain: each factor computes an energy value that can be interpreted as the negative log likelihood of the configuration of the variables it connects with. The total energy of the system is the sum of the factors' energies, so that the maximum likelihood configuration of variables can be obtained by minimizing the total energy.

Figure 3.1 shows the structure used in Hidden Markov Models (HMM) and Kalman Filters, including Extended Kalman Filters (EKF) which can model non-linear dynamics. HMMs can capture longer range dependencies, but they are limited to discrete sequences. Discretizing the state space of a high-dimensional continuous dynamical process to make it fit into the HMM framework is often impractical. Conversely, EKFs deal with continuous state spaces with non-linear dynamics, but much of the machinery for inference and for training the parameters is linked to the problem of

marginalizing over hidden state distributions and to propagating and estimating the covariances of the state distributions. This has lead several authors to limit the discussion to dynamics and observation functions that are linear, radial-basis functions networks (Wan and Nelson, 1996; Ghahramani and Roweis, 1999) or single-hidden layer perceptrons (Ilin et al., 2004). More recently, Gaussian Processes with dynamics on latent variables have been introduced (Wang et al., 2006b), but they suffer from a quadratic dependence on the number of training samples.

3.1.2 Dynamical Factor Graphs

By contrast with current state-space methods, our primary interest is to model processes whose underlying dynamics are essentially deterministic, but can be highly complex and non-linear. Hence our model will allow the use of complex functions to predict the state and observations, and will sacrifice the probabilistic nature of the inference. Instead, our inference process (including during learning) will produce the most likely (minimum energy) sequence of states given the observations. We call this method *Dynamic Factor Graph* (DFG), a natural extension of Factor Graphs specifically tuned for sequential data.

To model complex dynamics, the proposed model allows the state at a given time to depend on the states and observations over several past time steps. The corresponding DFG is depicted in Figure 3.2. The graph structure is somewhat similar to that of Taylor and Hinton's Conditional Restricted Boltzmann Machine (Taylor et al., 2006). Ideally, training a CRBM would consist in minimizing the negative log-likelihood of the data under the model. But computing the gradient of the log partition function with respect to the parameters is intractable, hence Taylor and Hinton propose to use a form of the contrastive divergence procedure, which relies on

Monte-Carlo sampling. To avoid costly sampling procedures, we design the factors in such a way that the partition function is constant, hence the likelihood of the data under the model can be maximized by simply minimizing the average energy with respect to the parameters for the optimal state sequences. To achieve this, the factors are designed so that the conditional distributions of state $\mathbf{z}(t)$ given previous states and observation, and the conditional distribution of the observation $\mathbf{y}(t)$ given the state $\mathbf{z}(t)$ are both Gaussians with a fixed diagonal covariance matrix. Other types of distributions (e.g. Laplace) with constant partition function are possible, all depending on how the energy (error) is measured (e.g. sum of L_1 norms for Laplace distribution). As long as the noise term is independent of time t, we can use the constant partition function assumption.

In a nutshell, the proposed training method is as follows. Given a training observation sequence, the optimal state sequence is found by minimizing the energy using a gradient-based minimization method. Second, the parameters of the model are updated using a gradient-based procedure so as to decrease the energy. These two steps are repeated over all training sequences. The procedure can be seen as a sort of deterministic generalized EM procedure in which the latent variable distribution is reduced to its mode, and the model parameters are optimized with a stochastic gradient method. The procedure assumes that the factors are differentiable with respect to their input variables and their parameters. This simple procedure will allow us to use sophisticated non-linear models for the dynamical and observation factors, such as stacks of non-linear filter banks (temporal convolutional networks). It is important to note that *the inference procedure operates at the sequence level*, and produces the most likely state sequence that best explains the entire observation. In other words, future observations may influence previous states.

In the DFG shown in Figure 3.1, the dynamical factors compute an energy term

of the form $E_d(t) = \| \mathbf{z}(t) - f(\mathbf{x}(t), \mathbf{z}(t-1)) \|^2$, which can seen as modeling the state $\mathbf{z}(t)$ as $f(\mathbf{x}(t), \mathbf{z}(t-1))$ plus some Gaussian noise variable with a fixed diagonal covariance $\epsilon(t)$ (inputs $\mathbf{x}(t)$ are not used in experiments in this chapter). Similarly, the observation factors compute the energy $E_o(t) = \| \mathbf{y}(t) - g(\mathbf{z}(t)) \|^2$, which can be interpreted as $\mathbf{y}(t) = g(\mathbf{z}(t)) + \omega(t)$, where $\omega(t)$ is a Gaussian random variable with fixed diagonal covariance.

Our chapter is organized in three additional sections. First, we explain the gradient-based approximate algorithm for parameter learning and deterministic latent state inference in the DFG model (3.2). We then evaluate DFGs on toy, benchmark and real-world datasets (3.3). Finally, we compare DFGs to previous methods for deterministic nonlinear dynamical systems and to training algorithms for Recurrent Neural Networks (3.4).

3.2 Methods

The following subsections detail the deterministic nonlinear (neural networks-based) or linear architectures of the proposed Dynamic Factor Graph (3.2.1) and define the EM-like, gradient-based inference (3.2.2) and learning (3.2.4) algorithms, as well as how DFGs are used for time series prediction (3.2.3).

3.2.1 A Dynamic Factor Graph

Similarly to Hidden Markov Models, our proposed Dynamic Factor Graph contains an observation and a dynamical factors/models (see Figure 3.1), with corresponding observed outputs and latent variables.

The *observation model* g links latent variable $\mathbf{z}(t)$ (an m-dimensional vector) to the observed variable $Y(t)$ (an n-dimensional vector) at time t under Gaussian noise

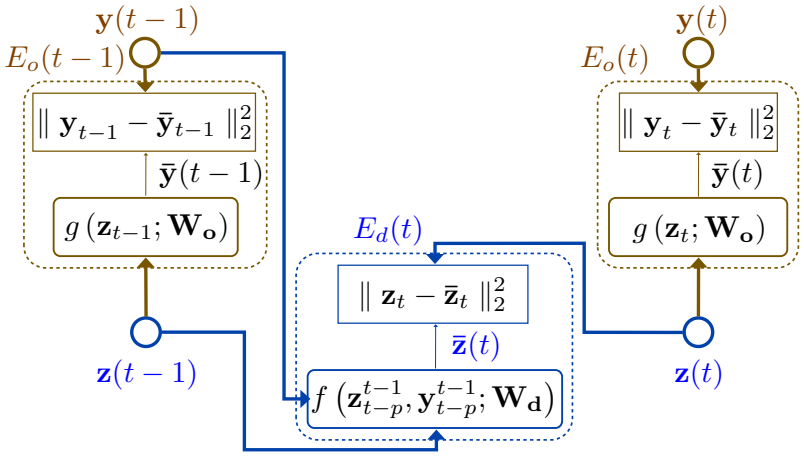

Figure 3.3: Energy-based graph of a DFG with a 1^{st} order Markovian architecture and additional dynamical dependencies on past observations. Observations $\mathbf{y}(t)$ are inferred as $\bar{\mathbf{y}}(t)$ from latent variables $\mathbf{z}(t)$ using the observation model parameterized by $\mathbf{W}_o$. The (non)linear dynamical model parameterized by $\mathbf{W}_d$ produces transitions from a sequence of latent variables $\mathbf{z}_{t-p}^{t-1}$ and observed output variables $\mathbf{y}_{t-p}^{t-1}$ to $\mathbf{z}(t)$ (here $p = 1$). The total energy of the configuration of parameters and latent variables is the sum of the observation $E_o(.)$ and dynamic $E_d(.)$ errors.

model $\omega(t)$ (because the quadratic observation error is minimized). g can be nonlinear, but we considered in this chapter linear observation models, i.e. an $n \times m$ matrix parameterized by a weight vector $\mathbf{W}_o$. This model can be simplified even further by imposing each observed variable $y_i(t)$ of the multivariate time series $\mathbf{Y}$ to be the sum of k latent variables, with $m = k \times n$, and each latent variable contributing to only one observed variable. In the general case, the generative output is defined as:

$$\mathbf{y}(t) = \bar{\mathbf{y}}(t) + \omega(t), \text{ where } \bar{\mathbf{y}}(t) \equiv g(\mathbf{W}_o, \mathbf{z}(t)) \tag{3.1}$$

In its simplest form, the linear or nonlinear *dynamical model* f establishes a causal relationship between a sequence of p latent variables $\mathbf{z}_{t-p}^{t-1}$ and latent variable $\mathbf{z}(t)$, under Gaussian noise model $\epsilon(t)$ (because the quadratic dynamic error is minimized). (3.2) thus defines p^{th} order Markovian dynamics (see Figure 3.1 where $p = 1$). The

dynamical model is parameterized by vector $\mathbf{W_d}$.

$$\mathbf{z}(t) = \bar{\mathbf{z}}(t) + \epsilon(t), \text{ where } \bar{\mathbf{z}}(t) \equiv f\left(\mathbf{W}_d, \mathbf{z}_{t-p}^{t-1}\right) \tag{3.2}$$

Typically, one can use simple multivariate autoregressive linear functions to map the state variables, or can also resort to nonlinear dynamics modeled by a Convolutional Network (LeCun et al., 1998a) with convolutions (FIR filters) across time, as in Time-Delay Neural Networks (Lang and Hinton, 1988; Wan, 1993).

Other dynamical models, different from the Hidden Markov Model, are also possible. For instance, latent variables $\mathbf{z}(t)$ can depend on a sequence of p past latent variables $\mathbf{z}_{t-p}^{t-1}$ and p past observations $\mathbf{y}_{t-p}^{t-1}$, using the same error term $\epsilon(t)$, as explained in (3.3) and illustrated on Figure 3.2.

$$\mathbf{z}(t) = \bar{\mathbf{z}}(t) + \epsilon(t), \text{ where } \bar{\mathbf{z}}(t) \equiv f\left(\mathbf{W}_d, \mathbf{z}_{t-p}^{t-1}, \mathbf{y}_{t-p}^{t-1}\right) \tag{3.3}$$

Figure 3.3 displays the interaction between the observation (3.1) and dynamical (3.3) models, the observed $\mathbf{Y}$ and latent $\mathbf{Z}$ variables, and the quadratic error terms.

As will be explained in the next sections, hidden variables $\mathbf{Z}$ are initialized randomly, and several priors on their distribution (e.g. bounded representation, sparsity or smoothness) are incorporated thanks to regularization.

3.2.2 Inference in Dynamic Factor Graphs

Let us define the following *total* (3.4), *dynamical* (3.5) and *observation* (3.6) energies (quadratic errors) on a given time interval $[t_a, \ldots, t_b]$, where respective weight coefficients α, β are positive constants (in this chapter, $\alpha = \beta = 0.5$):

$$E\left(\mathbf{W}_d, \mathbf{W}_o, \mathbf{Y}_{t_a}^{t_b}\right) = \sum_{t=t_a}^{t_b} \left[\alpha E_d(t) + \beta E_o(t)\right] \tag{3.4}$$

$$E_d(t) \equiv \min_{\mathbf{Z}} E_d\left(\mathbf{W}_d, \mathbf{z}_{t-p}^{t-1}, \mathbf{z}(t)\right) \tag{3.5}$$

$$E_o(t) \equiv \min_{\mathbf{Z}} E_o\left(\mathbf{W}_o, \mathbf{z}(t), Y(t)\right) \tag{3.6}$$

Inferring the sequence of latent variables $\{\mathbf{z}(t)\}_t$ in (3.4) and (3.5) is equivalent to simultaneous minimization of the sum of dynamical and observation energies at all times t:

$$E_d\left(\mathbf{W}_d, \mathbf{z}_{t-p}^{t-1}, \mathbf{z}(t)\right) = \| \bar{\mathbf{z}}(t) - \bar{\mathbf{z}}(t) \|_2^2 \tag{3.7}$$

$$E_o\left(\mathbf{W}_o, \mathbf{z}(t), \mathbf{y}(t)\right) = \| \bar{\mathbf{y}}(t) - \mathbf{y}(t) \|_2^2 \tag{3.8}$$

Observation and dynamical errors are expressed separately, either as Normalized Mean Square Errors (NMSE) or Signal-to-Noise Ratio (SNR).

3.2.3 Prediction in Dynamic Factor Graphs

Assuming fixed parameters $\mathbf{W}$ of the DFG, two modalities are possible for the prediction of unknown observed variables $\mathbf{Y}$.

- *Closed-loop (iterated) prediction*: when the continuation of the time series is unknown, the only relevant information comes from the past. One uses the dynamical model to predict $\bar{\mathbf{z}}(t)$ from $\mathbf{y}_{t-p}^{t-1}$ and inferred $\mathbf{z}_{t-p}^{t-1}$, set $\mathbf{z}(t) = \bar{\mathbf{z}}(t)$, use the observation model to compute prediction $\bar{\mathbf{y}}(t)$ from $\mathbf{z}(t)$, and iterate as long as necessary. If the dynamics depend on past observations, one also needs

to rely on predictions $\bar{\mathbf{y}}(t)$ in (3.3).

- *Prediction as inference*: this is the case when only some elements of $\mathbf{Y}$ are unknown (e.g. estimation of missing motion-capture data). First, one infers latent variables through gradient descent, and simply does not backpropagate errors from unknown observations. Then, missing values $\bar{y}_i(t)$ are predicted from corresponding latent variables $\mathbf{z}(t)$. In this way, we can incorporate a dependency on future values of the observed time series.

3.2.4 Training of Dynamic Factor Graphs

Learning in an DFG consists in adjusting the parameters $\mathbf{W} = \left[\mathbf{W}_d^T, \mathbf{W}_o^T\right]$ in order to minimize the loss $\mathcal{L}(\mathbf{W}, \mathbf{Y}, \tilde{\mathbf{Z}})$:

$$\mathcal{L}(\mathbf{W}, \mathbf{Y}, \mathbf{Z}) = E(\mathbf{W}, \mathbf{Y}) + R_z(\mathbf{Z}) + R(\mathbf{W}) \tag{3.9}$$

$$\tilde{\mathbf{Z}} = \arg\min_{\mathbf{Z}} \mathcal{L}(\tilde{\mathbf{W}}, \mathbf{Y}, \mathbf{Z}) \tag{3.10}$$

$$\tilde{\mathbf{W}} = \arg\min_{\mathbf{W}} \mathcal{L}(\mathbf{W}, \mathbf{Y}, \tilde{\mathbf{Z}}) \tag{3.11}$$

where $R(\mathbf{W})$ is a regularization term on the weights $\mathbf{W}_d$ and $\mathbf{W}_o$, and $R_z(\mathbf{Z})$ represents additional constraints on the latent variables further detailed. Minimization of this loss is done iteratively in an Expectation-Maximization-like fashion in which the states $\mathbf{Z}$ play the role of auxiliary variables, as explained in Chapter 2. During inference, values of the model parameters are clamped and the hidden variables are relaxed to minimize the energy. The inference described in part (3.2.2) and equation (3.10) can be considered as the *E-step* (state update) of a gradient-based version of the EM algorithm. During learning, model parameters $\mathbf{W}$ are optimized to give lower

energy to the current configuration of hidden and observed variables. The parameter-adjusting *M-step* (weight update) described by (3.11) is also gradient-based.

In its current implementation, the E-step inference is done by gradient descent on $\mathbf{Z}$, with learning rate η_z typically equal to 0.5. The convergence criterion is when energy (3.4) stops decreasing. The M-step parameter learning is implemented as a stochastic gradient descent (diagonal Levenberg-Marquard) (LeCun et al., 1998b) with individual learning rates per weight (re-evaluated every 10000 weight updates) and global learning rate η_w typically equal to 0.01. These parameters were found by trial and error (cross-validation) on a grid of possible values.

The state inference is not done on the full sequence at once, but on *mini-batches* (typically 20 to 100 samples), and the weights get updated once after each mini-batch inference, similarly to the Generalized EM algorithm. During one epoch of training, the batches are selected randomly and overlap in such a way that each state variable $Z(t)$ is re-inferred at least a dozen times in different mini-batches. This learning approximation echoes the one in regular stochastic gradient with no latent variables and enables to speed up the learning of the weight parameters.

The learning algorithm turns out to be particularly simple and flexible. The hidden state inference is however under-constrained, because of the higher dimensionality of the latent states and despite the dynamical model. For this reason, this chapter proposes to (in)directly regularize the hidden states in several ways. First, one can add to the loss function an L_1 regularization term $R(\mathbf{W})$ on the weight parameters. This way, the dynamical model becomes "sparse" in terms of its inputs, e.g. the latent states. Regarding the term $R_z(\mathbf{Z})$, an L_2 norm on the hidden states $\mathbf{z}(t)$ limits their overall magnitude, and an L_1 norm enforces their sparsity both in time and across dimensions. Regularization coefficients λ_w and λ_z typically range from 0 to 0.1.

Algorithm 1 Pseudo-Code of the EM-Like Learning and Inference in DFGs

while *epoch* $\leq n_{epochs}$ **do**
  for randomly selected $I \subset [1, T]$ **do**
    repeat
      for $t \in I$ **do**
        Forward-propagate $\mathbf{z}_{t-p}^{t-1}$ through f to get $\bar{\mathbf{z}}_t$
        Forward-propagate $\mathbf{z}_t$ through g to get $\bar{\mathbf{y}}_t$
        Back-propagate errors from $\| \mathbf{z}_t - \bar{\mathbf{z}}_t \|_2^2$, add to $\Delta \mathbf{z}_t$
        Back-propagate errors from $\| \mathbf{y}_t - \bar{\mathbf{y}}_t \|_2^2$, add to $\Delta \mathbf{z}_t$
      end for
      Update latent states $\mathbf{z}_{t \in I}$ using gradients $\Delta \mathbf{z}_{t \in I}$
    until convergence, when energy $E(I)$ stops decreasing
    for $t \in I$ **do**
      Back-propagate errors from $\| \mathbf{z}_t - \bar{\mathbf{z}}_t \|_2^2$, add to $\Delta \mathbf{W}$
      Back-propagate errors from $\| \mathbf{y}_t - \bar{\mathbf{y}}_t \|_2^2$, add to $\Delta \mathbf{W}$
    end for
    Update parameters $\mathbf{W}$ using gradients $\Delta \mathbf{W}$
  end for
end while

3.2.5 Smoothness Penalty on Latent Variables

The second type of constraints on the latent variables is the *smoothness penalty*. In an apparent contradiction with the dynamical model (3.2), this penalty forces two consecutive variables $z_i(t)$ and $z_i(t+1)$ to be similar. One can view it as an attempt at inferring slowly varying hidden states and at reducing noise in the states (which is particularly relevant when observation $\mathbf{Y}$ is sampled at a high frequency). By consequence, the dynamics of the latent states are smoother and simpler to learn. Constraint (3.12) is easy to derivate w.r.t. a state $z_i(t)$ and to integrate into the gradient descent optimization (3.10):

$$R_z\left(\mathbf{z}_t^{t+1}\right) = \sum_i (z_i(t) - z_i(t+1))^2 \tag{3.12}$$

In addition to the smoothness penalty, we have investigated the decorrelation of

multivariate latent variables $\mathbf{z}(t) = (z_1(t), z_2(t), \ldots, z_m(t))$. The justification was to impose to each component $\mathbf{z}_i$ to be independent, so that it followed its own dynamics, but we have not obtained satisfactory results yet. As reported in the next section, the interaction of the dynamical model, weight sparsification and smoothness penalty already enables the separation of latent variables.

3.3 Experimental Evaluation

First, working on toy problems, we investigate the latent variables that are inferred from an observed time series. We show that using smoothing regularizers, DFGs are able to perfectly separate a mixture of independent oscillatory sources (3.3.1), as well as to reconstruct the Lorenz chaotic attractor in the inferred state space (3.3.2). Secondly, we apply DFGs to two time series prediction and modeling problems. Subsection (3.3.3) details how DFGs outperform the best known algorithm on the CATS competition benchmark for time series prediction. In (3.3.4) we reconstruct realistic missing human motion capture marker data in a walk sequence.

3.3.1 Asynchronous Superimposed Sine Waves

The goal is to model a time series constituted by a sum of 5 asynchronous sinusoids: $y(t) = \sum_{j=1}^{5} \sin(\lambda_j t)$ (see Fig. 3.4a). Each component $x_j(t)$ can be considered as a "source", and $y(t)$ is a mixture. This problem has previously been tackled by employing Long-Short Term Memory (LSTM) (Hochreiter and Schmidhuber, 1995), a special architecture of Recurrent Neural Networks that needs to be trained by genetic optimization (Wierstra et al., 2005).

After EM training and inference of hidden variables $\mathbf{z}(t)$ of dimension $m = 5$, frequency analysis of the inferred states on the training (Fig. 3.4b) and testing (Fig.

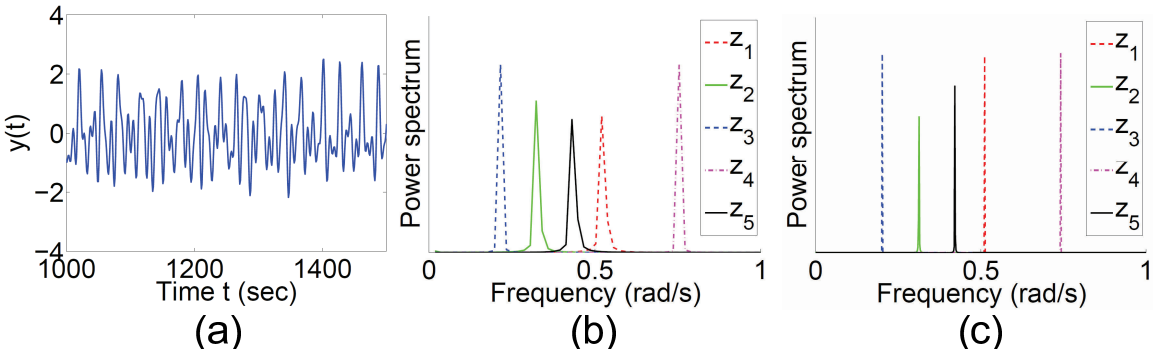

Figure 3.4: (a) Superposition of five asynchronous sinusoids: $y(t) = \sum_{j=1}^{5} \sin(\lambda_j t)$ where $\lambda_1 = 0.2$, $\lambda_2 = 0.311$, $\lambda_3 = 0.42$, $\lambda_4 = 0.51$ and $\lambda_5 = 0.74$. Spectrum analysis shows that after learning and inference, each reconstructed state z_i isolates only one of the original sources x_j, both on the training (b) and testing (c) datasets.

3.4c) datasets showed that each latent state $z_i(t)$ reconstructed one individual sinusoid. In other words, the 5 original sources from the observation mixture $y(t)$ were inferred on the 5 latent states. The observation SNR of 64dB, and the dynamical SNR of 54dB, on both the training and testing datasets, proved both that the dynamics of the original time series $y(t)$ were almost perfectly reconstructed. DFGs outperformed LSTMs on that task since the multi-step iterated (closed-loop) prediction of DFG did not decrease in SNR even after thousands of iterations, contrary to (Wierstra et al., 2005) where a reduction in SNR was already observed after around 700 iterations.

As architecture for the dynamical model, 5 independent Finite Impulse Response (FIR) filters of order 25 were chosen to model the state transitions: each of them acts as a band-pass filter and models an oscillator at a given frequency. One can hypothesize that the smoothness penalty (3.12), weighted by a small coefficient of 0.01 in the state regularization term $R_z(\mathbf{Z})$ helped shape the hidden states into perfect sinusoids. Note that the states or sources were made independent by employing five independent dynamical models for each state. This specific usage of DFG can be likened to Blind Source Separation from an unique source, and the use of independent filters for the

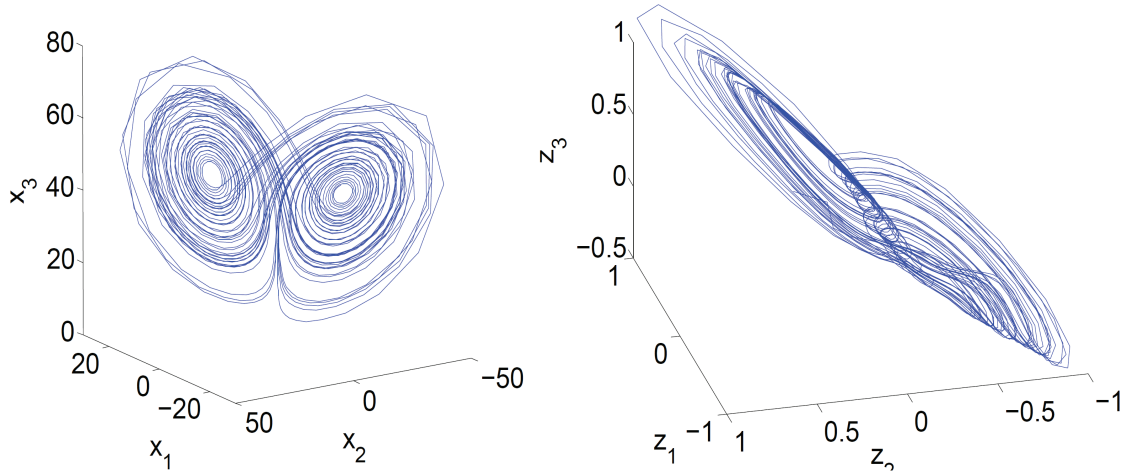

Figure 3.5: Lorenz chaotic attractor (left) and the reconstructed chaotic attractor from the latent variables $\mathbf{z}(t) = \{z_1(t), z_2(t), z_3(t)\}$ after inference on the testing dataset (right).

latent states (or sources) echoes the approach of BSS using linear predictability and adaptive band-pass filters.

Obviously, the above problem could have been solved trivially using spectral analysis, and the point of this small exercise was simply to illustrate the inference of a simple hidden representation underlying a more complex time series. The following examples actually make use of nonlinear dynamics that cannot be recovered by spectral analysis.

3.3.2 Lorenz Chaotic Data

As a second application, we considered the 3-variable (x_1, x_2, x_3) Lorenz dynamical system (Lorenz, 1963) generated by parameters $\rho = 16, b = 4, r = 45.92$ as in (Mattera and Haykin, 1999) (see Fig. 3.5a). Observations consisted in one-dimensional time series $y(t) = \sum_{j=1}^{3} x_j(t)$.

The DFG was trained on 50s (2000 samples) and evaluated on the following 40s

Table 3.1: Comparison of 1-step prediction error using Support Vector Regression, with the errors of the dynamical and observation models of DFGs, measured on the Lorenz test dataset and expressed as signal-to-noise ratios.

Architecture	SVR	DFG
Dynamic SNR	41.6 *dB*	46.2 *dB*
Observation SNR	-	31.6 *dB*

(1600 samples) of $\mathbf{Y}$. Latent variables $Z(t) = (z_1(t), z_2(t), z_3(t))$ had dimension $m = 3$, as it was greater than the attractor correlation dimension of 2.06 and equal to the number of explicit variables (sources). The dynamical model was implemented as a 3-layered convolutional network. The first layer contained 12 convolutional filters covering 3 time steps and one latent component, replicated on all latent components and every 2 time samples. The second layer contained 12 filters covering 3 time steps and all previous hidden units, and the last layer was fully connected to the previous 12 hidden units and 3 time steps. The dynamical model was autoregressive on $p = 11$ past values of $\mathbf{Z}$, with a total of 571 unique parameters. "Smooth" consecutive states were enforced (3.12), thanks to the state regularization term $R_z(\mathbf{Z})$ weighted by a small coefficient of 0.01. After training the parameters of DFG, latent variables $\mathbf{Z}$ were inferred on the full length of the training and testing dataset, and plotted in 3D values of triplets $(z_1(t), z_2(t), z_3(t))$ (see Fig. 3.5b).

The 1-step dynamical SNR obtained with a training set of 2000 samples was higher than the 1-step prediction SNR reported for Support Vector Regression (SVR) (Mattera and Haykin, 1999) (see Table 3.1). According to the Takens theorem (Takens, 1981), it is possible to reconstruct an unknown (hidden) chaotic attractor from an adequately long window of observed variables, using time-delay embedding on $y(t)$, but we managed to reconstruct this attractor on the latent states $(z_1(t), z_2(t), z_3(t))$ inferred both from the training or testing datasets (Fig. 3.5). Although one of the

Table 3.2: Prediction results on the CATS competition dataset comparing the best algorithm (Kalman Smoothers (Sarkka et al., 2004)) and Dynamic Factor Graphs. E_1 and E_2 are unnormalized MSE, measured respectively on all five missing segments or on the first four missing segments.

Architecture	Kalman smoother	DFG
E1 (5 segments)	4.08	3.90
E2 (4 segments)	3.46	2.88

"wings" of the reconstructed butterfly-shaped attractor is slightly twisted, one can clearly distinguish two basins of attraction and a chaotic orbit switching between one and the other. The reconstructed latent attractor has correlation dimensions 1.89 (training dataset) and 1.88 (test dataset).

3.3.3 CATS Time Series Competition

Dynamic Factor Graphs were evaluated on time series prediction problems using the CATS benchmark dataset (Lendasse et al., 2004). The goal of the competition was the prediction of 100 missing values divided into five groups of 20, the last group being at the end of the provided time series. The dataset presented a noisy and chaotic behaviour commonly observed in financial time series such as stock market prices.

In order to predict the missing values, the DFG was trained for 10 epochs on the known data (5 chunks of 980 points each). 5-dimensional latent states on the full 5000 point test time series were then inferred in one E-step, as described in section 3.2.3. The dynamical factor was the same as in section 3.3.2. As shown in Table 3.2, the DFG outperformed the best results obtained at the time of the competition, using a Kalman Smoother (Sarkka et al., 2004), and managed to approximate the behavior of the time series in the missing segments.

Table 3.3: Reconstruction error (NMSE) for 4 sets of missing joint angles from motion capture data (two blocks of 65 consecutive frames, about 2s, on either the left leg or entire upper body). DFGs are compared to standard nearest neighbors matching. Because of different normalizations, we cannot directly compare our performance to the one achieved by CRBMs in (Taylor et al., 2006), but in both cases, we observe a comparable reduction in error of the order of 20%.

Method	Nearest Neighb.	DFG
Missing leg 1	0.77	0.59
Missing leg 2	0.47	0.39
Missing upper body 1	1.24	0.9
Missing upper body 2	0.8	0.48

3.3.4 Estimation of Missing Motion Capture Data

Finally, DFGs were applied to the problem of estimating missing motion capture data. Such situations can arise when "the motion capture process [is] adversely affected by lighting and environmental effects, as well as noise during recording" (Taylor et al., 2006). The estimation of missing markers is a difficult problem that was traditionally handled using simple algorithmic solutions, such as nearest neighbors, piece-wise linear modeling (Liu and McMillan, 2006), or Kalman Filtering (Aristidou et al., 2008). Motion capture data[1] $\mathbf{Y}$ consisted of three 49-dimensional time series representing joint angles derived from 17 markers and coccyx, acquired on a subject walking and turning, and downsampled to 30Hz. Two sequences of 438 and 3128 samples were used for training, and one sequence of 260 samples for testing.

We reproduced the experiments from (Taylor et al., 2006), where Conditional Restricted Boltzman Machines (CRBM) were utilized. On the test sequence, two different sets of joint angles were erased, either the left leg (1) or the entire upper

[1]We used motion capture data from the MIT database as well as sample Matlab code for motion playback and conversion, developed or adapted by Taylor, Hinton and Roweis, available at: `http://www.cs.toronto.edu/~gwtaylor/`.

body (2). After training the DFG on the training sequences, missing joint angles $y_i(t)$ were inferred through the E-step inference. The DFG was the same as in sections 3.3.2 and 3.3.3, but with 147 hidden variables (3 per observed variable) and no smoothing. Table 3.3 shows that DFGs significantly outperformed nearest neighbor interpolation (detailed in (Taylor et al., 2006)), by taking advantage of the motion dynamics modeled through dynamics on latent variables. Contrary to nearest neighbors matching, DFGs managed to infer smooth and realistic leg or upper body motion. Videos comparing the original walking motion sequence, and the DFG- and nearest neighbor-based reconstructions are available at
`http://cs.nyu.edu/~mirowski/pub/mocap/`. Figure 3.6 illustrates the DFG-based reconstruction (we did not include nearest neighbor interpolation resuts because the reconstructed motion was significantly more "hashed" and discontinuous).

3.4 Discussion

In this section, we establish a comparison with other nonlinear dynamical systems with latent variables (3.4.1) and suggest that DFGs could be seen as an alternative method for training Recurrent Neural Networks (3.4.2).

3.4.1 Comparison with Nonlinear Dynamical Systems

An earlier model of nonlinear dynamical system with hidden states is the Hidden Control Neural Network (Levin, 1993), where latent variables $\mathbf{z}(t)$ are added as an additional input to the dynamical model on the observations. Although the dynamical model is stationary, the latent variable $\mathbf{z}(t)$ modulates its dynamics, enabling a behavior more complex than in pure autoregressive systems. The training algorithm iteratively optimizes the weights $\mathbf{W}$ of the Time-Delay Neural Network (TDNN) and

latent variables $\mathbf{Z}$, inferred as

$\tilde{\mathbf{Z}} \equiv argmin_{\mathbf{Z}} \sum_t \parallel \mathbf{y}(t) - f_{\tilde{\mathbf{W}}}(\mathbf{y}(t-1), \mathbf{z}(t)) \parallel^2$.

The latter algorithm is likened to approximate maximum likelihood estimation, and iteratively finds a sequence of dynamic-modulating latent variables and learns dynamics on observed variables. DFGs are more general, as they allow the latent variables $\mathbf{z}(t)$ not only to modulate the dynamics of observed variables, but also to generate the observations $\mathbf{y}(t)$, as in DBNs. Moreover, (Levin, 1993) does not introduce dynamics between the latent variables themselves, whereas DFGs model complex nonlinear dynamics where hidden states $\mathbf{z}(t)$ depend on past states $\mathbf{y}_{t-p}^{t-1}$ and observations $\mathbf{z}_{t-p}^{t-1}$. Because our method benefits from highly complex non-linear dynamical factors, implemented as multi-stage temporal convolutional networks, it differs from other latent states and parameters estimation techniques, which generally rely on radial-basis functions (Wan and Nelson, 1996; Ghahramani and Roweis, 1999).

The DFG introduced in this chapter also differs from another, more recent, model of DBN with deterministic nonlinear dynamics and explicit inference of latent variables. In (Barber, 2003), the hidden state inference is done by message passing in the forward direction only, whereas our method suggests hidden state inference as an iterative relaxation, i.e. a forward-backward message passing until "equilibrium".

In a limit case, DFGs could be restricted to a deterministic latent variable generation process like in (Barber, 2003). One can indeed interpret the dynamical factor as hard constraints, rather than as an energy function. This can be done by setting the dynamical weight α to be much larger than the observation weight β in (3.4).

3.4.2 A New Algorithm for Recurrent Neural Networks

An alternative way to model long-term dependencies is to use recurrent neural networks (RNN). The main difference with the proposed DFG model is that RNN use fully deterministic noiseless mappings for the state dynamics and the observations. Hence, there is no other inference procedure than running the network forward in time. Unlike with DFG, the state at time t is fully determined by the previous observations and states, and does not depend on future observations.

Exact gradient descent learning algorithms for Recurrent Neural Networks (RNN), such as Backpropagation Through Time (BPTT) or Real-Time Recurrent Learning (RTRL) (Williams and Zipser, 1995), have limitations. The well-known problem of vanishing gradients is responsible for RNN to forget, during training, outputs or activations that are more than a dozen time steps back in time (Bengio et al., 1994). This is not an issue for DFG because the inference algorithm effectively computes "virtual targets" for the function f at every time step.

The faster of the two algorithms, BPTT, requires $O(T|\mathbf{W}|)$ weight updates per training epoch, where $|\mathbf{W}|$ is the number of parameters and T the length of the training sequence. The proposed EM-like procedure, which is dominated by the E-step, requires $O(aT|\mathbf{W}|)$ operations per training epoch, where a is the average number of E-step gradient descent steps before convergence (a few to a few dozens if the state learning rate is set properly).

Moreover, because the E-step optimization of hidden variables is done on mini-batches, longer sequences T simply provide with more training examples and thus facilitate learning; the increase in computational complexity is linear with T.

3.4.3 Ideas of Further Experiments

A number of further experiments could have been conducted in this doctoral work. For instance, one could try to model a time series $\mathbf{Y}$ where only a subset of the dimensions (a subset of the measurements) is relevant, the rest being noise (or highly corrupted by nonlinear noise); it would then be interesting to know whether a properly regularized (with L_1 sparsity constraints) DFG algorithm could learn to ignore the noisy entries of $\mathbf{Y}$.

One could also try to use the DFG model to classify sequences based on their energy (as a proxy for likelihood); a further extension could even consist in learning DFGs discriminatively.

A third problem to explore would be the combination of both nonlinear dynamics and changes of dynamics: I suspect that a hierarchical model, with small range dynamical dependencies (for modeling nonlinear dynamics) and long-range dynamical dependencies (for modeling "switching" dynamics) would be more appropriate. A glimpse of the solution is provided in Chapter 6, where a Latent Dirichlet Allocation-based topic model encodes long-range changes of dynamics (but it is appropriate for discrete observations $\mathbf{Y}$).

3.5 Conclusions

This chapter introduces a new method for learning deterministic nonlinear dynamical systems with highly complex dynamics. Our approximate training method is gradient-based and can be likened to Generalized Expectation-Maximization.

We have shown that with proper smoothness constraints on the inferred latent variables, Dynamical Factor Graphs manage to perfectly reconstruct multiple oscil-

latory sources or a multivariate chaotic attractor from an observed one-dimensional time series. DFGs also outperform Kalman Smoothers and other neural network techniques on a chaotic time series prediction tasks, the CATS competition benchmark. Finally, DFGs can be used for the estimation of missing motion capture data. Proper regularization such as smoothness or a sparsity penalty on the parameters enable to avoid trivial solutions for high-dimensional latent variables.

This initial work on DFG was subsequently applied to the inference of genetic regulatory networks from mRNA expression levels, which is the object of next chapter.

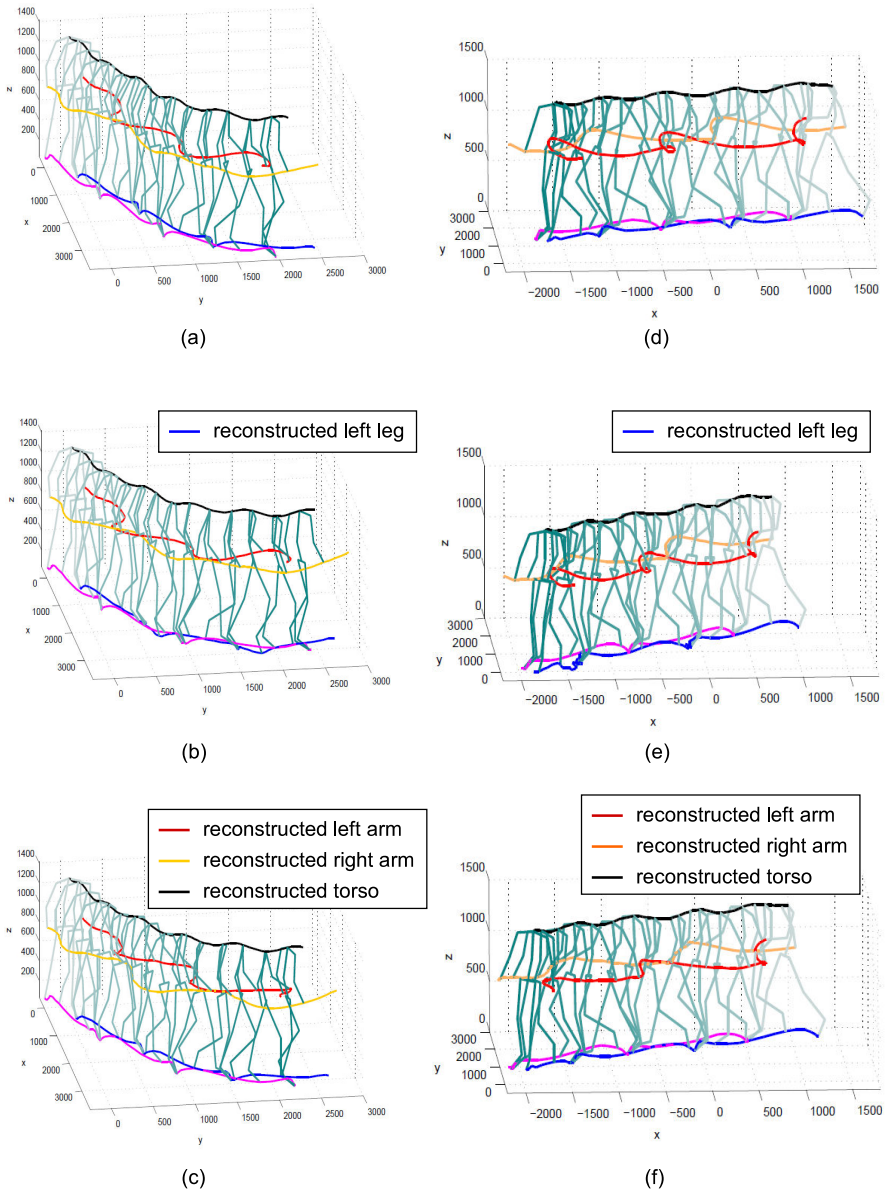

Figure 3.6: Application of a DFG for the reconstruction of missing joint angles from motion capture marker data (1 test sequence of 260 frames at 30Hz). 4 sets of joint angles were alternatively "missing" (erased from the test data): 2 sequences of 65 frames, of either left leg or the entire upper body. (a) Subsequence of 65 frames at the beginning of the test data. (b) Reconstruction result after erasing the left leg markers from (a). (c) Reconstruction results after erasing the entire upper body markers from (a). (d) Subsequence of 65 frames towards the end of the test data. (e) Reconstruction result after erasing the left leg markers from (d). (f) Reconstruction results after erasing the entire upper body markers from (d).

Chapter 4

Application to the Inference of Gene Regulation Networks

> Time flies like an arrow;
> fruit flies like a banana.
>
> Groucho Marx

We present in the chapter how Dynamic Factor Graphs can be used in molecular biology, as a new and flexible algorithm for learning state-space models representing gene regulation networks. In one embodiment, our factor graph model contains observation (transcriptional) and dynamic factors, connected to two types of variables: observed mRNA expression levels, and hidden transcription factor sequences (e.g. protein concentrations). In a second embodiment, the latent variables simply correspond to a de-noised version of the observed mRNA expression levels, and we try to model dynamics on idealized hidden variables instead of noisy mRNA.

Our formalisms covers most state-space models in the biological literature, while giving them a common learning and inference procedure that is simpler and faster than MCMC, Variational Bayes approaches for Dynamic Bayesian Networks and Gaussian Processes. Learning our factor graphs is still done by maximizing their joint likeli-

hood, but we use an approximate gradient-based MAP inference to obtain the most likely configuration of the hidden sequence.

Our biological state-space model has been applied to two different studies, one about reverse-engineering a gene regulation network by understanding gene-gene interactions, and another about inferring levels of protein transcription factors, which are typically difficult to measure, using only mRNA data.

The first set of experiments, submitted for publication to Genome Biology (Krouk et al., Provisionally accepted for publication), focuses on NO_{3-}, a nitrogen source and a signaling molecule that controls many aspects of plant development. We try to learn a gene network involved in plant adaptation to fluctuating nitrate environments, and specifically to build core regulatory networks involved in *Arabidopsis* root adaptation to NO_{3-} provision. Our experimental approach is to monitor genome response to NO_{3-} at 7 time points, using micro-array chips. A state-space model inferred from the micro-array data successfully predicted gene behavior in unlearnt conditions, and suggested to investigate a specific gene, that was then shown to be involved in the NO_{3-} response.

In a second set of experiments, we demonstrate our algorithm on several datasets: the p53 protein dataset (related to human cancer), the Mef2 protein from the *Drosophila* and the TGF-β protein (human cancer). We show that our algorithm is able the infer the time course of a single or multiple transcription factor proteins.

4.1 Machine Learning Approaches to Modeling GRNs

4.1.1 Gene Regulatory Networks

An excellent biological definition for our problem is provided by (Segal et al., 2003). "*The complex functions of a living cell are carried out through the concerted activity of many genes* [...]. *This activity is often coordinated by the organization of the genome into regulatory modules, or sets of co-regulated genes* [...]". Genes encode proteins, and the proteins themselves serve as transcription factors to other genes. One of the goals of modern molecular biology is to identify the interactions between genes (via proteins) in order to understand, now that the genome has been sequenced, the actual functioning of the living organisms.

In that context, one can grossly simplify the highly complex biology by a Genetic Regulatory Network (GRN), which can be formalized by a graph connecting gene, mRNA or protein nodes, and where the links among nodes stand for regulatory interactions (Alvarez-Buylla et al., 2007).

4.1.2 mRNA Micro-arrays

The tool of choice are so-called gene chips, or *DNA micro-arrays*. Micro-arrays correspond to small, organism-specific, collections of tiny probes that can bind mRNA[1]. Each probe corresponds to a specific gene. After the hybridization process, the micro-arrays are scanned to measure the concentration of bound mRNA at each probe (Krouk, personal communication). By conducting specific experiments (e.g. response to stress conditions, cell development and differentiation), one can initiate a regulatory circuit (Spellman et al., 1998). Then, by destructively sampling microarray

[1]Standard micro-arrays are the *Affymetrix* chips.

data every few minutes of the experiment, one can obtain a short, high-dimensional time series of expression levels for thousands of genes. Using the assumption that the temporal behavior of the multivariate time series represents causal dependencies between the time series, we can search for protein-encoding transcripts in the genome.

The mRNA time series are typically extremely short (a few measures, sampled every few minutes to hours). This short duration is a major limitation, given the number of genes. Moreover, each micro-array experiment is destructive, and therefore the cells which are sampled at consecutive time points are not the same (Krouk, personal communication). Each sampling experiment is however repeated a few times, and one gene expression level has several replicates differing slightly in their value. Often, the reported gene expression level is the average of these replicates, but one can consider the replicates separately. Using replicates, one can artificially multiply the number of microarray time series to obtain more sequences, hence more time points (Shasha, personal communication).

4.1.3 Reverse-engineering of Gene Regulation Networks

Time series of gene expression levels can provide us with a detailed picture of the behavior of a Genetic Regulation Network (GRN) over time, and help understand the biological functions of an organism.

Unfortunately, the micro-array measurements of mRNA expression levels contain highly noisy, scarce, and incomplete information. Typically, the concentration levels of proteins, which serve as transcription factors to genes, are absent because they are difficult to measure. Moreover, their specific influence on genes is unknown and requires reverse engineering (Jaeger and Monk, 2010). In their review article, Jaeger and Monk pointed out that this reverse-engineering task in the presence of few time-

point measurements, many genes, measurement errors and random fluctuations in the environment is inherently difficult (Jaeger and Monk, 2010), the main limitation coming from the paucity of data relative to the number of possible connections between the genes (and the proteins).

An additional challenge of systems biology is to be able to model systems precisely enough that the model can predict untested conditions, which is equivalent to constructing a robust dynamical system.

Dynamical Predictive Modeling of Regulatory Gene Networks

Among the several approaches to this modeling problem, dynamical models have gained prominence as they simultaneously encode the topology of the gene interaction graph, and its functional evolution model. Such a model can in turn also be used for predictive modeling of gene expression at further time steps or upon perturbation.

These dynamical models essentially consist of a mathematical function that governs the transitions of the state of a GRN over time. Interactions between genes and transcription factors (e.g. proteins) can be simplified as a dynamical model involving their concentration levels. Typically, dynamical models of mRNA levels consist of ordinary differential equations (ODEs) (Jaeger and Monk, 2010). For a given gene i, ODEs can, for instance, define the rate of change of mRNA level $y_i(t)$ as a function of the weighted influences of M transcription factors $z_j(t)$, with an optional mRNA's degradation term (coefficient d_i) and a basal rate term (coefficient b), as in Equation (4.1). The coefficient of the degradation term can be replaced with a kinetic constant τ_i on the derivative on $y_i(t)$, as in Equation (4.2).

$$\frac{\partial y_i(t)}{\partial t} = g_i\left(\mathbf{z}(t)\right) - d_i y_i(t) + b_i \quad (4.1)$$

$$\tau\frac{\partial y_i(t)}{\partial t} = g_i\left(\mathbf{z}(t)\right) - y_i(t) + b_i \quad (4.2)$$

In the equations above, the transcription factors $\mathbf{z}_t$ can be the unknown protein levels, or in a very simplistic setting, other mRNA levels (in which case $\mathbf{z}_t = \mathbf{y}_t$). In one set of experiments (on p53, Mef2 and TGF-β proteins), we used $\mathbf{z}_t$ to model unknown protein levels, while in another set of experiments on the *Arabidopsis*, we directly used the observed mRNA levels. In the case of protein transcription factors, the relationship between a protein $z_i(t)$ and its encoding gene $y_i(t)$ is generally modeled as a first-order ODE involving $z_i(t)$ and $y_i(t)$: hence, assuming $\mathbf{z}_t = \mathbf{y}_t$ is not terribly wrong.

In our studies, we considered dynamics with the mRNA degradation term (the so-called *kinetic* model (Bonneau et al., 2006, 2007)) and without it (the so-called *Brownian motion* (Wang et al., 2006b) model). Assuming degradation (kinetic ODE) worked better in our experiments with the *Arabidopsis*.

Since micro-array data are discretely sampled over time, Equation (4.1) or (4.2) is linearized; hence it explains how gene expressions at time t influence gene expressions at time $t + 1$.

The data paucity limitation defined two major groups of methods for computational inference of gene regulation networks: a) either a nonlinear or state-space based modeling of the complex interactions between a restricted number of genes with hidden protein transcription factors, or b) simpler, but linear, models of TF-gene interactions (Bonneau et al., 2006, 2007; Wang et al., 2006b; Shimamura et al., 2009), relying on larger (hundreds to thousands) number of mRNA micro-array measure-

ments[2].

Hidden Variable Approaches: State-Space Models

State-space models (SSM) are a general category of machine learning algorithms that model the dynamics of a sequence of data by encoding the joint likelihood of observed $\mathbf{Y}$ and hidden $\mathbf{Z}$ variables. State-space models assume an observed sequence $\mathbf{y}(t)$ (in our case, gene expression data) to be generated from an underlying unknown sequence $\mathbf{z}(t)$ also called "hidden states". Consecutive hidden states form a Markov chain $\mathbf{z}(1), \ldots, \mathbf{z}(T-1), \mathbf{z}(T)$.

A popular probabilistic example of state-space models that have been applied to gene expression data are Dynamical Bayesian Networks (Murphy and Mian, 1999) such as Linear Dynamical Systems (Beal et al., 2005; Hirose et al., 2008; Rangel et al., 2004; Yamaguchi et al., 2007, 2010; Angus et al., 2010). Examples of such LDS , are (Beal et al., 2005) and (Angus et al., 2010) who infered the profiles of 14 hidden transcription factors for 10 observed genes. Their modeling was however done either without predictive validation (Beal et al., 2005), or on synthetically generated data (Angus et al., 2010). Other researchers (Hirose et al., 2008; Yamaguchi et al., 2007, 2010) used a trainable Kalman smoother-like approach to learn 4 to 5 hidden variables (so-called modules) explaining the behavior of hundreds of genes, but neither validated their model on out-of-sample data points, nor drew conclusions on gene-gene interactions.

LDS also suffer from their linearity, and may be insufficient to model the nonlin-

[2]In the above enumeration, we actually omitted one group of methods that consist in highly nonlinear Boolean Networks with binary ON/OFF values for gene expression levels, and linear, nonlinear or stochastic dynamics (Lahdesmaki et al., 2003; Alvarez-Buylla et al., 2007). In such boolean networks, one typically starts from a hypothesis on the GRN, and then simulates the dynamics of a boolean network, looking for attractors. The objective does not consist in fitting mRNA expression levels.

ear regulation of genes by proteins; whereas the derivation of the variational Bayes solution to nonlinear dynamical systems might be difficult.

Hidden Variable Approaches: Gaussian Processes

The other main approaches devised to solve the ODEs involved in gene regulation networks consists in Gaussian Processes (GPs) (Lawrence and Sanguinetti, 2007; Gao et al., 2008; Alvarez et al., 2009), which model the latent protein concentration as a latent function $z_j(t)$ that follows a Gaussian prior with a specified covariance.

That model was further improved in (Zhang et al., 2010), using Gaussian Process Latent Variable models (Wang et al., 2006a) to infer the profile of a single transcription factor (the tumor suppressor p53) and explained the activity of a large collection of genes using that TF only. GPs however require to analytically derive the covariance function and can be computationally expensive.

Large-Scale Linear Models Without Hidden Variables

Because the SSM or GP models described in the previous sections can prove computationally expensive and define too many degrees of freedom w.r.t. available data, the simplification "mRNA = transcription factor" is often used, and a simple linear model is employed.

Examples of first-order linear dynamical models on gene expressions include the Inferelator by (Bonneau et al., 2006, 2007). The Inferelator consists of a kinetic ODE, that follows the Wahde and Hertz equation (Wahde and Hertz, 2001) and where transcription factors contribute linearly. This ODE also includes an mRNA degradation term. Some instances of the Inferelator introduce nonlinear AND, OR and XOR relationships between pairs of genes, based on a previous bi-clustering of genes. One has to note that the Inferelator has been mostly applied to datasets with

hundreds of data-points (e.g. the *Halobacterium*).

Other examples include the first-order vector autoregressive models VAR(1) (Shimamura et al., 2009), or the *Brownian motion* (which is a VAR(1) model on the change of the mRNA concentration (Wang et al., 2006b)). Lozano et al. suggested using a dynamic dependency on the past 2, 3, or 4 time-steps (Lozano et al., 2009), but this was impractical in our case given the relatively small number of micro-array measurements in our experiments.

4.1.4 Biological Datasets Used in Our Experiments

Arabidopsis Thaliana's Response to NO_{3-}

This research, from the hypothesis and experimental protocol through the experimental manipulation and data analysis, was devised and conducted by Dr. Gabriel Krouk, at the time post-doctoral researchers in Prof. Gloria Coruzzi's[3] Plant Systems Biology lab[4] at the NYU Center for Genomics and Systems Biology at New York University. Additional feedback about GRN inference was provided from the author and from Prof. Dennis Shasha.

Higher plants constitute a main entry of nitrogen in food chains, and acquire nitrogen mainly as NO_{3-}. Soil concentration of this mineral ion can fluctuate dramatically in the rhizosphere, often resulting in limited growth and yield. Thus, understanding plant adaptation to fluctuating nitrogen levels is a challenging task with potential consequences for health, the environment, and economy (Krouk et al., 2010).

The first genomic approaches studying NO_{3-} responses were published 10 years ago (Wang et al., 2000). To date, data from more than 100 Affymetrix ATH1 chips have been published that monitor gene expression in response to NO_{3-} provision.

[3]Research page at: http://biology.as.nyu.edu/object/GloriaCoruzzi.html
[4]http://coruzzilab.bio.nyu.edu/home/

Analysis of the N-treated microarray data sets from several different labs demonstrated that at least a tenth of the genome can be regulated by nitrogen provision, depending on the context (Gutierrez et al., 2007). Despite these extensive efforts of characterization, only a limited number of molecular actors that alter NO_{3-} induced gene regulation have been identified so far.

In this study, our aim was to provide a systems view of NO_{3-} signal propagation though dynamic regulatory gene networks. To do so, a high-resolution dynamic NO_{3-} transcriptome from plants treated with nitrate from 0 to 20 min was generated. The micro-arrays contained 7 full-genome mRNA measures at 0, 3, 6, 9, 12, 15 and 20 min; in the cross-validation leave-out-last study, we used measures between 0 and 15 min to fit the model for each gene i (by tuning the parameters of associated dynamical functions), and tested the fitted model on the last time step (prediction of the mRNA level at 20 min).

Two micro-array replicates were acquired in this study, listed in Table 4.1. Since each replicate is independent of all micro-arrays preceding and following in time, there were four possible transitions between any two time points t and $t+1$, and we therefore used 4 replicate sequences to train the machine learning algorithm.

p53, Mef2 and TGF-β Protein Datasets

Our first dataset consisted in the p53 human genome data from (Barenco et al., 2006). p53 is a "*tumor repressor activated during DNA damage.* [...] *Irradiation is performed to disrupt the equilibrium of the p53 network stimulating transcription of p53 target genes. Seven samples* [of mRNA] *in three replicas* [were] *collected as the raw time course data*" (Gao et al., 2008)[5]. Previous studies on that dataset included (Barenco

[5]We used both the pre-processes data available at Neil Lawrence's website: http://staffwww.dcs.shef.ac.uk/people/N.Lawrence/software.html, and the raw mRNA associated to the experiment conducted by (Barenco et al., 2006), and available as supplemental

Table 4.1: Number of microarrays used for the study of the Gene Regulation Network of the *Arabidopsis* that is involved in the plant's reaction to nitrates. The table is sorted by time-point and experimental condition. All the 26 microarrays are considered independent experiments. Note that we based our predictive modeling only on the nitrate data.

Time-point	NO_{3-}	KCl
0 min	2 replicates	-
3 min	2 replicates	2 replicates
6 min	2 replicates	2 replicates
9 min	2 replicates	2 replicates
12 min	2 replicates	2 replicates
15 min	2 replicates	2 replicates
20 min	2 replicates	2 replicates

et al., 2006; Lawrence and Sanguinetti, 2007; Gao et al., 2008; Alvarez et al., 2009; Zhang et al., 2010). The predicted p53 protein levels were compared to experimental Western Blot measures.

We also considered the data associated with the development of the mesoderm in Drosophila, involving the Mef2 transcription factor (Gao et al., 2008)[6]. Protein levels were not available, but we compared our predictions to the ones made in the study.

Finally, we demonstrate that our experimental approach can infer the levels of 3 proteins from 70 mRNAs on the human Transforming Growth Factor (TGF) β data from (Keshamouni et al., 2009). Our predictions for protein levels were compared to the experimental data acquired a new methodology, iTRAQ. Both data were supplied in the journal article.

material.

[6]We used data available at Neil Lawrence's website.

4.2 Gradient-Based Biological State-Space Models

We propose a new and simple algorithm for learning SSMs representing gene regulation networks, that can incorporate nonlinear protein-gene interactions or focus on gene-gene interactions. It is grounded in the factor graph formalism (Kschischang et al., 2001), which expresses the joint likelihood of the hidden and observed variables as a product of likelihoods at each factor. Our SSM includes two types of factors: observation and dynamic factors, which may be connected to two types of variables: observed mRNA expression levels, and hidden transcription factor sequences (either transcription factors, e.g. protein concentrations, or a noise-free time-course of mRNA), as illustrated respectively on Figure 4.2 or on Figure 4.1.

A "Plug-And-Play" Architecture for SSMs

Our model is flexible because one can essentially "plug-and-play" different types of factors to suit various types of SSMs in the biological literature. Each factor is expressed in the negative log domain, and computes an energy value that can be interpreted as the negative log likelihood of the configuration of the variables it connects with. The total energy of the system is the sum of the factors' energies, so that the maximum likelihood configuration of variables can be obtained by minimizing the total energy. Learning our factor graphs is still done by maximizing their joint likelihood, but we use an approximate gradient-based MAP inference to obtain the most likely configuration of the hidden sequence. Such approximate approaches have been applied on chaotic and motion capture time series modeling problems (Mirowski and LeCun, 2009). Our algorithm is also faster than MCMC or Variational Bayes approaches for Dynamic Bayesian Networks and than Gaussian Processes.

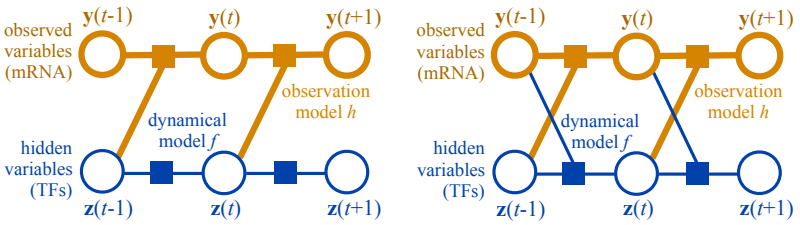

Figure 4.1: Two factor graph representations of the state-space model for gene regulation networks. In both DFGs, the observation models incorporate a dependency on the previous mRNA expression level $\mathbf{y}_{t-1}$, as we are modeling the rate of change of $\mathbf{Y}$ by a first-order linearized ODE. Left: the dynamical model f follows random walk or $AR(1)$ dynamics. Right: the dynamical model f incorporates the influence of the mRNA in protein encoding.

4.2.1 Representing Protein TF Levels as Hidden Variables

We assume, as in Barenco et al. (2006); Gao et al. (2008), that for a gene i, the rate of change of the mRNA level follows a dynamic that involves its basal transcription rate b_i, its decay rate d_i and a weighted contribution of its M transcription factors $z_j(t)$. The contribution of each TF can be modeled as a linear (identity) Barenco et al. (2006) or nonlinear activation function σ. The transcriptional dynamics can thus be expressed as an ODE (4.3). After linearization between two consecutive time steps t and $t + \Delta t$, the kinetic function (4.3) can be approximated by a Markovian model (4.4), namely a function h_i with added Gaussian noise term ϵ_i:

$$\frac{dy_i}{dt} = b_i - d_i y_i(t) + \sum_{j=1}^{M} s_{i,j}\sigma\left(z_j(t)\right) + \epsilon_{i,t} \tag{4.3}$$

$$y_{i,t+\Delta t} = h_i\left(y_{i,t}, \mathbf{z}_t\right) + \epsilon_{i,t} = b'_i + (1 - d'_i)y_{i,t} + \sum_{j=1}^{M} s'_{i,j}\sigma\left(z_{j,t}\right) + \epsilon_{i,t} \tag{4.4}$$

In this study, we considered two kinds of dynamics on the hidden TFs $\mathbf{z}_j$, illustrated on Figure 4.1. In a first, simplistic model, we can assume that $z_j(t)$ follows a Gaussian random walk, which is equivalent to imposing a Gaussian prior on $z_j(t)$

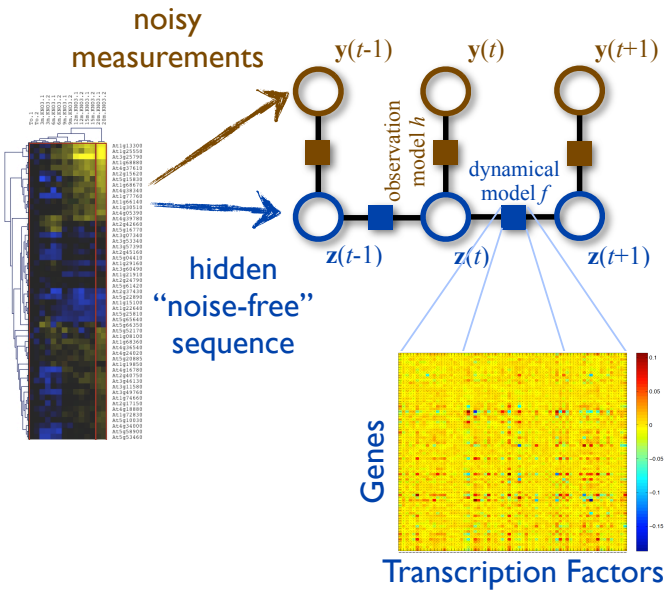

Figure 4.2: Factor graph representation of the state-space model used for modeling gene-gene interactions under the assumption that mRNA are a noisy observation of an "idealized" gene expression level time-course. The observation factor is the identity function.

as in Lawrence and Sanguinetti (2007); Gao et al. (2008): $z_{j,t+\Delta t} = f_j\left(z_{j,t}\right) + \eta_{j,t} = z_{j,t} + \eta_{j,t}$.

The second dynamic actually takes into account the encoding of proteins by their corresponding genes (mRNA), and models that interaction as an ODE. The encoding of each TF j is modulated by the mRNA levels of the associated gene with sensitivity w_j, with decay term δ_j. After linearization, this ODE can be approximated by Eq. (4.6), i.e. a function f_j with additional Gaussian noise η_i:

$$\frac{dz_j}{dt} = -\delta_j z_j(t) + w_j y_j(t) + \eta_{j,t} \tag{4.5}$$

$$z_{j,t+\Delta t} = f_j\left(y_{j,t}, z_{j,t}\right) + \eta_{i,t} = (1-\delta_i')z_{j,t} + w_j' y_{j,t} + \eta_{j,t} \tag{4.6}$$

4.2.2 Representing Noise-Free mRNA as Hidden Variables

In a departure from previous state-space model frameworks, our second approach uses the hidden variables to represent an idealized, "true" sequence of gene expressions $\mathbf{z}(t)$ that would be measured if there were no noise. The set of all genes at time t is modeled by a "latent" (i.e., hidden) variable (denoted $\mathbf{z}(t)$), about which noisy observations $\mathbf{y}(t)$ are made. Specifically, we a) model the dynamics on hidden states $\mathbf{z}(t)$ instead of modeling them directly on the Affymetrix data $\mathbf{y}(t)$, as well as b) have the hidden sequence $\mathbf{z}(t)$ generate the actual observed sequence $\mathbf{y}(t)$ of mRNA, while incorporating measurement uncertainty. Such an approach has been used in robotics to cope with errors coming from sensors.

As shown in Figure 4.2, the relationship between consecutive latent variables $\mathbf{z}(t)$ and $\mathbf{z}(t+1)$ is a Markov chain: each latent gene's expression value at time $t+1$ is assumed to depend only on the state of potentially all the latent gene expressions at the previous time point t. For each gene i, this relationship stems from the kinetic ODE involving the rate of mRNA change (with a kinetic time constant τ), mRNA degradation, and a linear function f_i of transcription factor concentrations for that specific gene. So-called "Brownian motion" dynamics correspond to kinetic dynamics without the mRNA degradation term. In linearized (discretized) form, the overall dynamical model f can be represented by an $N \times M$ matrix $\mathbf{F}$ where N is the total number of genes and M the number of transcription factors ($M \leq N$, and transcription factors are given indexes from 1 to M), plus a bias term $\mathbf{b}$ and a Gaussian error term with zero mean and fixed covariance:

$$\tau \frac{\mathrm{d}z_i(t)}{\mathrm{d}t} + z_i(t) = f_i\left(\mathbf{z}(t)\right) + \eta_i(t) \tag{4.7}$$

$$\frac{\tau}{\Delta t}\left(z_i(t+1) - z_i(t)\right) + z_i(t) = \sum_{j=1}^{N_i} F_{i,j} z_j(t) + b_i + \eta_i(t) \tag{4.8}$$

This linear Markovian model which represents a kinetic (RNA degrades) or Brownian motion (RNA doesnÕt degrade) ODE, is the simplest and requires the fewest parameters (there is one parameter per TF-gene interaction, and an additional offset for each target gene). We conjecture that model thus helps to avoid over-fitting scarce gene data.

The observation model h is essentially an $N \times N$ identity matrix with a Gaussian error term:

$$y_i(t) = h\left(z_i(t)\right) + \epsilon_i(t) \tag{4.9}$$

$$y_i(t) = z_i(t) + \epsilon_i(t) \tag{4.10}$$

Because our algorithm is efficient, simple and tractable, as explained in next section, it can handle larger numbers of genes (we focussed on 76 genes) than other state-space model approaches, given enough genes Beal et al. (2005), Angus et al. (2010), Zhang et al. (2010).

4.2.3 Learning Gradient-Based DFGs

The above functions f_i and h_j are only a subset of the possible factors that our method can handle, and they could be substituted by any function that is differentiable with

respect to both its parameters and the latent variables. Unlike methods based on Gaussian Processes Lawrence and Sanguinetti (2007); Alvarez et al. (2009); Zhang et al. (2010), on expensive MCMC sampling Barenco et al. (2006), or on Variational Bayes Beal et al. (2005), our method only requires to compute the gradients of all functions f_i and h_j, both w.r.t. parameters $\mathbf{\Theta}$ and w.r.t. latent variables $\mathbf{Z}$.

Expectation-Maximization-Like Coordinate Descent

Learning and inference are performed by minimizing the negative log-likelihood loss of the factor graph (i.e. is a sum of square errors because of the Gaussian prior on the error/noise terms). On a sequence $\mathbf{Y}$ of T micro-array measurements (including replicate sequences) over N genes, corresponding latent variables $\mathbf{Z}$, under an observation (and dynamic) models parameterized by $\mathbf{\Theta}$, and for given hyperparameters γ (which controls the weight of the dynamical and observation errors) and λ (for the L_1-norm regularization), the loss is expressed as (4.11). Latent variables $\mathbf{Z}$ and parameters $\mathbf{\Theta}$ are initialized to small random values. Then the iterative procedure consists of a) the *inference* step, where the loss (4.11) is minimized with respect to the latent variables $\mathbf{Z}$ thanks to gradient descent; and of b) the *learning* step, where the loss (4.11) of the observation (and dynamical, if relevant) modules is minimized w.r.t. parameters $\mathbf{\Theta}$ using conjugate gradient optimization or Least-Angle Regression and Shrinkage (LARS) if the factor is linear (Tibshirani, 1996). We use small learning rates and validate the hyperparameters γ and λ on the training data (typically, $\lambda = 0.01$ and $\gamma = 1$).

$$L(\mathbf{Y}, \mathbf{Z}; \mathbf{\Theta}, \gamma, \lambda) = \sum_{t=1}^{T} \left(\frac{\gamma}{2} \sum_{j=1}^{M} \eta_{j,t}^2 + \frac{1}{2} \sum_{i=1}^{N} \epsilon_{i,t}^2 \right) + \lambda \parallel \Theta \parallel_1 \tag{4.11}$$

The learning algorithm is run for 100 or 1000 consecutive epochs over all the

replicate sequences. In order to retain the optimal set of parameters of f, one selects the epoch where the dynamic or observation error on the training dataset is minimal.

In the case of model architecture from Section 4.2.2. one run of the learning procedure provides with a matrix $\mathbf{F}$ of signed (positive: excitatory or negative: inhibitory) interactions between transcription factors and genes. Each element $F_{i,j}$ represents the action of the j-th transcription factor on the i-th gene.

Hyperparameters and Recovering Existing Methods

Two main hyper-parameters were explored in our learning experiments: the amount of L1-norm regularization λ (explained in the Methods) and the Lagrange-like coefficient γ linked to the state-space model. When trying to learn GRN from mRNA (in Section 4.2.2), we used the kinetic coefficient τ as an additional hyperparameter.

Note that when the state-space coefficient is $\gamma = 0$, and using the configuration from Section 4.2.2), we can recover non-SSM algorithms: (Efron et al., 2004), as used for instance by Bonneau et al. (Bonneau et al., 2006, 2007) and Elastic Nets (Zou and Hastie, 2005), as used for instance by Shimamura et al. (Shimamura et al., 2009). In that case, we simply have $\mathbf{Y} = \mathbf{Z}$. Moreover, if we do not use the mRNA degradation term in the kinetic ODE, and use instead "Brownian motion" dynamics, and if we set the state-space coefficient to $\gamma = 0$, we recover an approach comparable to the one published by Wang et al. (Wang et al., 2006b) (although their optimization algorithm was based on the SVD of the micro-array data).

Regularization

During the learning step, sparse gene regulation networks are obtained by penalizing dense solutions using L_1-norm regularization, which amounts to adding a λ-weighted penalty to the dynamical error term, as in the LASSO initially described by Tibshirani

Tibshirani (1996). Employing regularization on parameters also helps avoiding local optima in the solutions.

LARS is a fast implementation of Tibshirani's popular LASSO regression with L1-norm regularization (Tibshirani, 1996). Elastic Nets are an improvement over LARS and LASSO, and their main advantage is to group variables (in our case genes) as opposed to choosing one gene and leaving out correlated ones.

Selection of Gene Regulation Network by Bootstrapping

Using a bootstrapping approach based on random initialization of latent variables $\mathbf{z}(t)$, we further repeat the SSM iterative procedure 20 times and take the final average model.

In the case of the dynamical model on noise-free mRNA described in Section 4.2.2, we use bootstrapping to determine the statistically significant gene-gene links. The above-explained algorithm for learning state-space models starts with random initial values for both the dynamical model (in other words, matrix $\mathbf{F}$) and for the latent variables $\mathbf{Z}$. We repeat the whole procedure 20 times in order to perform the following bootstrapping evaluation. Each run k of the algorithm might converge to a slightly different solution $\mathbf{F}^*(k)$. We then take the average TF-gene interactions weights obtained from all solutions $\mathbf{F}^*(k)$ and call it $\mathbf{F}^*$. The table on Figure 4.4 reports comparative results on the average solutions. In parallel, we also generate 1000 random permutations of each matrix $\mathbf{F}^*(k)$, defined respectively as $\mathbf{P}^*(k,1), \mathbf{P}^*(k,2), \ldots, \mathbf{P}^*(k,1000)$, and then compute 1000 average matrices $\mathbf{P}^*(1), \mathbf{P}^*(2), \ldots, \mathbf{P}^*(1000)$ of those "scrambled" matrices (we take the averages over the 20 runs). We compare each average element $F^*_{i,j}$ to the empirical distribution of the 1000 permuted averages and thus obtain an empirical p-value. The final genetic regulation network consists in elements $F^*_{i,j}$ that have a p-value $p < 0.001$.

4.3 GRN of the *Arabidopsis* Response to NO_3^-

In this study, instead of learning the dynamics directly on the gene expression sequence, we took into account uncertainty and acquisition errors, and used a state-space model. The latter defined the observed gene expression time series (denoted as $\mathbf{y}(t)$) as being generated by a hidden "true" sequence of gene expressions $\mathbf{z}(t)$. This approach enabled us to both incorporate uncertainty about the measured mRNA and to model the gene regulation network by simple linear dynamics on the hidden variables (so-called "states"), thus reducing the number of (unknown) free parameters and the associated risk of over-fitting the observed data.

Our DFG-based method delivered a coherent regulatory model that was good enough to predict the direction of gene change (up regulation or down regulation) on future data points. This coherence allowed us to propose a gene influence network involving transcription factors and "sentinel genes" involved in the primary NO_3^- response (such as NO_3^- transporters or NO_3^- assimilation genes). The role of a predicted hub in this network was evaluated in further biological experiments by over-expressing it, and indeed lead to changes in the NO_3^- driven gene expression of sentinel genes.

4.3.1 Comparative Study of State-Space Model Optimization

Out of the 550 N-regulated genes we extracted 67 genes which correspond to all the predicted transcription factors and 9 N-regulated genes that belonged to the N-assimilation pathway (including sentinel genes). Their mRNA over 7 time points and for 2 replicates is shown on Figure 4.3. The transcription factors have been used as explanatory variables (inputs to f) as well as explained values (output from f), whereas the N-assimilation genes are only explained values. We then optimized the

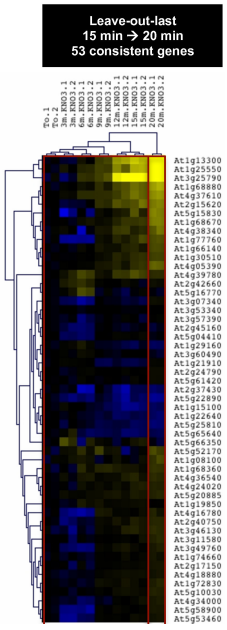

Figure 4.3: 76-gene micro-array used for the *Arabidopsis* study. The last time-point, corresponding to time $t = 20$ min, was out-of-sampled and used for evaluating the predictive capability of our dynamical model of gene regulation.

state-space model, using different algorithms, in order to fit it to the observed data matrix, and compared all our results in the table on Figure 4.4. We also compared our SSM approach to non-SSM approaches (Bonneau et al., 2006, 2007; Wang et al., 2006b; Efron et al., 2004; Zou and Hastie, 2005; Shimamura et al., 2009) in in the table on Figure 4.5.

For each type of ODE (kinetic or "Brownian motion") and type of optimization algorithm, we exhaustively explored the space of hyper-parameters (γ, λ, ρ) in order to optimize the quality of fit of each model to the first six time-points (0 min, 3 min, 6 min, 9 min, 12 min and 15 min). As can be seen in the table on Figure 4.4, we identified the state-space model relying on the kinetic ODE, and with either LARS or conjugate gradient optimizations, as the two best (having the highest Signal-to-Noise Ratio (SNR)) optimization algorithms on the MAS5 training datasets. The signal-to-

Dynamics	Normal-ization	Optimization	Best hyperparameters (w.r.t. SNR on leave-1 train dataset)			Perf. on train set	Perf. on test set
			gamma (state-space coeffi-cient)	tau (kinetic time constant)	lambda (regulariza-tion para-meter)	SNR (in dB) on leave-1 train dataset	Percentage of correct signs on leave-1 test dataset
kinetic	**MAS5**	**gradient**	**1**	**3**	**0.0001**	**32.4**	**68%**
kinetic	**MAS5**	**LARS**	**0.1**	**3**	**0.1**	**32.4**	**74%**
kinetic	MAS5	Elastic Nets	0.1	7	0.05	32.2	71%
Brownian	MAS5	gradient	0.1	n/a	0.0001	32.1	65%
Brownian	MAS5	LARS	0	n/a	0.05	32.1	63%
Brownian	MAS5	Elastic Nets	0	n/a	0.05	32.1	63%
Naïve trend prediction	*MAS5*		*n/a*	*n/a*	*n/a*	*n/a*	*52%*

Figure 4.4: The kinetic ODE and both the conjugate gradient and LARS optimization algorithms obtain the best fit to $[0, 15]$ min data, with good leave-out-last predictions. Each line in the table represents the type of ODE for the dynamical model of TF-gene regulation (either kinetic, with mRNA degradation, or ÒBrownian motion", without mRNA degradation), the type of micro-array data normalization, and the optimization algorithm for learning the parameters of the dynamical model. For each of those, we selected the best hyperparameters, namely the state-space coefficient γ, the kinetic time constant τ (in minutes) and the parameter regularization coefficient λ, based on the quality of fit to the training data ($[0, 15]$ min), as measured by the signal-to-noise ratio, in dB. We then performed a leave-out-last prediction and counted the number of times the sign of the mRNA change between 15 min and 20 min was correct. We compared these results to a naŢve extrapolation (based on the trend between 12 min and 15 min) and obtained statistically significant results at $p = 0.0145$. Reproduced from the table published in (Krouk et al., Provisionally accepted for publication).

noise ratio is a monotonic function of the Normalized Mean Square Error (NMSE) on the predicted values of mRNA; all algorithms used in this article aim at minimizing the NMSE, i.e. at maximizing the SNR.

Having chosen the two best algorithms using all time points up to and including 15 min as training data, we performed a "leave-out-last" test, consisting of predicting both the direction and magnitude of the change of the genes between 15 and 20 min. Using those algorithms with those parameter settings, we made predictions about whether gene expression levels would increase (positive sign) or decrease (negative

			Best hyperparameters (w.r.t. SNR on leave-1 train dataset)			Perf. on train set	Perf. on test set	
Dynamics	Normal-ization	Optimization	gamma (state-space coeffi-cient)	tau (kinetic time constant)	lambda (regulariza-tion para-meter)	SNR (in dB) on leave-1 train dataset	Percentage of correct signs on leave-1 test dataset	Reference
kinetic	**MAS5**	**gradient**	**1**	**3**	**0.0001**	**32.4**	**68%**	**This article**
kinetic	**MAS5**	**LARS**	**0.1**	**3**	**0.1**	**32.4**	**74%**	**This article**
kinetic	MAS5	LARS	0	3	0.05	32.1	74%	Bonneau 2006
kinetic	MAS5	Elastic Nets	0	3	0.05	32.1	74%	Shimamura 2009
Brownian	MAS5	gradient	0	n/a	0.005	32.1	66%	Wang 2006
Brownian	MAS5	LARS	0	n/a	0.05	32.1	63%	Wang 2006
Brownian	MAS5	Elastic Nets	0	n/a	0.05	32.1	63%	Wang 2006
Naïve trend prediction	*MAS5*		*n/a*	*n/a*	*n/a*	*n/a*	*52%*	

Figure 4.5: The quality of fit of our State-Space Model approach slightly outperforms the non-SSM approaches. We compared our State-Space Model-based technique (SSM, with a non-zero state-space model parameter gamma) to previously published algorithms for learning gene regulation networks by enforcing gamma=0 (see Methods). We notice that the LARS algorithm (Tibshirani, 1996), used in the Inferelator by Bonneau et al. (Bonneau et al., 2006, 2007), as well as Elastic Nets (Zou and Hastie, 2005; Shimamura et al., 2009), obtain a slightly worse quality of fit (signal-to-noise ratio, in dB) than when combined with our state-space modeling, for the same leave-out-last performance as our SSM + LARS. Not using an mRNA degradation term, as in Wang et al. (Wang et al., 2006b), degrades the leave-out-last performance. Reproduced from the table published in (Krouk et al., Provisionally accepted for publication).

sign) in 20 min compared with 15 min.

As the table on Figure 4.4 shows, a state-space model relying on the kinetic ODE and with LARS optimization (kinetic LARS) gives correct results 74% of the time on a set of 53 genes (47 TFs and 6 N-assimilation genes) that are "consistent" among the two biological replicates in their behavior (consistently up or down-regulated in both replicates) for the transition from 15 min to 20 min. When we considered all 76 genes, regardless of their "consistency" across replicates, kinetic LARS still gave correct results 71% of the time. Corresponding figures for the other chosen algorithm (kinetic ODE with conjugate gradient optimization) yielded 68% correct results on

both the 53 consistent genes and on all 76 genes. By contrast, a naive algorithm, that would extrapolate the trend between 12 min and 15 min, was correct for only 52% of the consistent genes, just slightly better than random (this result implies that 48% of the consistent genes changed "direction" at 15 min). Thus, our state-space model does significantly better ($p = 0.0145$) than the naive trend forecast based on a binomial test on a coin that is biased to be correct 52% of the time.

Using the hyper-parameters (γ, λ, ρ) corresponding to the two best solutions (kinetic LARS and kinetic conjugate gradient), we retrained two State Space Models on all the available data (0 to 20 min) to obtain corresponding gene regulatory networks. Finally, we performed a statistical analysis of the bootstrap networks, in order to retain TF-gene links that were statistically significant at $p = 0.001$. We ultimately selected the conjugate gradient-optimized network as it gave a less sparse solution (394 links) than the LARS-optimized GRN (22 links). We used this network (next section) to analyze the NO_{3-} response of sentinel genes to transcription factors.

Although the number of samples in the dataset is extremely small (7 time-points, corresponding to 26 different time points using replicate time series), all the dynamical models (our state-space model in particular) were able to learn the system well enough to predict the direction of changes to gene expression. This suggests that we might have learnt some consistent and biologically meaningful networks involved in NO_{3-} response pathway. Since the dynamical functions f model the gene regulation network learned during the leave-out-last test, we conclude by presenting the function f obtained from the full time sequence 0-20 min. This function f can be displayed as an influence matrix (Figure 4.7), or as a gene network where each node is a gene and edges represent potential influences.

The study of this network as a whole system is discussed below.

4.3.2 Over-Expression of a Potential Network Hub (SPL9) Modifies NO_{3-} Response of Sentinel Genes.

In order to probe the role of a transcription factor/hub in the predicted network presented on Figure 4.7, transgenic plants (pSLP9:rSPL9) expressing an altered version of the mRNA for the SPL9 transcription factor plants were compared to WT (wild type) plants for their response to NO_{3-} provision, using another mRNA measuring technique called QPCR. Results are shown on Figure 4.6.

The SPL9 gene has been selected for several reasons: (i) it is induced at very early time points (3 and 6 minutes), (ii) the inferred network predicts that SPL9 potentially controls at least 6 genes including 2 sentinel genes. This places it as the 3rd most influential TF on sentinels, and (iii) it is the most strongly influenced gene in both number of connections as well as the magnitude of the regulations controlling it.

What follows is the biologist's interpretation of the QPCR study, described in further details in (Krouk et al., Provisionally accepted for publication).

> As such SPL9 constitutes a potential crucial bottleneck in the flux of information mediated by the proposed network. We first considered SPL9 mutants and monitored sentinel expression in this genetic background. However even if some defects have been observed no consistent phenotype could have been reported. This can be easily explained by the topological redundancy of the network. Thus one could expect that its over-expression triggers a detectable effect on the sentinels and on the network behavior. SPL9 is a transcription factor identified to control shoot development and flowering transitions, and it also appears as a potential central regulator in our network derived from the state space model.

In our experimental set-up, transgenic SPL9 mRNA is over-expressed an average 20 to 4 times in the plants. In parallel, mRNA transcription levels of several sentinel genes has been followed in this SPL9 transgenic line. The most dramatic effect recorded is for the NIR gene. Interestingly, the NIR gene has previously been demonstrated to be one of the most robustly NO_{3-} regulated gene based on a meta analysis of microarray data from N-treated plants (Gutierrez et al., 2007). Thus, over-expression of the SPL9 gene leads to significantly advance the NIR NO_{3-} response by about 10 min, and attenuates its magnitude of regulation for later time points (60 min). Less dramatic but still significant (over 3 independent experiments) effects has been recorded for NRT1.1/CIPK23 genes, belonging the NO_{3-} sensing module, and for the NIA2 gene. These results demonstrate a role of the SPL9 transcription factor in the control of the NO_{3-} primary response. To further investigate the role of SPL9 over-expression on the transcription levels of genes in the network over time. SPL9 is also regulated transiently as well as earlier than the sentinel genes we measured their dynamics of mRNA accumulation in this experiment. Interestingly, SPL9 seems to have an effect on the vast majority of the genes that we have tested. The diversity of the mis-regulations is high. For instance for 4 out of the 14 tested genes display an early effect (between 0 and 20min) of the SPL9 over-expression. However, 11 genes display modified gene expression in transgenic plants at later time points (40 and 60min).

This high-resolution time course analysis demonstrated that the previously known primary nitrate response is actually preceded by very fast (within 3 min) gene expression modulation, involving genes/functions needed to prepare plants to use/reduce

NO_{3-}. The experiments and methods allow us to propose a temporal working model for NO_{3-}-driven gene networks. The over-expression of a predicted gene hub encoding an early induced transcription factor indeed leads to the modification of the NO_{3-} response kinetic of sentinel genes such as NIR, NIA2, and NRT1.1.

4.4 Inferring Protein Levels from Micro-arrays

4.4.1 Inferring Human p53 Protein Levels from mRNA

In a first series of experiments, we reproduced the results from Lawrence and Sanguinetti (2007); Gao et al. (2008); Alvarez et al. (2009); Zhang et al. (2010) who tried to infer the single human p53 (tumor repressor) protein level from 5 mRNA expression levels (not including the mRNA of TP53) in reaction to irradiation Barenco et al. (2006). Using data preprocessed by Gao et al. (2008), we investigated sharing the latent variables $\mathbf{Z}$ across the 3 replicates, random walk dynamics on $\mathbf{Z}$ and the use of nonlinear activation (Michaelis-Menten "bottleneck" kinetics) $\sigma(z(t)) = z(t)/(\mu + z(t))$.

Using the micro-array data available with Barenco et al. (2006), we added a 6th gene (p53-encoding TP53) and enforced TP53-governed kinetics (Eq. 4.6) on p53, with or without sharing the latent variables $\mathbf{Z}$ across replicates. Figure 4.8 shows that the experimental profile of p53 was well recovered from 6-gene datasets. All experiments were repeated 10 times, starting from random initializations, and the errors bars were small. The TF value at time $t = 0$ was set to 0, and the sensitivity of p21 was set to 1, as in Gao et al. (2008). In terms of reconstruction error, all experiments achieved an observation Signal-to-Noise Ratio of about 16dB, and the 6-gene experiments had a dynamic SNR of about 13dB.

4.4.2 Inferring *Drosophila* Mef2 Protein Levels from mRNA

A similar experiment was repeated with 7-gene data used for the inference of the Mef2 protein in the *Drosophila* Gao et al. (2008), where one of the genes encoded Mef2 and the 6 others genes were targets of the TF. As illustrated on Figure 4.9, the inferred TF was similar to the one in Gao et al. (2008) but the mRNA fitted the observed data more closely than in Gao et al. (2008), with 10dB SNR.

4.4.3 Inferring Multiple Protein Levels: Human p53, TGF-β

Coming back to p53 data, but using 50 mRNAs, we investigated the inference of multiple (3) hidden TFs. No constraints were enforced on the TFs, but for each realization, we ultimately sorted the TFs according to their average cross-correlation among replicates (TF3 being the most correlated). As Figure 4.10 shows, the profile of most-correlated TF3 was consistent among the realizations and had a comparable shape to the Western blot experimental p53 measures from Barenco et al. (2006).

Finally, we applied our model to a new human cancer dataset containing both mRNA and protein levels. Using only mRNA, we succeeded in inferring the protein levels of 3 proteins (β-actin, cofilin and moesin) involved in the TGF-β Epithelial-Mesenchymal Transition. We used normalized mRNA data averaged over replicates and taken from Keshamouni et al. (2009), defined 4 TFs, with an encoding kinetic (Eq. 4.6) on 3 TFs (respectively encoded by ACTB, CFL1 and MSN), and set the TFs levels to be equal to 1 at time $t = 8$h (because the experimental protein time series started at that point and were defined as ratios). The learning experiment was repeated 5 times with random initializations. Figure 4.10 shows that the first 3 inferred TFs match the profile of experimental protein ratios measured using the iTRAQ method.

4.5 Conclusions and Further Work

Using experimental validation, we demonstrated that our simple and fast gradient-based state-space model algorithm can infer protein profiles from mRNA datasets, and match experimental measures of protein concentration levels.

We have also shown that they can be applied to the problem of reverse-engineering gene regulation networks from mRNA, by using hidden variables to model the noise in mRNA data. Using predictive modeling, we were able to predict the direction taken by gene expression levels on out-of-sample micro-arrays, confirming that our dynamic model succeeded in capturing the influences of the gene regulatory network.

We are now planning on further evaluating our method for reverse-engineering GRNs by directly modeling transcription factors and by replacing gene-gene interactions by gene-TF and TF-gene interactions. In our factor graph notation, that corresponds to replacing a model with dynamics on hidden variables $\mathbf{Z}$ and an identity observation function $\mathbf{Y} = h(\mathbf{Z})$ by a proper transcription function $\frac{\partial \mathbf{y}_t}{\partial t} = h(\mathbf{z}_t)$ and a translation function $\frac{\partial \mathbf{z}_t}{\partial t} = f(\mathbf{y}_t)$. Our current work is inspired by the module-networks SSM approaches described in (Hirose et al., 2008; Yamaguchi et al., 2007, 2010) and by the fully-fledged Dynamic Bayesian Network approaches in (Rangel et al., 2004; Beal et al., 2005).

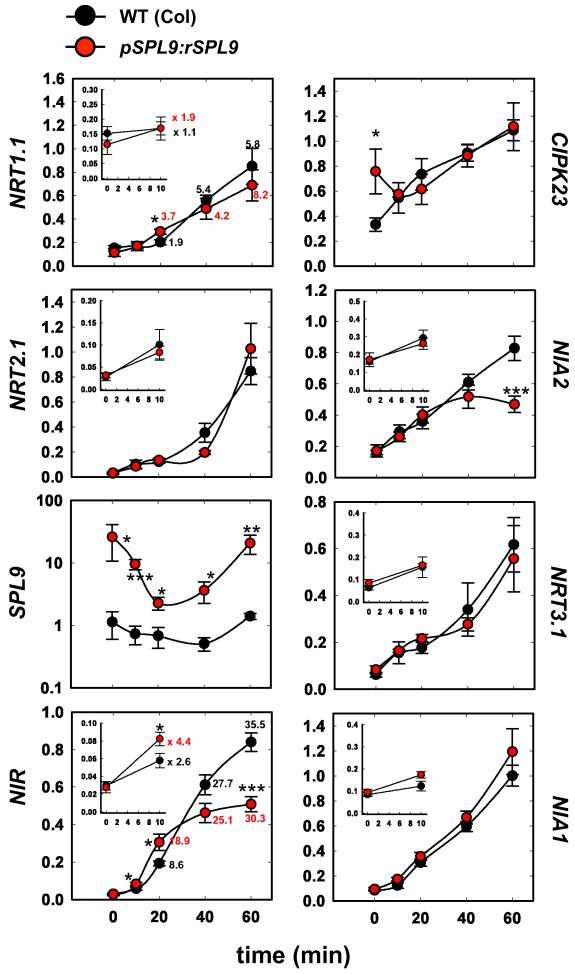

Figure 4.6: Gene knock-out validation for the Arabidopsis GRN inference The "wild-type" expression (WT, in black) corresponds to the normal time-course of mRNA levels, while the *pSPL9:rSPL9* time-course (in red) corresponds to mRNA levels after the gene SPL9 has been knocked-out.

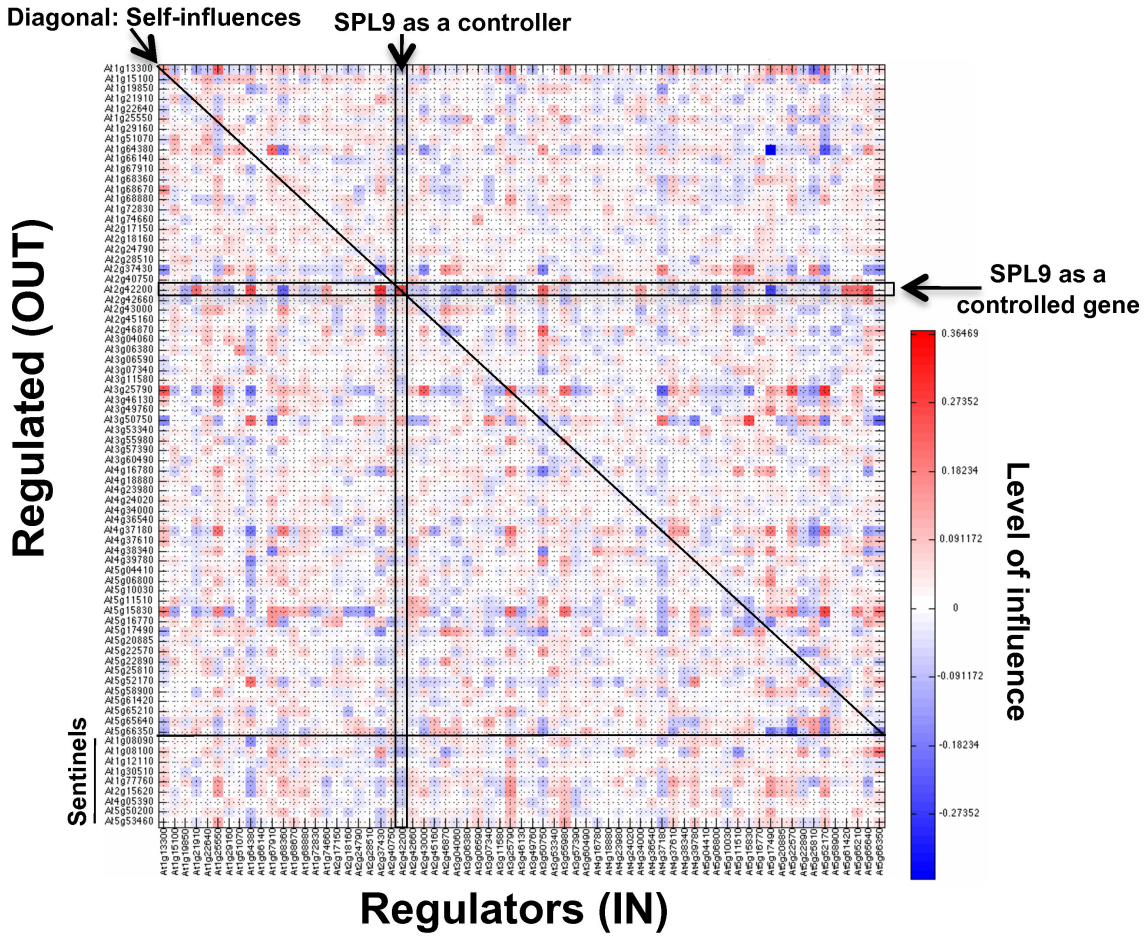

Figure 4.7: Gene Regulation Network involved in the Arabidopsis's response to NO_{3-}, represented as a matrix of signed gene-gene influences.

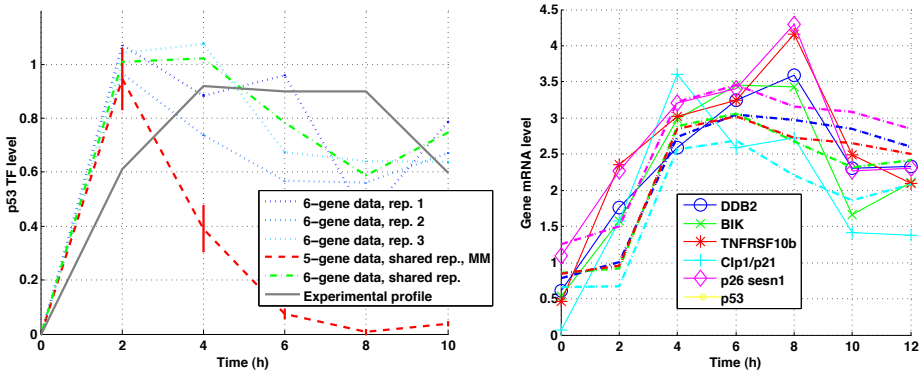

Figure 4.8: Left: inferred p53 protein levels using different techniques, compared with the experimental data using Western blots. Right: mRNA levels from replicate 1, as measured (solid line) and predicted by the 6-gene shared model (dashed line).

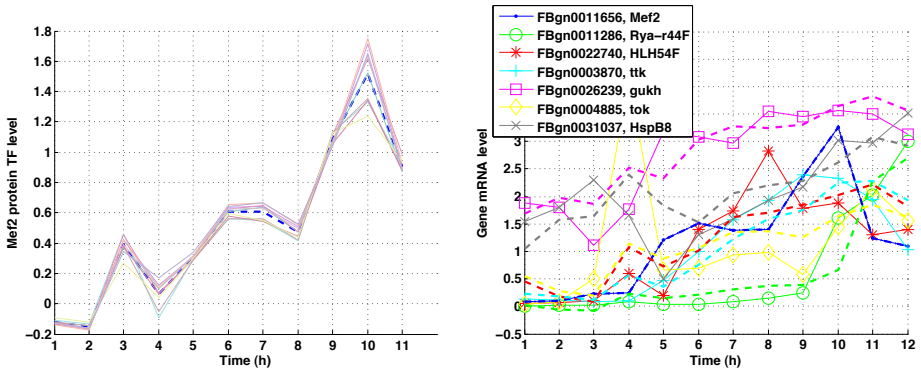

Figure 4.9: Left: inferred Mef2 protein (10 different realizations). Right: mRNA levels from replicate 1, as measured (solid line) and predicted by the model (dashed line).

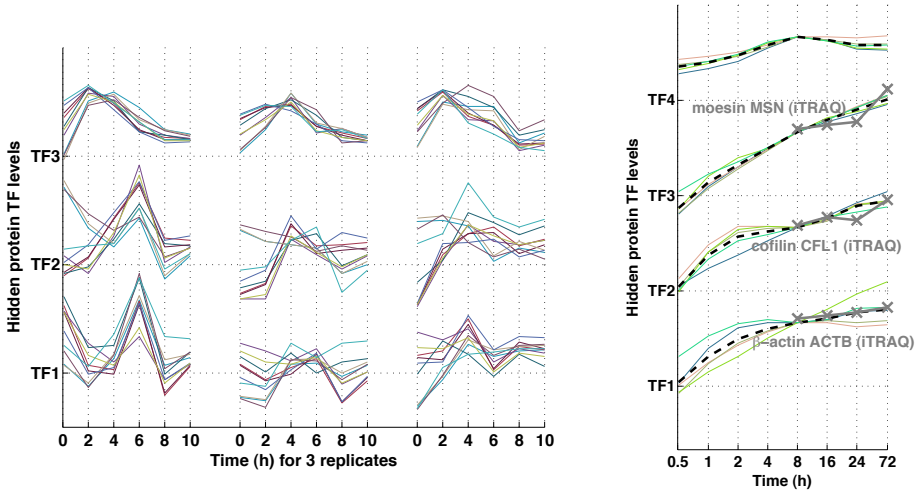

Figure 4.10: Left: inferred profiles of 3 latent variables, across 3 replicates, for the 50-gene p53 dataset. For each of the 10 realizations, the latent factors were sorted by cross-correlation among replicates. TF3 has the strongest cross-correlation and resembles the p53 experimental profile. Right: inferrred profiles of 4 latent variables for the 70-gene TGF-β dataset. TF1, TF2 and TF3 are respectively encoded by the ACTB, CFL1 and MSN genes and show very good fit to experimental iTRAQ ratios.

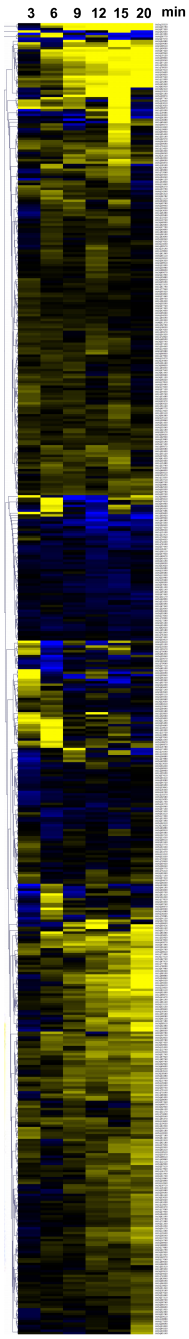

Figure 4.11: Partial view of the microarray data collected from 26 *Affymetrix* gene chips on the *Arabidopsis Thaliana* in response to NO_{3-} and to a control stimulation by KCl. The values show the $\log_2$ of the ratio between the mRNA levels for each gene in response to NO_{3-} and the same genes' mRNA levels in response to KCl. Values have been averaged over the 2 replicates, and are shown for time-points at 3, 6, 9, 12, 15 and 20 min.

Chapter 5

Application to Topic Modeling of Time-Stamped Documents

The Times They Are a-Changin'

Bob Dylan

This chapter introduces new applications for Dynamic Factor Graphs, consisting in topic modeling, text classification and information retrieval. DFGs are tailored here to sequences of time-stamped documents.

Based on the auto-encoder architecture, our nonlinear multi-layer model is trained stage-wise to produce increasingly more compact representations of bags-of-words at the document or paragraph level, thus performing a semantic analysis. It also incorporates simple temporal dynamics on the latent representations, to take advantage of the inherent (hierarchical) structure of sequences of documents, and can simultaneously perform a supervised classification or regression on document labels, which makes our approach unique. Learning this model is done by maximizing the joint likelihood of the encoding, decoding, dynamical and supervised modules, and is possible using an approximate and gradient-based maximum-a-posteriori inference.

We demonstrate that by minimizing a weighted cross-entropy loss between his-

tograms of word occurrences and their reconstruction, we directly minimize the topic-model perplexity, and show that our topic model obtains lower perplexity than the Latent Dirichlet Allocation on the NIPS and State of the Union datasets. We illustrate how the dynamical constraints help the learning while enabling to visualize the topic trajectory. Finally, we demonstrate superior information retrieval and classification results on the Reuters collection, as well as an application to volatility forecasting from financial news.

This work will be presented at the 2010 NIPS Deep Learning Workshop (Mirowski et al., 2010c), and has been submitted for publication.

5.1 Information Retrieval, Topic Models and Auto-Encoders

We propose in this article a new model for sequences of observations of discrete data, specifically word counts in consecutive (or time-stamped) text documents, such as online news, recurrent scientific publications or periodic political discourses. We build upon the classical bag-of-words approach, which ignores the syntactic dependencies between words, and focuses on the text semantics by looking at vocabulary distributions at the paragraph or document level. Our method can automatically discover and exploit sequences of low-dimensional latent representations of such documents. Unlike most latent variable or topic models, our latent representations can be simultaneously constrained both with simple temporal dependencies and with document labels. One of our motivations is the sentiment analysis of streams of documents, and has interesting business applications, such as ratings prediction. In this work, we predict the volatility of a company's stock, by capturing the opinion of investors

manifested in online news about that company.

5.1.1 Document Representation for Information Retrieval

Simple word counts-based techniques, such as the Term Frequency - Inverse Document Frequency (TF-IDF) remain a standard method for information retrieval (IR) tasks (for instance returning documents of the relevant *category* in response to a query). TF-IDF can also be coupled with a classifier (such as an SVM with linear or Gaussian kernels) to produce state-of-the-art text classifiers (Joachims, 1998; Debole and Sebastiani, 2005). We thus show in Results section 5.3.3 how our low-dimensional document representation measures up to TF-IDF or TF-IDF + SVM benchmarks on information retrieval and text categorization tasks.

Plain TF-IDF relies on a high-dimensional representation of text (over all V words in the vocabulary) and compact representations are preferable for index lookup because of storage and speed issues. A candidate for such low-dimensional representations is Latent Semantic Analysis (LSA) (Deerwester et al., 1990), which is based on singular value decomposition (SVD). Alternatively, one can follow the dimensionality reduction by independent components analysis (ICA), to obtain statistically independent latent variables (Kolenda and Kai Hansen, 2000) (and, as we show in the Results section, ICA-based LSA can achieves a better performance than simple LSA in both information retrieval and text categorization tasks). Unfortunately, because they perform lossy compression and are not trained discriminatively w.r.t. the task, SVD and ICA achieve worse IR performance than the full TF-IDF.

Instead of linear dimensionality reduction, our approach is to build *auto-encoders*. An auto-encoder is an architecture trained to provide with a latent representation (*encoding*) of its input, thanks to a nonlinear *encoder* module and an associated

decoder module. Auto-encoders can be stacked and made into a deep (multi-layer) neural network architecture (Bengio et al., 2006; Hinton and Salakhutdinov, 2006; Ranzato et al., 2007; Salakhutdinov and Hinton, 2007). A (semi-)supervised deep auto-encoder for text has been introduced in (Ranzato and Szummer, 2008) and achieved state-of-the-art classification and IR.

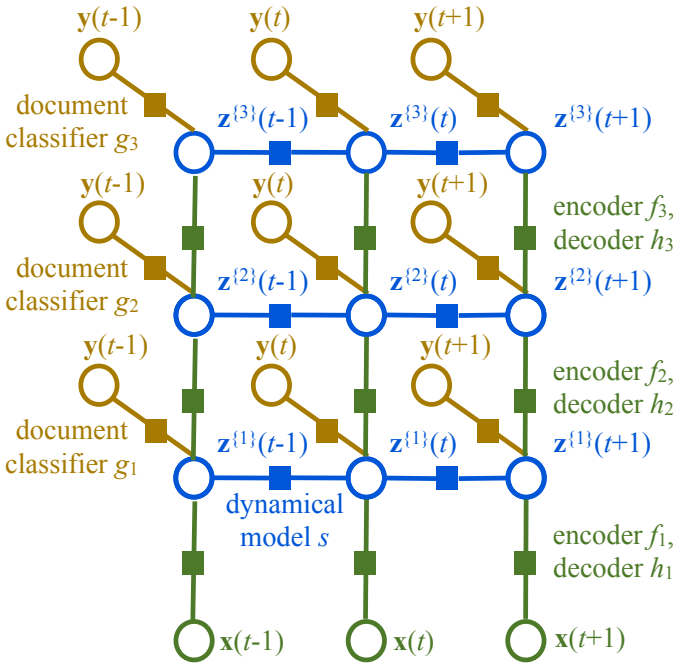

Figure 5.1: Factor Graph Representation of Our Deep Auto-Encoder Architecture with Dynamical Dependencies Between *Latent* Variables.

There are three crucial differences between our model and Ranzato and Szummer's (Ranzato and Szummer, 2008). First of all, our model makes use of latent variables. These variables are inferred though the minimization of an energy (over a whole sequence of documents) that involves the reconstruction, the temporal dynamics, the code prediction, and the category (during supervised learning), whereas in (Ranzato and Szummer, 2008), the codes are simply computed deterministically by feed-forward encoders (their inference does not involve energy minimization and relaxation). It is

the same difference as between a dynamic Bayesian net and a simple feed-forward neural net. Secondly, our cross-entropy loss function is specifically constructed to minimize topic model perplexity, unlike in (Ranzato and Szummer, 2008). Instead of merely predicting word counts (through an un-normalized Poisson regression), we predict the smoothed word distribution. This allows us to actually model topics probabilistically. Lastly, our model has a hierarchical temporal structure, and because of its more flexible nature, is applicable to a wider variety of tasks.

5.1.2 Probabilistic Topic Modeling with Dynamics on the Topics

Several auto-encoders have been designed as probabilistic graphical models in order to model word counts, using binary stochastic hidden units and a Poisson decoder (Gehler et al., 2006; Salakhutdinov and Hinton, 2007) or a Softmax decoder (Salakhutdinov and Hinton, 2009). Despite not being a true graphical model when it comes to the inference of the latent representation, our own auto-encoder approach is also based on the Softmax decoder, and, as explained in Methods section 5.2.3, we also do take into account varying document lengths when training our model. Moreover, and unlike (Gehler et al., 2006; Salakhutdinov and Hinton, 2007, 2009), our method is supervised and discriminative, and further allows for a latent dynamical model.

Another kind of graphical models specifically designed for word counts are topic models. Our benchmark is the Latent Dirichlet Allocation (Blei et al., 2003), which defines a posterior distribution of K topics over each document, and samples words from sampled topics using a word-topic matrix and the latent topic distribution. We also considered its discriminative counterpart, Supervised Topic Models (Blei and McAulife, 2007) with a simple linear regression module, on our financial prediction

task (in Results section 5.3.4). We show in Results section 5.3.1 that we managed to achieve lower perplexity than LDA.

Some topic models have introduced dynamics on the topics, modeled as Gaussian random walks (Blei and Lafferty, 2006), or Dirichlet processes (Pruteanu-Malinici et al., 2010). A variant to explicit dynamics consists in modeling the influence of a "time" variable (Wang and McCallum, 2006). Some of those techniques can be expensive: in Dynamic Topic Models (Blei and Lafferty, 2006), there is one topic-word matrix per time step, used to model drift in topic definition. Moreover, inference in such topic models is intractable and replaced either by complex Variational Bayes, or by Gibbs sampling. Finally, all the above temporal topic models are purely generative.

The major problem with the Gaussian random walks underlying (Blei and Lafferty, 2006) is that they describe a smooth dynamic on the latent topics. This might be appropriate for domains such as scientific papers, where innovation spreads gradually over time (Blei and Lafferty, 2006), but might be inexact for political or financial news, with sudden "revolutions" (as vehemently advocated in (Taleb, 2007)). For this reason, we considered Laplace random walks, that allow for "jumps", and illustrated in section 5.3.2 the trajectory of the U.S. State of the Union speeches.

5.2 Methods: Dynamic Auto-Encoders

For each text corpus, we assume a vocabulary of V unique tokens, which can be words, word stems, or named entities[1]. The input to the system is a V-dimensional bag-of-words representation $\mathbf{x}_i$ of each document i, in the form of a histogram of word counts $n_{i,v}$, with $N_i = \sum_{v=1}^{V} n_{i,v}$. To avoid zero-valued priors on word occurrences,

[1]We built a named-entity recognition pipeline, using libraries from the General Architecture for Text Engineering (http://gate.ac.uk), and relying on gazetteer lists enriched with custom lists of company names.

probabilities $\mathbf{x}_i$ can be smoothed with a small coefficient β (here set to 10^{-3}):

$$\mathbf{x}_i \equiv \frac{n_{i,v} + \beta}{N_i + \beta V} \tag{5.1}$$

5.2.1 Auto-Encoder Architecture on Bag-of-Words Histograms

The goal of our system is to extract a hierarchical, compact representation from very high-dimensional input vectors $\mathbf{X} = \{\mathbf{x}_i\}_i$ and potential scalar or multivariate labels $\mathbf{Y} = \{\mathbf{y}_i\}_i$. This latent representation consists in D layers $\mathbf{Z}^{\{l\}} = \{\mathbf{z}_i^{\{l\}}\}_i$ (where $l \in \{1, D\}$) of decreasing dimensionality $V > K_1 > K_2 > \cdots > K_D$ (see Fig. 5.1). We produce this representation using deep (multi-layer) auto-encoders (Bengio et al., 2006; Hinton and Salakhutdinov, 2006; Ranzato et al., 2007; Salakhutdinov and Hinton, 2007) with additional dynamical constraints on the latent variables. Each layer of the auto-encoder is composed of modules, which consist in a parametric deterministic function plus an error (loss) term, and can be interpreted as conditional probabilities.

The *encoder* module of the l-th layer transforms the inputs (word distribution $\mathbf{x}_i$ if $l = 1$) or variables from the previous layer $\mathbf{z}_i^{\{l-1\}}$ into a latent representation $\mathbf{z}_i^{\{l\}}$. The encoding function $f_l(\mathbf{z}_i^{\{l-1\}}) + \epsilon_i = \mathbf{z}_i^{\{l\}}$ or $f_l(\mathbf{x}_i) + \epsilon_i = \mathbf{z}_i^{\{1\}}$is parametric (with parameters noted $\mathbf{W_e}$). Typically, we use the classical *tanh* sigmoid non-linearity, or a sparsifying non-linearity $x^3/(x^2 + \theta)$ where θ is positive[2]. The mean square loss term ϵ_i represents Gaussian regression of latent variables.

Conversely, there is a linear *decoder* module (parameterized by $\mathbf{W_d}$ on the same l-th layer that reconstructs the layer's inputs from the latent representation $h_l(\mathbf{z}_i^{\{l\}}) +$

[2]The sparsifying nonlinearity is asymptotically linear but shrinks small values to zero. θ should be optimized during the learning, but we decided, after exploratory analysis on training data, to set it to a fixed value of 10^{-4}

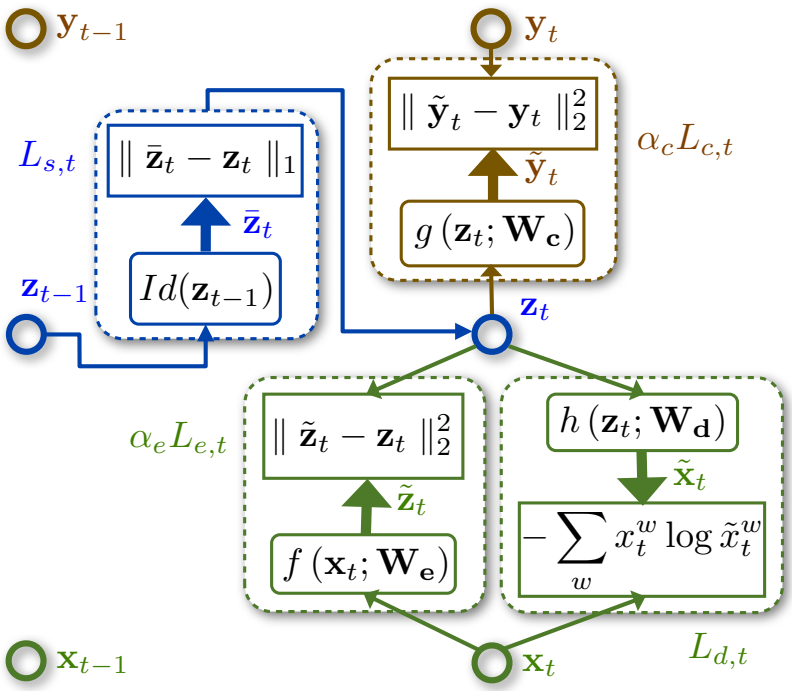

Figure 5.2: Energy-based view of the first layer of the dynamic auto-encoder. The reconstruction factor comprises a decoder module h with cross-entropy loss $\mathcal{L}_{d,t}$ w.r.t. word distribution $\{x_t^w\}_{w=1}^V$, and an encoder module f with Gaussian loss $\mathcal{L}_{e,t}$, for a total factor's loss $\alpha_e \mathcal{L}_{e,t} + \mathcal{L}_{d,t}$. The latent variables $\mathbf{z}_t$ are averaged by time unit into $\mathbf{Z}_{t'-1}, \mathbf{Z}_{t'}, \ldots$, and the latter follow Gaussian or Laplace random walk dynamics defined by the dynamical factor and associated loss $\alpha_s \mathcal{L}_{s,t'}$ (for simplicity, we assumed here 1 document for time unit t' and one for previous time unit $t'-1$). There is an optional supervised classification/regression module g (here with a Gaussian regression loss $\alpha_c \mathcal{L}_{c,t}$).

$\delta_i = \mathbf{z}_i^{\{l-1\}}$, with a Gaussian loss δ_i. Layer 1 is special, with a normal encoder but with a Softmax decoder h_1 and a cross-entropy loss term, as in (Salakhutdinov and Hinton, 2009):

$$\bar{x}_i^v = \frac{\exp(\mathbf{W}_{\mathbf{d}v} \mathbf{z}_i^{\{1\}})}{\sum_{v'} \exp(\mathbf{W}_{\mathbf{d}v'} \mathbf{z}_i^{\{1\}})} \tag{5.2}$$

The dynamical module of the l-th layer corresponds to a simple random walk from a document at time step t to next document at time step $t+1$: $\mathbf{z}_{t+1}^{\{l\}} = \mathbf{z}_t^{\{l\}} + \eta_i$. The error

term η_i can be either a sum of squared element-wise differences (L_2-norm) between the consecutive time-unit averages of latent codes of documents (i.e. a Gaussian random walk, that enforces smooth dynamics), or a sum of absolute values of those element-wise differences (L_1-norm, i.e. Laplace random walk).

There can be multiple documents with the same timestamp, in which case, there should be no direct constraints between $\mathbf{z}_{a,t}$ and $\mathbf{z}_{b,t}$ of two documents a and b sharing the same time-stamp t. In the case of such hierarchical temporal dynamics, we define a dynamic between consecutive values of the averages $< \mathbf{z} >_t$ of the latent variables from same time-unit documents (for a set I_t of N_t articles published on the same day t, each average is defined as $< \mathbf{z} >_t \equiv 1/N_t \sum_{i \in I_t} \mathbf{z}_i$). The intuition behind the time-specific averages of topics is that they capture the topic "trend" for each time stamp (e.g. year for NIPS proceedings or for State-of-the-Union speeches).

Finally, there is a classification/regression module g_l that classifies l-th layer latent variables. Typically, we considered multi-variate logistic regression (for classification problems) or linear regression with logistic loss or Gaussian loss, respectively.

Those models can be learned in a greedy, sequentially layer-wise approach (Bengio et al., 2006), by considering each layer as an approximated graphical model (see Fig. 5.2) and by minimizing its negative log-likelihood using an Expectation Maximization (EM) procedure with an approximate maximum-a-posteriori inference (see next sub-section 5.2.2). We finally prove how our learning procedure minimizes the topic model perplexity (sub-section 5.2.3).

5.2.2 Dynamic Factor Graphs and the MAP Approximation

As explained in the previous chapters of the thesis, we use the Dynamic Factor Graph formalism to express the joint likelihood of all visible and hidden variables. We re-

trieve through a MAP inference the most likely sequence of hidden topics $\mathbf{Z}$ (minimization of an unnormalized negative log-likelihood). Our gradient-based EM algorithm is a coordinate descent on the log-likelihood over the sequence:

$$\mathcal{L}(\mathbf{X}, \mathbf{Y}; \mathbf{W}) = \min_{\mathbf{Z}} \left\{ \begin{array}{ll} \mathcal{L}_d(\mathbf{X}, \mathbf{Z}; \mathbf{W}_d) & + \\ \alpha_c \mathcal{L}_c(\mathbf{Z}, \mathbf{Y}; \mathbf{W}_c) & + \\ \alpha_e \mathcal{L}_e(\mathbf{X}, \mathbf{Z}; \mathbf{W}_e) & + \\ \alpha_s \mathcal{L}_s(\mathbf{Z}) & \end{array} \right\} \tag{5.3}$$

Each iterative inference (E-step) and learning (M-step) consists in a full relaxation w.r.t. latent variables or parameters, like in the original EM algorithm. We use simple gradient descent to minimize negative log-likelihood loss w.r.t. latent variables, and conjugate gradient with line search to mimize $\mathcal{L}$ w.r.t. parameters. Because each relaxation is until convergence and done separately, everything else being fixed, the various hyperparameters for learning the modules can be tuned independently, and the only subtlety is in the choice of the weights α_c, α_e and α_s. The α_* coefficients control the relative importance of the encoder, decoder, dynamics and supervised modules in the total energy, and they can be chosen by cross-validation.

We add an additional Laplace prior on the weights and latent variables (using L_1-norm regularization, and multiplying learning rates by $\lambda_w = \lambda_z = 10^{-4}$). Finally, we normalize the decoder to unit column weights as in the sparse decomposition (Olshausen and Field, 1997). Because we initialize the latent variable by first propagating the inputs of the layer through the encoder, then doing a relaxation, the relaxation always gives the same latent variables for given parameters, inputs and labels.

As a variation on a theme, we can directly encode $\mathbf{x}_i$ using the encoders $f_1, f_2, \ldots, f_D$, like in (Ranzato and Szummer, 2008), in order to perform fast inference (e.g. for information retrieval or for prediction, as we did on experiments in sections 5.3.3 or

5.3.4).

Algorithm 2 EM-Type Learning of the Latent Representation at Layer l of the Dynamic Factor Graph

if $l = 1$ **then**
  Use bag-of-words histograms $\mathbf{X}$ as inputs to the first layer
else
  Use K_{l-1}-dimensional hidden representation $\mathbf{Z}^{\{l-1\}}$ as inputs to layer l
end if
Initialize the latent variables $\mathbf{Z}^{\{l\}}$ using K_l-dimensional ICA
while *epoch* $\leq n_{epochs}$ **do**
  // M-step on the full training sequence:
  Optimize the softmax ($l = 1$) or Gaussian decoder h_l by minim. loss $\mathcal{L}$ w.r.t. $\mathbf{W}_d$
  Optimize the nonlinear encoder f_l by minimizing loss $\mathcal{L}$ w.r.t. $\mathbf{W}_e$
  Optimize the logistic classifier or linear regressor g_l by minim. loss $\mathcal{L}$ w.r.t. $\mathbf{W}_c$
  // E-step on the full training sequence:
  Infer the latent variables $\mathbf{Z}^{\{l\}}$ using the **encoder** f_l
  Store associated loss $\mathcal{L}'(epoch)$
  Continue inference of $\mathbf{Z}^{\{l\}}$ by minim. loss $\mathcal{L}$ (Eq. 5.11) w.r.t. $\mathbf{Z}^{\{l\}}$ (relaxation)
  if encoder-only loss $L'(epoch)$ is the lowest so far **then**
    Store the "optimal" parameters $\{\mathbf{W}_e, \mathbf{W}_d, \mathbf{W}_c\}$
  end if
end while
Infer $\mathbf{Z}^{\{l\}}$ using "optimal" parameters and the encoder f_l only
Optional: continue the inference by minimizing loss $\mathcal{L}$ w.r.t. $\mathbf{Z}^{\{l\}}$

5.2.3 Minimizing Topic Model Perplexity

In the field of topic models, the perplexity measures the difficulty of predicting documents after training model $\mathbf{\Omega}$, and is evaluated on held out test sets. Under an independence assumption, and on a set $\{\mathbf{w}_i\}_{i=1}^{T}$ of T documents, containing N_i words

each, perplexity is defined in (Blei et al., 2003) as the exponential of the cross-entropy:

$$P \equiv p\left(\{\mathbf{w}_i\}_{i=1}^{T}|\Omega\right)^{-\frac{1}{\sum_{i=1}^{T} N_i}} \tag{5.4}$$

$$= \exp\left(-\frac{\sum_{i=1}^{T} \log p\left(\mathbf{w}_i|\mathbf{\Omega}\right)}{\sum_{i=1}^{T} N_i}\right) \tag{5.5}$$

In most topic models, each document i is associated with a latent representation θ_i (e.g. the multinomial posterior distribution over topics in LDA), and one assumes the document to be a bag of N_i conditionally independent words $\mathbf{w}_i = \{w_{i,n}\}_{n=1}^{N_i}$. Hence, the marginal distribution of $\mathbf{w}_i$ is:

$$p\left(\mathbf{w}_i|\mathbf{\Omega}\right) = \int_{\theta_i} p\left(\theta_i|\mathbf{\Omega}\right)\left(\prod_{n=1}^{N_i} p(w_{i,n}|\theta_i,\mathbf{\Omega})\right) d\theta_i \tag{5.6}$$

$$\approx \prod_{n=1}^{N_i} p(w_{i,n}|\tilde{\theta}_i,\mathbf{\Omega}) \tag{5.7}$$

Estimating the likelihood of a document given a topic model is intractable even for small number of topics, documents and vocabulary size, although approximate techniques based on particle filtering were recently suggested in (Buntine, 2009). Here, we use the standard approximation made by LDA, which is that the topic assignment distribution $\tilde{\theta}_i$ is inferred for each document d from observed word occurrences using variational inference (Blei et al., 2003) or Gibbs sampling (Griffiths and Steyvers, 2004). In our maximum-a-posteriori approach, we replace the full distribution over θ_i by a delta distribution with a mode at $\tilde{\theta}_i$ that maximizes the likelihood. We rewrite

equation (5.6):

$$\log p\left(\mathbf{w}_i|\tilde{\theta}_i, \mathbf{\Omega}\right) = \sum_{n=1}^{N_i} \log p(w_{i,n}|\tilde{\theta}_i, \mathbf{\Omega}) \tag{5.8}$$

$$= N_i \sum_{v=1}^{V} \frac{n_{i,v}}{N_i} \log p(v|\tilde{\theta}_i, \mathbf{\Omega}) \tag{5.9}$$

By defining the empirical conditional distribution of words in document d as $p_i(v) \equiv \frac{n_{i,v}}{N_i}$, which we substitute in (5.8), and by noting the model conditional distribution as $q_i(v) \equiv p(v|\tilde{\theta}_i.\mathbf{\Omega})$, equation (5.8) become proportional to the cross-entropy between the empirical and the model conditional distributions over words for document i: $H\left(p_i(v), q_i(v)\right) = -\sum_v p_i(v) \log q_i(v)$. Given this derivation and MAP approximation, the perplexity of our topic model can be expressed in terms of a weighted sum of cross-entropies (the weights are proportional to the documents' lengths):

$$P \approx \tilde{P} = \exp\left(\frac{1}{\sum_{i=1}^{T} N_i} \sum_{i=1}^{T} N_i H(p_i, q_i)\right) \tag{5.10}$$

Minimizing LDA perplexity (5.4) is equivalent to minimizing the negative log-likelihood of the model probabilities of words in all documents, i.e. to a maximum likelihood solution. This is what we do in our approximate maximum-a-posteriori (MAP) solution, by minimizing a weighted cross-entropy loss (5.11) with respect to both the model parameters $\mathbf{\Omega}$ and the latent representations $\{\theta_i\}_{i=1}^{T}$. Using an unnormalized latent document representation $\mathbf{z}_i$ (instead of LDA's simplex θ_i), and in lieu of model distribution q_i, our model reconstructs a V-dimensional *output* vector $\bar{\mathbf{x}}_i$ of positive values summing to 1 through the sequence of decoding functions (we write it $\tilde{\mathbf{x}}_i = h(\mathbf{z}_i)$). However, instead of integrating over the latent variables as in (5.6), we minimize the *reconstruction loss* (5.11) over the hidden representation. For a document i, the cross-

entropy $-\sum_v x_{i,v} \log \bar{x}_{i,v}$ is measured between the actually observed distribution $\mathbf{x}_i$, and the predicted distribution $\bar{\mathbf{x}}_i$.

$$\mathcal{L}_d\left(\{p_i\}_{i=1}^T; \mathbf{\Omega}\right) \equiv \min_{\{q_i\}_i} \left(\sum_{i=1}^T N_i H(p_i, q_i) \right) \tag{5.11}$$

$$= \min_{\tilde{\mathbf{x}}_i} \left(-\sum_{i=1}^T \mathbf{x}_i^T \log \tilde{\mathbf{x}}_i \right) \tag{5.12}$$

5.3 Results Obtained with Dynamic Auto-Encoders

5.3.1 Perplexity of Unsupervised Dynamic Auto-Encoders

In order to evaluate the quality of Dynamic Auto-Encoders as topic models, we performed a comparison of DAE vs. Latent Dirichlet Allocation. More specifically, for a 100-30-10-2 DAE architecture, we compared the perplexity of 100-topic LDA vs. the perplexity of the 1st layer of the DAE, then the perplexities of 30-topic LDA vs. the 2nd DAE layer, and so on for 10-topic and 2-topic LDA.

The dataset, consisting in 2483 NIPS articles published from 1987 to 2003, was separated into a training set (2286 articles until 2002) and a test set (197 articles from 2003). We kept the top $V = 2000$ words with the highest TF-IDF score. 100-, 30-, 10- and 2-topic LDA "encodings" (Blei et al., 2003) were performed using Gibbs sampling inference[3] (Griffiths and Steyvers, 2004). Our 100-30-10 DAE with encoding weight $\alpha_e = 0$ achieved lower perplexity[4] than LDA on the first two layers (see Table 5.1). We also empirically compared L_1 or L_2 dynamical penalties vs. no dynamics ($\alpha_s = 0$).

[3]Using Xuan-Hieu Phan's GibbsLDA++ package, available at http://gibbslda.sourceforge.net/, we trained Gibbs-sampled sLDA for 2000 iterations, with standard and recommended priors $\alpha = 50/M$ and $\beta = 20/V$

[4]Note that we did not evaluate the perplexity of unigram representations of text, which have been shown in (Blei et al., 2003) to perform much worse than LDA.

Table 5.1: Test Set Perplexity on NIPS Articles. We used a 100-30-10 DAE with 3 different dynamical models (none, Laplace L_1 random walk, Gaussian L_2 random walk). Each layer of DAE is compared to LDA with the same number K of latent topics. The last, 10-unit layer is outperformed by 10-topic LDA, which might be a consequence of training the model stage-wise, without a global end-to-end optimization from $\mathbf{X}$ up to the last layer $\mathbf{Z}^{\{3\}}$.

K	**LDA**	$\mathbf{DAE}_{\alpha_s=0}$	$\mathbf{DAE}^{L_1}_{\alpha_s=1}$	$\mathbf{DAE}^{L_2}_{\alpha_s=1}$
100	657	**518**	**522**	**522**
30	760	**698**	**695**	**695**
10	848	903	909	960

There was little difference between the three types on the first 2 layers. However, L_1 norm (Laplace) dynamics instead of (Gaussian) L_2 helped for further layers, as on the 3rd layer, no dynamics and L_1 decreased perplexity by 10%. Moreover, L_1 allowed a large "jump" in topic space between 2001 and 2002 (that jump was smeared out by L_2 dynamics).

5.3.2 Plotting Topic Trajectories

We reproduced a study on the U.S. State of the Union speeches from (Pruteanu-Malinici et al., 2010). We selected the top $V = 2000$ common words and named entities (using the same method as in section 5.3.4), and defined a training set consisting in 17,350 paragraphs from 196 yearly speeches through 1989, and a test set of 1965 paragraphs from 19 speeches (1990 to 2010). After training a 100-30-10-2 DAE with L_1 dynamics, we visualized the 2D topic trajectories taken by the yearly averages of latent variables on the 4th layer, and compared them with a non-dynamical DAE (same architecture) and a 3-topic LDA (with 2 degrees of freedom). As Figure 5.3 shows, using dynamics on the latent variables during the E-step inference helps

to produce a latent representation that can be useful when we expect a dynamical structure in the data.

The latter 2D latent representation provided us with a historical interpretation. It appeared that the five strongest discontinuities in the L_1 norm between 4-th hidden topics were, in that order: Harry Truman (1946), Ronald Reagan (1982, inaugural), Andrew Jackson (1829, inaugural), Woodrow Wilson (1913, inaugural) and Franklin Roosevelt (1934, inaugural), and on the test data, George W Bush (2001, inaugural), William Clinton (1996) and Barack Obama (2009, inaugural), which seemed to confirm historical intuitions.

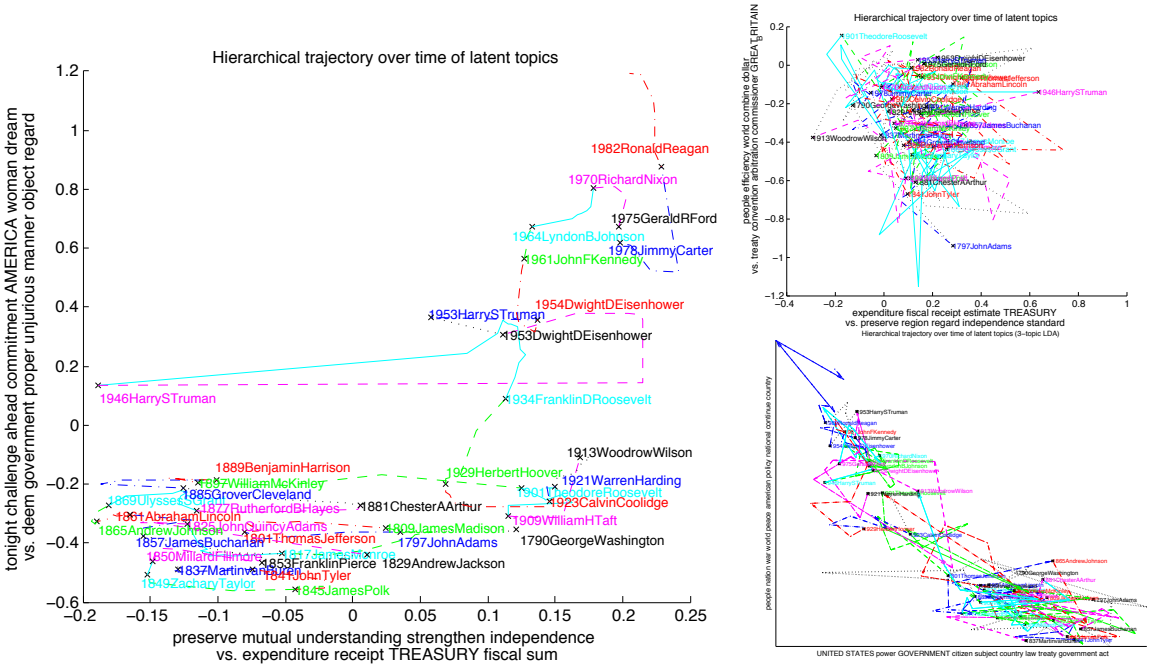

Figure 5.3: 2D "Trajectories" of State-of-the-Union Addresses. Left: We visualize the 4th layer yearly topic averages (over paragraphs) of 196 addresses, produced by a 100-30-10-2 DAE, with dynamical weight $\alpha_s = 1$. On each axis, "vs." opposes the words at the two extremes of that axis. Latent variables were inferred per paragraph and averaged by year. Top right: same figure for a DAE without dynamics ($\alpha_s = 0$). Bottom right: same figure for a 3-topic LDA (2 degrees of freedom).

Table 5.2: Test Set Perplexity on State-of-the-Union Addresses (using the same architectures as in Table 5.1).

K	**LDA**	$\mathbf{DAE}_{\alpha_s=0}$	$\mathbf{DAE}^{L_1}_{\alpha_s=1}$
100	739	**197**	**218**
30	951	**481**	**514**
10	1154	**1008**	**859**
2	1428	1553	**1206**

5.3.3 Text Categorization and Information Retrieval

The standard Reuters-21578 "ModApte" collection[5] contains 12,902 financial articles published by the Reuters news aggregator, split into 9603 train and 3998 test samples. Each article belongs to zero, one or more categories (in this case, the type of commodity described), and we considered the traditional set of the 10 most populated categories (note that both (Gehler et al., 2006) and (Ranzato and Szummer, 2008) mistakenly interpreted that collection as a dataset of 11,000 train and 4000 test single-class articles). We generated stemmed word-count matrices from raw text files using the Rainbow toolbox[6], selecting the top $V = 2000$ word stems with respect to an information gain criterion, and arranging articles by publication date.

To our knowledge, TF-IDF is the best representation for IR on the Reuters collection, and the state-of-the-art classification technique on that set remains Support Vector Machines with linear or Gaussian kernels (Joachims, 1998). We focused on linear SVMs and used the standard *liblinear* software package[7], and performed a five-fold cross-validation to select the regularization hyperparameter C through exhaustive search on a coarse, then on a fine grid.

[5] Available at Alessandro Moschitti's webpage: http://dit.unitn.it/∼moschitt/corpora.htm
[6] Andrew McCallum's toolbox is available at http://www.cs.cmu.edu/∼mccallum/bow/rainbow/
[7] See http://www.csie.ntu.edu.tw/∼cjlin/liblinear/

We compared our 100-30-10-2 DAE with a single-hidden-layer Multi-Layer Perceptron encoder to TF-IDF, TF-IDF+ICA (Kolenda and Kai Hansen, 2000), TF-IDF+SVD (Deerwester et al., 1990), LDA (Blei et al., 2003; Griffiths and Steyvers, 2004), and auto-encoders (Ranzato and Szummer, 2008). The Area Under the Precision-Recall (AUPR) curve for information retrieval (interpolated as in (Davis and Goadrich, 2006)) by TF-IDF was 0.51, and 0.54 using 10-dimensional LDA (which was by far the best among unsupervised techniques). After optimizing the inference weights on the training data ($\alpha_e = \alpha_c = 10$ and $\alpha_s = 1$), our DAE vastly outperformed TF-IDF and unsupervised techniques in terms of AUPR (see Table 5.3). For the multi-class classification task, we computed multi-class precision, recall and F_1 scores using micro and macro-averaging (Joachims, 1998; Debole and Sebastiani, 2005). Using an SVM with linear kernel trained on the latent variables, we matched full TF-IDF ($F_{1,\mu} = 0.91$, $F_{1,M} = 0.83$)[8] and outperformed TF-IDF+ICA (see Table 5.4).

Auto-encoders (Ranzato and Szummer, 2008) with the same architecture as DAE performed slightly better than DAE in terms of AUPR for IR, which might be attributed to the fact that they have no relaxation step on the latent variables during learning, only direct inference, which might help to better train the encoder. We can nevertheless claim that DAEs are close to the state of the art for information retrieval and text classification.

5.3.4 Prediction of Stock Market Volatility from Online News

There is some evidence in recent history that financial markets (over)react to public information. In a simpler setting, one can restrict this observation to company-specific news and associated stock movements, quantified with volatility σ^2. The problems of stock price movement or volatility forecasting from financial news have

[8]TF-IDF with Gaussian SVR achieved ($F_{1,\mu} = 0.92$, $F_{1,M} = 0.84$).

Table 5.3: Test Set Area Under the Prediction-Recall for Information Retrieval on Reuters-21578 Articles. We used a 100-30-10-2 DAE with 2 different dynamical models (none vs. Laplace L_1 random walk). Each layer of DAE is compared to LDA, TFIDF+ICA or TFIDF+SVD with the same number K of latent topics (TFIDF+ICA performed the best). We outperformed full TFIDF (0.51) and all unsupervised techniques. We also compared our architecture to auto-encoders in (Ranzato and Szummer, 2008) with a similar 100-30-10-2 architecture.

K	**LDA**	$\mathbf{DAE}^{\alpha_c=10}_{\alpha_s=0}$	$\mathbf{DAE}^{\alpha_c=10}_{L_1,\alpha_s=1}$	$\mathbf{DAE}^{\alpha_c=100}_{\alpha_s=0}$	$\mathbf{DAE}^{\alpha_c=100}_{L_1,\alpha_s=1}$	**R&S**
100	0.42	0.86	0.86	**0.90**	**0.89**	0.87
30	0.49	0.85	0.81	0.62	0.63	0.93
10	0.54	0.86	0.80	0.81	0.78	0.89
2	0.25	**0.73**	**0.78**	**0.71**	**0.75**	0.70

Table 5.4: Test Set Macro/Micro-Averaged F_1 Scores Using Linear SVM on Reuters-21578 Articles. We used the same architectures as in Table 5.3.

K	**ICA**	$\mathbf{DAE}^{\alpha_c=10}_{\alpha_s=0}$	$\mathbf{DAE}^{\alpha_c=10}_{L_1,\alpha_s=1}$	$\mathbf{DAE}^{\alpha_c=100}_{\alpha_s=0}$	$\mathbf{DAE}^{\alpha_c=100}_{L_1,\alpha_s=1}$	**R&S**
100	0,90, 0.81	0.91, 0.84	0.91, 0.84	**0.92, 0.86**	0.92, 0.85	0.92, 0.85
30	0.86, 0.70	0,91, 0.85	0.91, 0.83	**0.92, 0.86**	0.92, 0.85	0.92, 0.85
10	0.73, 0.40	0.91, 0.84	0.91, 0.84	**0.92, 0.86**	**0.92, 0.85**	0.92, 0.84
2	0.53, 0.09	**0.81, 0.52**	**0.85, 0.63**	**0.83, 0.54**	**0.83, 0.51**	0.75, 0.19

been formulated as supervised text categorization problems, and addressed in an intra-day setting, respectively in (Gidofalvi and Elkan, 2003) and in (Robertson et al., 2007). In the latter, it was proved that the arrival of some "shock" news about an asset j impacted its volatility (by switching to a "high-volatility" mode) for a duration of at least 15 min. In this article, we tried to solve a slightly more difficult problem than in (Robertson et al., 2007), by considering the volatility $\sigma^2_{j,t}$ estimated from daily stock prices[9] of a company j. We normalized volatility dividing it by the

[9]Stock market data were acquired at http://finance.yahoo.com. Volatility was estimated from daily open, close, high and low prices (Yang and Zhang, 2000).

median volatility across all companies j on that same day, then taking its logarithm: $y_{j,t} = \log \sigma^2_{j,t} - \log \bar{\sigma}^2_t$. Using the Bloomberg Professional service, we collected over 90,000 articles, published between January 1 and December 31, 2008, on 30 companies that were components of the Dow Jones index on June 30, 2008. We extracted each document's time stamp and matched it to the log-volatility measure $y_{j,t}$ at the earliest following market closing time. Common words and named entities were extracted, and numbers (dollar amounts, percentages) were binned. In order to make the problem challenging, we split the dataset into 51,362 test articles (after July 1, 2008, in a crisis market) and 38,968 training articles (up to June 30, 2008, corresponding to a more optimistic market).

Our benchmark was linear regression on the 2000-word TF-IDF representation, which achieved $R^2 = 0.267$. Support Vector Regression with Gaussian kernels[10] (and a Gaussian "spread" parameter equal to $\gamma = 1$) achieved a higher score of $R^2 = 0.285$. Note that kernel methods are expensive on this large Bloomberg dataset with 51k training examples. sLDA [11] (Blei and Lafferty, 2006) performed surprisingly poorly, with $R^2 < 0.1$, for 100, 30, 10 or 2 topics.

As we report in Table 5.5, our DAE with a 100-30-10-2 architecture, L_1 dynamics, *tanh* encoders f and linear decoders g achieves, at each hidden layer, a higher coefficient of determination R^2 on the test set than linear encodings (K-dimensional ICA on TF-IDF) or probabilistic topic models (K-topic LDA). We observe that the latent representation on the 3rd and 4th layer of our DAE architecture also performs better than the full high-dimensional sparse representation (TF-IDF). DAE were however outperformed by the auto-encoders from (Ranzato and Szummer, 2008), for similar

[10] We used the liblinear SVM library, available at: http://www.csie.ntu.edu.tw/ cjlin/libsvm/

[11] Using Jonathan Chang's LDA package available at http://cran.r-project.org/web/packages/lda, we trained Gibbs-sampled sLDA with 100 M steps and 20 E steps, with priors $\alpha = 50/M$ and $\beta = 20/V$

Table 5.5: Prediction of Median-Adjusted Log-Volatility From 2008 Financial News About the Dow 30 Components. We used linear regression fits on bag-of-words-derived representations ($V = 2000$). We report the coefficient of determination R^2 on the test set (articles published after June 30). The 3rd and 4th layer of DAE outperformed TF-IDF with linear regression ($R^2 = 0.267$) and the 4th layer matched TF-IDF with nonlinear Gaussian SVR ($R^2 = 0.285$) but not the non-relaxed auto-encoders by Ranzato & Szummer (Ranzato and Szummer, 2008).

K	**LDA**	**ICA**	**DAE**$_1^{L_1}$	R&S
100	0.134	0.219	0.261	0.293
30	0.083	0.155	0.263	0.297
10	0.062	-0.073	**0.271**	0.300
2	-0.036	-0.123	**0.283**	0.304

reasons as on the information retrieval tasks on the Reuters corpus from the previous section.

Finally, those compact representations of the early 2008 financial articles highlighted informative text features about stock market uncertainty: for instance, the two 2nd-layer hidden topics that were the most positive regressors of log-volatility had the following topic definitions (top 10 words): topic 1: *GM, sale, US, vehicle, BOEING, world, +20%, automaker, +10%, plant* and topic 2: *rating, credit, financial, information, debt, MOODY'S, FITCH, flow, security, AIG* .

Note that by construction, volatility has strong temporal correlation. A naive predictor for next-day volatility based solely on historical prices (or actually, on the previous' day volatility) gets a very high score of $R^2 = 0.99$. This might be the main reason why a text-based TF-IDF linear regressor of next-day log-volatility achieves a relatively good $R^2 = 0.274$, which compares to $R^2 = 0.267$ for same-day volatility.

5.4 Conclusions and Futher Work

We have introduced a new method for information retrieval, text categorization and topic modeling, that can be trained in a both purely generative and discriminative ways. It can give word probabilities per document, like in a topic model, and incorporates temporal dynamics on the topics. Moreover, learning and inference in our model is simple, as it relies on an approximate MAP inference and a greedy approach for multi-layer auto-encoders. This results in a few hours of learning time on moderately large text corpora, using unoptimized Matlab code. Our initial results on standard text collections are very promising. As further avenues of work, we are planning on designing better (nonlinear) encoder modules, and in optimizing the gradient-based algorithms for training individual components of the DAE, in order to speed-up the method for very large datasets.

5.4.1 Application to Epileptic Seizure Prediction from EEG

I am also planning on applying Dynamic Auto-Encoders to our patent-pending (Mirowski et al., 2009b) seizure prediction methodology. The latter consists in classifying patterns $\mathbf{x}_t$ of bi-variate EEG synchronization features into two types: *pre-ictal* (i.e. a few minutes before a seizure) and *interictal* (far from seizure). The motivation behind our work is that, despite the current lack of a complete neurological understanding of the pre-ictal brain state, researchers increasingly hypothesize that brainwave synchronization patterns might differentiate interictal, preictal and ictal (seizure) states (Le Van Quyen et al., 2003). The meaures that we use for synchronization are bivariate (between any two electrodes of multi-channel EEG), and can consist in such features as cross-correlation, nonlinear interdependence (Arnhold et al., 1999)

or Wavelet analysis-based phase-locking synchony (Le Van Quyen et al., 2001). In our previous published work (Mirowski et al., 2008, 2009a), we showed that by training patient-specific convolutional network classifiers, we can successfully predict all seizures without false positives on the test set, in 15 patients out of 21, using a publicly available EEG database[12], and thus obtaining state-of-the-art performance on that data, outperforming previous studies (Aschenbrenner-Scheibe et al., 2003; Maiwald et al., 2004; Schelter et al., 2006a,b; Schulze-Bonhage et al., 2006).

In my future work on epileptic seizure prediction, instead of treating it as a classification problem, I will approach it as a time-to-next-seizure y_t regression problem and introduce latent variables $\mathbf{z_t}$ with simple dynamics (L_2-norm Gaussian random walk) to add temporal consistency and thus reduce the chance of false alarms. For this reason, I will use the same auto-encoder architecture as on the volatility prediction problem, but with a simple Gaussian decoder on the first layer.

[12]This evaluation was conducted on the EEG dataset of the University of Freiburg, Germany, available at: https://epilepsy.uni-freiburg.de/

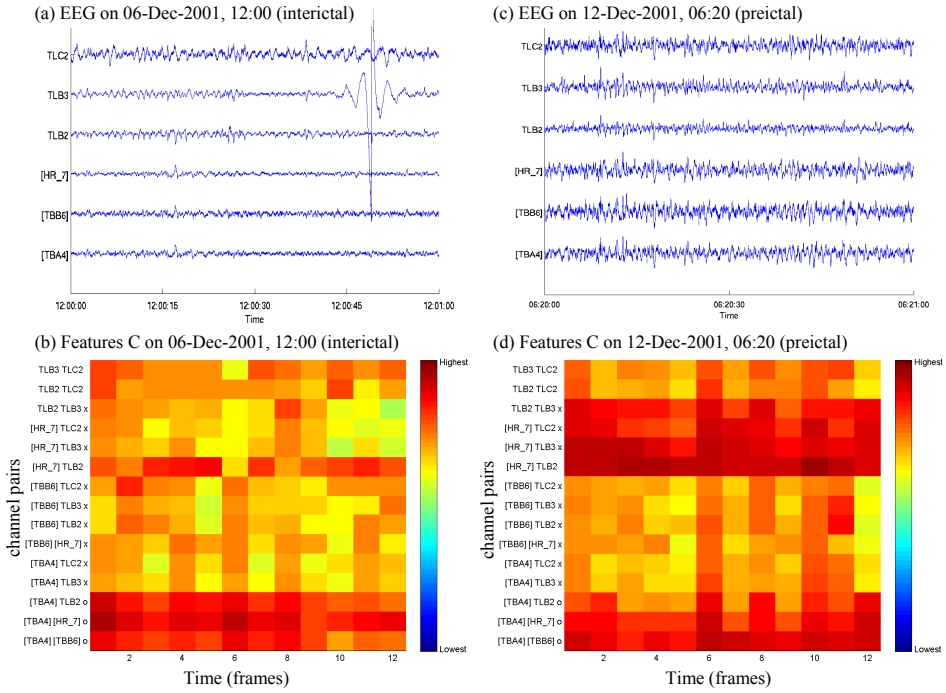

Figure 5.4: Examples of two 1-min EEG recordings (upper panels) and corresponding patterns of cross-correlation features (lower panels) for interictal (left panels) and preictal (right panels) recordings from patient 012. EEG was acquired on $M = 6$ channels. Cross-correlation features were computed on 5 s windows and on $p = M \times (M-1)/2 = 15$ pairs of channels. Each pattern contains 12 frames of bivariate features (1 min). Please note that channel TLB3 shows a strong, time-limited artifact; however, the patterns of features that we use for classification are less sensitive to single time-limited artifacts than to longer duration or repeated phenomena. This figure is reproduced from (Mirowski et al., 2009a).

Chapter 6

Application to Statistical Language Modeling

> Whenever I fire a linguist our system performance improves
>
> *At IBM Research in Speech Recognition*
>
> Frederick Jelinek

> Accepting [...] that I really said it, I must first of all affirm that I never fired anyone, and a linguist least of all.
>
> *In "Some of My Best Friends Are Linguists"*
>
> *Jelinek (2005)*
>
> Frederick Jelinek

This final applications chapter presents an adaptation of Dynamical Factor Graphs for language modeling. It was presented at the IEEE Spoken Language Technology workshop in December 2010 (Mirowski et al., 2010a), has been submitted for publication, and is the object of a patent application filed by AT&T Labs Research (Mirowski et al., 2010b). Because we are trying to model discrete events (words) using hidden variables, we resort to a major simplification in the latent variable inference. The

observation model is now simply a lookup table, which maps a 100-dimensional hidden vector to each word of the vocabulary, and contains no energy term. There is no proper relaxation on the hidden variables either, therefore we cannot call them *latent* anymore. On the upside, we gain the ability of full energy-based learning on the dynamics.

Probabilistic models of text such as n-grams require an exponential number of examples as the size of the context grows - a problem that is due to the discrete word representation. They were recently outperformed by language models that use a continuously valued and low-dimensional representation of words. In these models word probabilities result from non-linear dynamics in the latent space. We propose to build on Log-Bilinear models, and to enrich them with additional inputs such as part-of-speech tags, almost-parsed supertags, a mixture topic model and by using graph constraints based on word similarity. We demonstrate that our additions result in significantly lower perplexity on different text corpora, as well as improved word accuracy rate on speech recognition tasks, as compared to state-of-the-art N-gram and existing continuous language models.

6.1 Statistical Language Modeling

A key problem in natural language processing (both written and spoken) is designing a metric to score sentences according to their well-formedness in a language, also known as statistical language modeling. In speech recognition applications, statistical language models are generally used to rank the list of candidate hypotheses that are generated based on acoustic match to the input speech. An example is N-gram language models which assume that the probability of a word w_t depends only on a short, fixed history $\mathbf{w}_{t-n+1}^{t-1}$ of $n-1$ previous words (a Markov approximation). This

results in the joint likelihood of a sequence of T words being given by:

$$P\left(\mathbf{w}_1^T\right) = P\left(\mathbf{w}_1^{n-1}\right) \prod_{t=n}^{T} P\left(w_t | \mathbf{w}_{t-n+1}^{t-1}\right) \tag{6.1}$$

The conditional probabilities in N-gram models are estimated by keeping track of the n-gram counts in a training corpus. Their main limitation is that as the size of the history increases, the size of the corpus needed to reliably estimate the probabilities grows exponentially. In order to overcome this sparsity, back-off mechanisms (Katz, 1987) are used to approximate n^{th} order statistics with lower-order ones, and sparse or missing probabilities may be further approximated by smoothing (Chen and Goodman, 1996).

In contrast to discrete n-gram models, recently-developed Continuous Statistical Language Models (CSLM) (Bengio et al., 2003; Morin and Bengio, 2005; Schwenk and Gauvain, 2003; Schwenk, 2010; Blitzer et al., 2004; Mnih and Hinton, 2007, 2008; Mnih et al., 2009; Collobert and Weston, 2008; Sarikaya et al., 2010) *embed* the words of the $|W|$-dimensional vocabulary into a low-dimensional and continuously valued space $\Re^{|Z|}$, and rather than making predictions based on the sequence of discrete words $w_t, w_{t-1}, \ldots, w_1$ operate instead on the sequence of embedded word vectors $\mathbf{z}_t, \mathbf{z}_{t-1}, \ldots, \mathbf{z}_1$. The advantage of such models over discrete n-gram models is that they allow for a natural way of smoothing for unseen n-gram events. Furthermore, the representations for the words are discriminatively trained in order to optimize the word prediction task.

In this paper, we describe a novel CSLM that extends previously presented models. First, our model is capable of incorporating similarity graph constraints on word representations. Second, the model can efficiently use word meta-features, like part-of-speech tags or "almost parse" supertags (fragments of parse trees). Finally, the

model is also flexible enough to handle long range information derived from topic models. Thus our architecture synthesizes and extends many of the strengths of the state-of-the-art CSLMs (see Figure 6.1). While language modeling is our task and hence test perplexity is a natural evaluation metric, we also evaluate our model on word accuracy for speech recognition.

6.2 Proposed Extensions to Continuous Statistical Language Modeling

The best-known CSLM is the Neural Probabilistic Language Model (NPLM) (Bengio et al., 2003), which consists of a neural network that that takes as input a word window history, embeds this in latent space, $\mathbf{z}_{t-n+1}^{t-1}$ and is trained to directly predict the probability of the next word w_t (the probability is over the entire vocabulary). Trainable parameters of this system are both the word embedding function (the way in which words, w_t are projected to their low-dimensional representations, $\mathbf{z}_t$) as well as the network combination weights (how the $\mathbf{z}$'s in the context are combined to make the prediction). A variant of this model has been successfully applied to speech recognition (Schwenk and Gauvain, 2003) and machine translation (Schwenk, 2010).

Since the NPLM architecture does not allow constraints to be added to the word embeddings, we only adopt from this methods the non-linear architecture (single hidden layer neural network) and the trainability of the embedding. Instead we base our model on the Log-BiLinear (LBL) architecture (Mnih and Hinton, 2007, 2008; Mnih et al., 2009). This probabilistic energy-based model is trained to predict the embedding $\bar{\mathbf{z}}_t$ of the next word w_t. The key elements of the LBL architecture are explained in Sections 6.3.1, 6.3.2 and 6.3.3. We demonstrate in Section 6.4.2, that

LBL models outperform n-gram language models.

Other nonlinear classifiers (hierarchical logistic regression (Blitzer et al., 2004)) or state-space models (Tied-Mixture Language Models, (Sarikaya et al., 2010)) used for CSLM have been considered that initialize the word representation by computing a square word co-occurrence matrix (bigrams) and reducing its dimensionality through Singular Value Decomposition to the desired number of hidden factors $|Z|$. We follow this work in initializing the LBL word embeddings as explained in Section 6.3.4. We also explain there how one can impose similarity constraints on the word representation, using for instance information about word similarity from the WordNet taxonomy.

A third, major extension of our LBL model (section 6.3.5), is our incorporation of part-of-speech tag features as additional inputs, similar to the Deep Neural Networks with Multitask Learning (Collobert and Weston, 2008). The latter study, however, addresses different supervised NLP tasks other than language modeling. We also investigated the use of *supertags*, which are multi-level elements of a Tree-Adjoining Grammar (Joshi, 1987).

Finally, in Section 6.3.7, we investigate the influence of the long-range dependencies between words in the current and few previous sentences, or in the current document. For this reason, we integrate our CSLM with unsupervised topic models for text, in a spirit similar to HMM-LDA (Griffiths et al., 2005).[1] All the four proposed improvements over LBL are evaluated both in terms of language model perplexity and of speech recognition word accuracy in section 6.4.

[1]Their language model was a simple discrete bigram.

6.3 Architecture of Our Statistical Language Model with Hidden Variables

In a typical Continuous Statistical Language Model one tries to compute the probability distribution of the next word in a sequence using the distributed representation of the preceding words. One class of models tries to achieve this by capturing the dependencies/interactions between the distributed representation of the next word and the distributed representations of the preceding words in the sequence. This is achieved by defining an *energy* function (a cost) between the variables that capture these dependencies. Learning in such models involves adjusting the parameters such that low energies are assigned to the valid sequences of words and high energies to the invalid ones. This is typically achieved by maximizing the likelihood of the training corpus (LeCun et al., 2006).

6.3.1 Log-BiLinear Language Models

Log-Bilinear models, recently proposed by Mnih et al. in (Mnih and Hinton, 2007, 2008; Mnih et al., 2009) form our basic model class. Let us denote by $\mathbf{w}_1^T = [w_1 \dots w_T]$ a discrete word sequence of length T, and its corresponding low dimensional real-valued representation by $\mathbf{z}_1^T = [\mathbf{z}_1 \dots \mathbf{z}_T]$ (where $\forall t, z_t \in \Re^{|Z|}$). The LBL model tries to predict the distributed representation of the next word $\mathbf{z}_t$. It outputs $\bar{\mathbf{z}}_t$ using a linear function of the distributed representations of the preceding words $\mathbf{z}_{t-n+1}^{t-1}$, where $\mathbf{z}_{t-n+1}^{t-1}$ denotes a stacked history of the previous word embedding (a vector of length $(n-1)|Z|$):

$$\bar{\mathbf{z}}_t = \mathbf{C}\mathbf{z}_{t-n+1}^{t-1} + \mathbf{b}_\mathbf{C} = f_\mathbf{C}\left(\mathbf{z}_{t-n+1}^{t-1}\right) \tag{6.2}$$

Matrix $\mathbf{C}$ is a learnable parameter matrix that expresses the bilinear interactions between the distributed representations of the previous words and the representation of the current word. The vector $\mathbf{b_C}$ is the corresponding vector of biases. For any word w_v in the vocabulary with embedding z_v, the energy associated with respect to the current sequence is a bilinear function and is given by:

$$E(t, v) = -\bar{\mathbf{z}}_t^T \mathbf{z}_v - b_v \tag{6.3}$$

Intuitively, this energy can be viewed as expressing the similarity between the predicted distributed representation of the current word, and the distributed representation of any other word w_v in the vocabulary. The similarity is measured by the dot product between the two representations. Using these energies one can assign the probabilities to all the words w_v in the vocabulary:

$$P\left(w_t = w_v | \mathbf{w}_{t-n+1}^{t-1}\right) = \frac{e^{-E(t,v)}}{\sum_{v'=1}^{|W|} e^{-E(t,v')}}. \tag{6.4}$$

Training an LBL model involves maximizing the likelihood of all the words in a corpus, treating each word as a target. This is equivalent to minimizing the negative log likelihood $\mathcal{L}_t$ over a data set:

$$\mathcal{L}_t = E(t, v) + \log \sum_{v'=1}^{|W|} e^{-E(t,v')}. \tag{6.5}$$

6.3.2 Non-Linear Extension to LBL

The LBL model as described above is capable of capturing only linear interactions between representations of the previous words and the representation of the next

word, via the matrix $\mathbf{C}$. However, expressing it as an energy-based model allows us to add more complex interactions among the representations just as easily. This is achieved by simply increasing the complexity of the energy function. For instance, one can capture non-linear dependencies among the representations of the previous words, and the next word by adding a single hidden layer neural network, as proposed in (Mnih et al., 2009). In particular let matrices $\mathbf{A}$ and $\mathbf{B}$ be the two learnable parameter matrices and the vectors $\mathbf{b_A}$ and $\mathbf{b_B}$ be the corresponding biases. Let σ denote the tanh sigmoid transfer function which acts on hidden layer outputs. Then the prediction given by this nonlinear component, which captures non-linear dependencies among representations, is given by:

$$f_{\mathbf{A},\mathbf{B}}\left(\mathbf{z}_{t-n+1}^{t-1}\right) = \mathbf{B}\sigma(\mathbf{A}\mathbf{z}_{t-n+1}^{t-1} + \mathbf{b_A}) + \mathbf{b_B}. \tag{6.6}$$

Then, prediction by both the linear and the non-linear component of the LBL (LBLN) is given by the sum of the two terms:

$$\bar{\mathbf{z}}_t = f_{\mathbf{A},\mathbf{B}}\left(\mathbf{z}_{t-n+1}^{t-1}\right) + f_{\mathbf{C}}\left(\mathbf{z}_{t-n+1}^{t-1}\right). \tag{6.7}$$

The energy of the system is defined in exactly the same way as in equation (6.3), and the loss function is defined in the same way as in equation (6.5). The system is again trained by maximizing the likelihood of the training corpus.

6.3.3 Training the LBL(N) Model

Throughout this study the dimensions of the distributed representation of words was set to $|Z| = 100$, and the number of hidden units in the neural network were set to

500 (in the case of LBLN).

As mentioned in the previous section, training of LBLN models involves maximizing the log-likelihood of the target words in all the sequences of the training set, which is achieved by minimizing the negative log-likelihood (equation 6.5) for the corpus. This minimization is accomplished by a stochastic gradient descent procedure on mini-batches of 1000 words, as given in (Mnih and Hinton, 2007; Mnih et al., 2009). Typically, equation (6.5) is differentiated w.r.t. the prediction $\bar{\mathbf{z}}_t$, the target word representation $\mathbf{z}_w$ and the other word representations $\mathbf{z}_v$, and the gradients are propagated through the linear $\mathbf{C}$ and nonlinear $\mathbf{A}, \mathbf{B}$ modules up to the word representations $\mathbf{R}$ themselves, as well as to the respective biases. Following (Mnih and Hinton, 2007; Mnih et al., 2009), weight momentum μ is added to all parameters. In addition, the word embedding $\mathbf{R}$, and all weight matrices (except the biases) are subject to L_2-norm regularization. Table 6.1 summarizes the various hyperparameter values, some of which were taken from (Mnih et al., 2009) and others optimized by cross-validation on a small dataset.

We now discuss the various extensions to the LBLN model that we explored in the present study.

Table 6.1: Hyperparameters (Learning rates η, regularization λ and momentum μ coefficients) Used in the LBL Architecture of This Article. Values in boldface are taken from (Mnih et al., 2009).

η_C	η_A	η_B	η_R	η_F	λ	μ
$\mathbf{10^{-3}}$	$\mathbf{10^{-1}}$	$\mathbf{10^{-5}}$	$\mathbf{10^{-4}}$	10^{-4}	$\mathbf{10^{-5}}$	$\mathbf{0.5}$

6.3.4 Extension 1: Constraining the Hidden Word Embeddings

All the parameters $\mathbf{A}, \mathbf{B}, \mathbf{C}, \mathbf{R}$ are initialized randomly. We use the rule of thumb of generating zero-mean normally distributed words of variance equal to the inverse of the matrix *fan-in* (LeCun et al., 1998b). Biases are initialized to zero, with the exception of b_v, which are initially equal to the unigram statistics of the training data. Some CSLM architectures (Blitzer et al., 2004; Sarikaya et al., 2010) are however dependent on the initial hidden word representation, and in order to evaluate this dependency, we followed a procedure similar to (Sarikaya et al., 2010) which initializes $\mathbf{R}$ using Singular Value Decomposition on the bi-gram (n-gram) co-occurrence matrix.

As can be shown in section 6.4.4, the low-dimensional nature of the word embedding in CSLMs ($|Z| << |W|$, with $|Z| = 100$ and $|W|$ typically over 10,000) and the word co-occurrence in the text tend to cluster word representations $\mathbf{z}_w$ according to their syntactic co-occurrence and semantic equivalence. In order to speed-up the learning of our model and to potentially help achieve better performance, we considered imposing a graph constraint on the words. For each word w, we defined its neighborhood N_w obtained through the hierarchical WordNet[2] tree and using the *WordNet::Similarity* module[3] (specifically, we used Resnik similarity (Resnik, 1999), keeping in N_w only words whose Resnik score was higher than 8). During learning time, the graph constraint was imposed by adding a penalty term $\gamma \sum_{w=1}^{|W|} \parallel \mathbf{z}_w - \frac{1}{|N_v|} \sum_{v \in N_w} \mathbf{z}_v \parallel_2^2$ to the total log-likelihood (we set $\gamma = 1$).

[2]See http://wordnet.princeton.edu

[3]Available at http://wn-similarity.sourceforge.net/

6.3.5 Extension 2: Adding Part-Of-Speech Tags

The most important improvement over the LBL (Mnih and Hinton, 2007) and the LBLN (Mnih et al., 2009) was the addition of Part-of-Speech (POS) tags to each word. Conceptually, this step is identical to the word embedding: for each word, discrete POS tags (out of a vocabulary of $|X|$, here between 30 and 52) are mapped into a low-dimensional embedding $\Re^{|Z_X|}$ through a linear operation (matrix $\mathbf{F}$). The matrix $\mathbf{F}$ was also initialized randomly in the same way as discussed in Section 6.3.4. We also considered the case $|X| = |Z_X|$, with an identity transform $\mathbf{F} = \mathbf{I}_{|\mathbf{X}|}$. Those tags can then be concatenated with the $|Z_W|$-dimensional word representations into a history of $n-1$ word and feature representations, and used as an input to the predictive model (Figure 6.1), just like in (Collobert and Weston, 2008). As explained below, POS tag features can be trivially extended to accommodate other types of word features.

6.3.6 Extension 3: Incorporating Supertags

Supertags are elementary trees of a lexicalized tree grammar such as a Tree-Adjoining Grammar (TAG) (Joshi, 1987). Unlike context-free grammar rules which are single level trees, supertags are multi-level trees which encapsulate both predicate-argument structure of the anchor lexeme (by including nodes at which its arguments must substitute) and morpho-syntactic constraints such as subject-verb agreement within the supertag associated with the anchor. There are a number of supertags for each lexeme to account for the different syntactic transformations (relative clause, *wh*-question, passivization etc.). For example, the verb *give* will be associated with at least these two trees, which we will call tdi and tdi-dat, illustrated below:

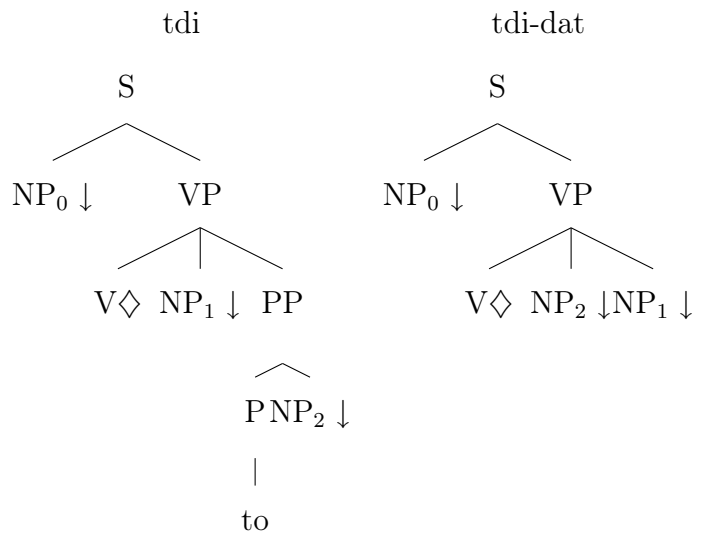

Supertagging is the task of disambiguating among the set of supertags associated with each word in a sentence, given the context of the sentence. In order to arrive at a complete parse, the only step remaining after supertagging is establishing the attachments among the supertags. Hence the result of supertagging is termed as an "almost parse" (Bangalore and Joshi, 1999). We use the same set of 500 supertags derived from the Penn Treebank as discussed in (Bangalore, 1997) in the experiments for this paper.

6.3.7 Extension 4: Topic Mixtures in LBL(N)

A fourth improvement over the LBL and LBLN architecture that we considered was the long-range dependency of the language model on the current topic, simplified as a dependency on the bag-of-words vocabulary statistics. Our main motivation was that such a context-dependent model would enable domain adaptation of the latent embedding and combination weights. This adaptation can be done at document-level (or paragraph-level). When proper document segmentation is not available, such as in broadcast transcripts, a "document" can be defined by considering the last D sentences, assuming that the speakers do not change topic too often.

We decided to implement a topic model based on the popular Latent Dirichlet Allocation[4] (Blei et al., 2003), a graphical model that is trained to extract a word-topic matrix from a collection of documents, and that can infer latent topic posterior distributions θ_d for each test document d. As can be seen on Fig. 6.1, the K-dimensional topic vector (where $\sum_k \theta_k = 1$) can be used as weights of a mixture model. Because the predictions made by each component of the mixture add-up for the final prediction $\overline{\mathbf{z}}_t$ (6.8), the implementation of the topic-dependent LBL(N) architecture is a simple extension of the previously described LBLN-based architectures.

$$\overline{\mathbf{z}}_t = \sum_{k=1}^{K} \theta_k \left(f_{\mathbf{C}_k} \left(\mathbf{z}_{t-n+1}^{t-1} \right) + f_{\mathbf{A}_k, \mathbf{B}_k} \left(\mathbf{z}_{t-n+1}^{t-1} \right) \right) \tag{6.8}$$

As can be seen in the next section, adding a topic model mixture holds promise in terms of language model perplexity but still requires additional experimental evaluation.

Note that we could have used the topic model developed in Chapter 5 of my thesis, but we initially preferred an out-of-the-box solution provided by LDA. Another reason for our choice of topic models was the fact that LDA computes a topic simplex (multinomial distribution over topics) which is very handy for mixture model weights.

6.4 Results Obtained with Feature-Rich Log-BiLinear Language Model

The following section summarizes several sets of experiments performed on four distinct datasets (section 6.4.1), aimed at assessing the test set perplexity of the respective language models (section 6.4.2), and at measuring the word accuracy performance

[4]We used the Gibbs-based implementation of LDA, available at http://gibbslda.sourceforge.net/

for speech recognition tasks (section 6.4.3). Finally, we illustrate the power of clustering words with low-dimensional representations (section 6.4.4).

6.4.1 Language Corpora

We have evaluated our models on five distinct, public datasets: 1) the *Airline Travel Information System* (ATIS), a small corpus containing short sentences concerning air travel, 2) the *Wall Street Journal* (WSJ) set, containing sentences from business news, 3) the *Reuters-21578* corpus[5] of business news articles, which is normally used for text categorization, 4) *TV broadcast news transcripts HUB-4* from the LDC (reference 2000S88), with audio information, and 5) the large *AP News* corpus used in (Bengio et al., 2003; Mnih and Hinton, 2007, 2008; Mnih et al., 2009). Table 6.2 summarizes the statistics of each dataset.

For the WSJ set, we used POS tags to identify and replace all numbers (tag CD) and proper nouns (tags NNP and NNPS), as well as words with 3 or fewer occurrences, by generic tags resulting in a considerable reduction in the vocabulary size. For the Reuters set, each article was split into sentences using the Maximum Entropy sentence-splitter by Adwait Ratnaparkhi[6], and then tagged using the Stanford Log-linear Part-of-Speech Tagger[7]. We replaced numbers and rare words (i.e. appearing less than four times) by special tags, as well as out-of-vocabulary test words by *{unk}*. For the HUB-4 corpus, we obtained 100-best hypotheses for each audio file in the test set using a speech recognition system comprising of a trigram language model that was trained on about 813,975 training sentences. In all the experiments but on AP News, 5% of the training data were set apart during learning for cross-validation (the model with the best performance on the cross-validation set was retained). The

[5]See: http://disi.unitn.it/moschitti/corpora.htm
[6]See: http://sites.google.com/site/adwaitratnaparkhi/
[7]See: http://nlp.stanford.edu/software/tagger.shtml

1M-word validation set of AP News had already been defined.

Table 6.2: Description of the datasets evaluated in this study: size of vocabulary $|W|$, number of training words T_{tr} and sentences/documents D_{tr}, number of test words T_{te} and sentences/documents D_{te}.

Dataset	$\|W\|$	T_{tr}	D_{tr}	T_{te}	D_{te}
ATIS	1,311	116k	11k	23k	2,369
WSJ	10,222	1,079k	46k	42k	2,266
Reuters	11,742	1,445k	10k	462k	3,299
AP News	17,964	13,995k	649k	963k	46k
HUB-4	25,520	813k	19k	32k	827

6.4.2 Decrease in Language Model Perplexity

Assuming a language model is defined by the conditional probability distribution q over the vocabulary, its perplexity intuitively corresponds to a word uncertainty given a context. On a corpus of T words, it is defined as:

$$p = \exp\left(-\frac{1}{T}\sum_{t=1}^{T}\log P\left(w_t|\mathbf{w}_{t-n+1}^{t-1}\right)\right) \tag{6.9}$$

In the absence of task-specific evaluation, such as word accuracy for speech recognition, perplexity is the measure of choice for language models. Therefore, and similar to (Bengio et al., 2003; Mnih and Hinton, 2007, 2008; Mnih et al., 2009), we used perplexity to compare our continuous language models to probabilistic n-gram models. We chose the best performing n-gram models that include a *back-off* mechanism for handling unseen n-grams (Katz, 1987) and the Kneser-Ney smoothing of probability estimates (Chen and Goodman, 1996), using an implementation provided by the SRI Language Modeling Toolkit[8] (Stolcke, 2002). We did not consider n-gram models ex-

[8]See: http://www-speech.sri.com/projects/srilm/

tended with POS tags. For each corpus, we selected the n-gram order that minimized the test set perplexity.

We performed an extensive evaluation of many configurations of the LBL-derived architectures and improvements. All the results presented here were achieved in less than 100 learning epochs (i.e. less than 100 passes on the entire training set), and with the set of hyperparameters specified in Table 6.1. As can be seen in Tables 6.3, 6.4, 6.5 and 6.6, most of the linear and all the non-linear LBL language models are superior to n-grams, as they achieve a lower perplexity. Various initializations (random or bi-gram/n-gram SVD-based) or *WordNet::Similarity* constraints do not seem to significantly improve the language model for LBLNs, and they might even be detrimental to linear LBLs.

We markedly reduced the perplexity of LBL and LBLN when using word features such as POS tags or supertags, as inputs to the model. The relative improvement was between 5% and 10% on ATIS (using all the 30 POS tags as inputs to the dynamical model), around 2%-5% on WSJ when using a 5-dimensional embedding of POS tags, of 5% on the Reuters corpus, and slightly below 3% for AP News. Supertags achieved a drastic reduction in perplexity between 20% and 25% on the WSJ set.

Table 6.3: Language model perplexity results on the ATIS test set. LBLN with 200 hidden nodes, $|Z_W| = 100$ dimensionial word representation and all $|Z_X| = 30$ POS tags achieved the lowest perplexity (below 11.6), outperforming the Kneser-Ney 4-gram model (13.5). Bigram SVD-derived initialization and *WordNet::Similarity* graph constraints on word embeddings did not improve LBLN results, and worsened LBL's.

	LBL	LBL POS	LBLN	LBLN POS
no constraints	15.45	14.30	12.32	**11.60**
rand. + graph	16.14	14.65	12.35	**11.48**
SVD init	15.96	14.51	12.37	**11.54**
SVD + graph	16.38	14.90	12.39	**11.61**

Taking advantage of the small size of the ATIS dataset, we investigated the influence of several hyper-parameters on the performance of the LBL model: the linear model learning rate η_C, as well as the word embedding learning rate η_R, the first layer η_A and second layer η_B nonlinear module learning rates. We conducted an exhaustive search on a coarse grid of the above hyper-parameters, assuming an LBL(N) architecture with $|Z_W| = 100$ dimensional word representation and $|H| = 0$, 50, 100 or 200 hidden nonlinear nodes, as well as $|Z_X| = 0$ or 3 dimensional embedding of POS tag features. Evidently, as suggested in (Mnih et al., 2009), the number of hidden non-linear nodes had a positive influence on the performance, and our addition of POS tags were beneficial to the language model. Regarding the learning rates, the most sensitive rates were η_R and η_C, then η_A and finally η_B. The optimal results were achieved for the hyper-parameter values in Table 6.1. We then selected the optimal LBLN architecture with $|Z_W| = 100$ and $|H| = 200$ and further evaluated the joint influence of the feature learning rate η_F, the graph constraint coefficient γ, the dimension of the POS tag embedding $|Z_X|$, and the random or bigram initialization of the word embeddings. The most important factor was η_F, which needed to be smaller than 10^{-3}, and the presence or absence of POS features (larger embedding sizes did not seem to significantly improve the model).

In a subsequent set of experiments, we evaluated the benefit of adding a topic model to the (syntactic) language model, focusing on the Reuters and AP News datasets (organized in documents) and on the HUB-4 transcripts (a window of five consecutive sentences was treated as a document; results reported in section 6.4.3). We used the standard Latent Dirichlet Allocation topic model to produce a simplex of topic posteriors $\{\theta_{t,1}, \ldots, \theta_{t,K}\}$ for $K = 5$ topics, for each "document", and used these coefficients as weights of a 5-mixture model. We retained, for each mixture component, the same LBL and LBLN architectures as in the previous experiments,

Table 6.4: Language model perplexity results on the WSJ test set. Kneser-Ney 5-grams attain a perplexity of 86.53. Similar architectures to the one in Table 6.5 were used. While the benefit of initializing the word representation and enforcing *WordNet::Similarity* graph constraints (noted as {**R**}) is not obvious, POS tags clearly reduce the perplexity of LBL and LBLN, and supertags are even better. We control for the size $|Z_X|$ of the feature embedding, showing that supertags are far superior to POS tags. Learning was stopped after 100 epochs, and results in italics show LBL models that did not reach their optimum.

	LBL	LBL {**R**}	LBLN	LBLN {**R**}
No features	*93.4*	*98.0*	84.9	84.4
$\|Z_X\|_{POS} = 5$	*90.3*	*95.8*	82.6	81.1
$\|Z_X\|_{POS} = 50$	*88.7*	*93.5*	83.0	82.6
$\|Z_X\|_{super} = 50$	69.6	72.4	**66.7**	**66.3**

and experimented with adding POS features. As Table 6.5 suggests, adding a topic model improved the plain LBL perplexity (but not LBLN's) on the medium-size Reuters set, and it significantly improved the perplexity on the large AP News corpus (the combined topic+POS reduction in perplexity was 8% on both LBL and LBLN).

6.4.3 Increase in Speech Recognition Word Accuracy

In Table 6.7, we present the results of speech recognition experiments using our language model. We used AT&T Watson ASR (Goffin et al., 2005) (with a trigram language model trained on HUB-4 training set) to produce 100-best hypotheses for each of the test audio files of the HUB-4 task. The 1-best and the 100-best oracle word accuracies are 63.7% and 66.6% respectively. Using a range of language models (including a 4-gram discrete LM), we re-ranked the 100-best hypotheses according to LM perplexity (ignoring the scores from ASR), and selected the top one from each list. The top-ranking hypothesis resulting from LBLN models had significantly better word accuracies than any discrete language models. Adding a topic mixture

Table 6.5: Language model perplexity results on the Reuters test set. All LBL(N)s had $|Z_W| = 100$ dimensional word representation, and LBLNs had 500 hidden nodes. Word representations were optionally initialized by SVD on 5-gram co-occurrence matrices. LBLNs with POS tags embedded into $|Z_X| = 5$ dimensions outperformed not only the Kneser-Ney 5-gram model, but also the vanilla LBLN. Adding a $K = 5$ dimensional topic mixture based on LDA posteriors (i.e. creating a 5-mixture model of LBL and LBLN) seemed to improve the perplexity of LBL but not of LBLN.

Method	Init.	POS $\|Z_X\|$	Topics	Perplex.
5-gram	-	-	-	80.78
LBL	rand.	-	-	78.30
LBL	rand.	-	5	73.12
LBLN	rand.	-	-	63.92
LBLN	SVD	-	-	63.67
LBLN	**rand.**	**5**	-	**60.34**
LBLN	**SVD**	**5**	-	**60.42**
LBLN	rand.	-	5	65.50
LBLN	SVD	-	5	66.74
LBLN	**rand.**	**5**	**5**	**61.85**
LBLN	**SVD**	**5**	**5**	**62.07**

model further increased the word accuracy on the HUB-4 dataset compared to vanilla LBLN. In order to measure the efficacy of the language model in selecting the correct hypothesis if it were present in the k-best list, we included the reference sentence as one of the candidates to be ranked. Table 6.8 shows that we significantly outperformed the best n-gram model on this task as well.

Finally, we compare the trade-off between the language model and the acoustic model. It can be seen that the acoustic model alone produces poor predictions. We noticed that combining the acoustic model with language model makes good predictions only when the language model is given a stronger (even infinite) weight, which is due to the fact that we are operating on a 100-best list.

Table 6.6: Language model perplexity results on the AP News test set. We evaluated LBL(N) architectures with $|Z_W| = 100$ dimensions for the word representation, and replicated the results from (Mnih et al., 2009) for the LBL and 500-hidden node LBLN architectures. We also evaluated the impact of adding 40 part-of-speech tags (with a $|Z_X| = 40$-dimensional representation) and K-topic models. Although the results that we obtained on vanilla LBL(N) had a little higher perplexity than in (Mnih et al., 2009), we nonetheless considerably improve upon LBLN using either POS features or topics (or both). We ultimately beat both the state-of-the-art LBLN and Gated LBLN architectures from (Mnih et al., 2009), as well as the Neural Probabilistic Language Model (Bengio et al., 2003) (marked with a $*$). We did not consider trivial improvements such as combining LBLs with probabilistic n-grams, or extending the size of the context to 10.

Method	$\|H\|$	POS $\|Z_X\|$	Topics	Perplex.
KN 5-gram	-	-	-	123.2
LBL	-	-	-	127.7
LBL	-	40	-	123.6
LBL	-	-	5	121.0
LBL	-	40	5	117.5
LBLN	500	-	-	104.4
LBLN	500	40	-	101.5
LBLN	**500**	-	**5**	**98.5**
LBLN	**500**	**40**	**5**	**96.1**
*NPLM**	500	-	-	109.0
*LBL**	-	-	-	117.0
*LBLN**	500	-	-	99.0
*GLBLN**	500	-	-	96.8

6.4.4 Examples of Word Embeddings on the AP News Corpus

For the visualization of the word embedding, we chose the AP News corpus (although it is smaller than the 386M word and 30k vocabulary Wikipedia set from (Collobert and Weston, 2008)). Table 6.9 illustrates the word embedding neighborhood of a few randomly selected "seed" words, after training an LBLN with POS tag features and a 5-topic mixture. Although word representations were initialized randomly and *WordNet::Similarity* was not enforced, we clearly succeeded in capturing functionally and

Table 6.7: Speech recognition results on the HUB-4 task. For each target sentence, 100-best lists were produced by the AT&T Watson system, and language models were used to select the candidate with lowest NLL score. We indicate the best and worst possible word accuracies that can be achieved on these lists ("Oracle"), as well as the one obtained by the acoustic model alone. LBLNs with 5-topic mixture models, and either POS tag features or bigram SVD-derived initialization achieve the highest word accuracy, outperforming a state-of-the-art speech recognition baseline, Kneser-Ney 4-gram models, and plain LBLNs.

Method	Accuracy
AT&T Watson	63.7 %
100-best list, acoustic model only	61.7 %
100-best list, "oracle"	66.6 %
Worst "oracle" on 100-best list	57.8 %
Back-off KN 4-gram	63.5 %
LBLN	64.1 %
LBLN+init	64.2 %
LBLN+POS(34)	64.1 %
LBLN+POS(34)+init	64.2 %
LBLN+topics	64.2 %
LBLN+topics+init	**64.6 %**
LBLN+POS(5)+topics	**64.3 %**
LBLN+POS(3)+topics+init	**64.6 %**

semantically (e.g. both synonymic and antonymic) similar words in the neighborhood of these seed words.

To provide with a simpler representation of the word embeddings, we further projected them onto a two-dimensional plan using the t-SNE algorithm (Van der Maaten and Hinton, 2008). Figures 6.2, 6.3, 6.4, 6.5 and 6.6 respectively illustrate the full word embedding, as well as details focusing on "country names", "US states", "occupations" and "verbs".

Table 6.8: Speech recognition results on HUB-4 transcripts. We used the same training and test sets as in Table 6.7, but with the true sentence to be predicted included among the 101-best candidates.

Method	Accuracy
Back-off KN 4-gram	86.9 %
LBLN+POS+init	**94.0 %**
"Oracle"	100 %

6.4.5 Computational Requirements

We implemented our LBL-derived architectures under Matlab. The training was linear in the size of the dataset (i.e. the number of words). As observed for previous CSLM models (Bengio et al., 2003) or (Mnih and Hinton, 2007), the bulk of the computations consisted in evaluating the word likelihood (6.4) and in differentiating the loss (6.5), which was theoretically linear in the size of the vocabulary $|W|$. However, thanks to the BLAS and LAPACK numerical libraries, it was sublinear in practice. Typically, training our LBL architectures on moderately sized datasets (*WSJ*, *Reuters* and *TV broadcasts*) would take about a day on a multi-core server. Because of the possible book-keeping overhead that might arise from sampling approximations, or because of the decreased language model performance (higher perplexity) when hierarchical word representation are used (Morin and Bengio, 2005), or of the LBL (Mnih and Hinton, 2008), we restrict ourselves to the exact solution.

6.5 Conclusions

We presented an energy based statistical language model with a flexible architecture that allows for novel and diverse extensions of the log-bilinear model formulated in (Mnih and Hinton, 2007, 2008; Mnih et al., 2009). We also explored initializations

Table 6.9: Examples of 10 closest neighbors in the $\Re^{100}$ word embedding space on AP News. We used the best LBLN+POS+topics architecture from Table 6.6. The 7 **seed words** were selected *randomly*, and cosine similarity was used to compare any two word vectors.

frustrations	**tried**	**immune**	**marble**
feelings	stopped	harmful	granite
achievements	threatened	resistant	velvet
accomplishments	sought	susceptible	bronze
advantages	decided	prone	silk
origins	returned	addictive	leather
vigor	met	abnormal	flower
successes	moved	transmitted	mahogany
weaknesses	kept	unsafe	brick
strength	refused	beneficial	neon
enthusiasm	offered	harmless	wooden

crime_rate	**technologies**	**savings_and_loans**
work_force	industries	thrift
standard_of_living	systems	law_firm
inflation_rate	foods	estate
budget_deficit	brands	investment_company
unemployment_rate	carriers	real_estate
demise	laboratories	transaction
stock_market	suppliers	bank_account
peso	enterprises	guaranty
value	products	cartel
net	methods	corporation

of word embeddings and word similarity constraints via a word-graph, with mixed results, but we demonstrated consistent and significant predictive improvements by incorporating part-of-speech tags or supertags as word features, as well as long range (document level) topic information. Our results show that our model significantly advances the state-of-the-art, beating both n-gram models and the best continuous language models on test perplexity. Finally, we demonstrated the utility of this improved language modeling by obtaining better word accuracy on a speech recognition task.

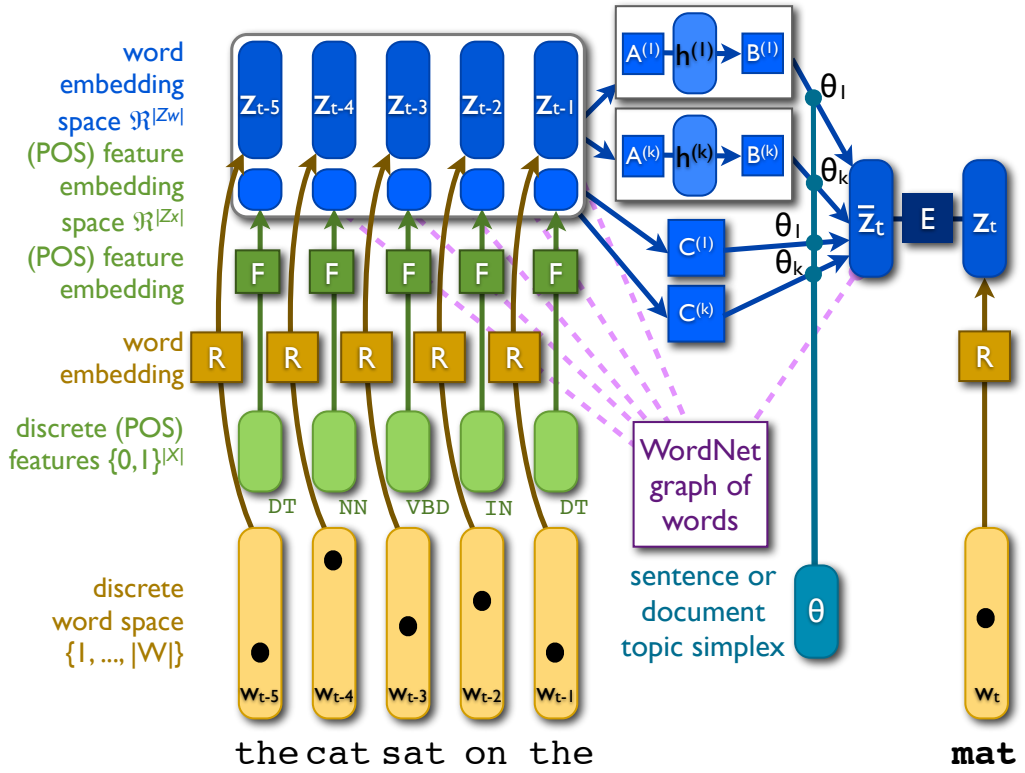

Figure 6.1: Enhanced log-biLinear architecture. Given a word history $\mathbf{w}_{t-n+1}^{t-1}$, a low-dimensional embedding $\mathbf{z}_{t-n+1}^{t-1}$ is produced using $\mathbf{R}$ and is fed into a linear $\mathbf{C}$ matrix, as well as into a non-linear (neural network) architecture (parameterized by $\mathbf{A}$ and $\mathbf{B}$) to produce a prediction $\bar{\mathbf{z}}_t$. If one uses a topic model with K topics, the predictor becomes a mixture of K modules, controlled by topic weights $\theta_1, \ldots, \theta_K$ obtained for the current sentence of document from a topic model such as LDA. That prediction is compared to the embedding of all words in the vocabulary using a log-bilinear loss E, which is normalized to give a distribution. Part-of-Speech features can be also embedded using matrix $\mathbf{F}$, alongside the words, and the embeddings can have WordNet::Similarity constraints.

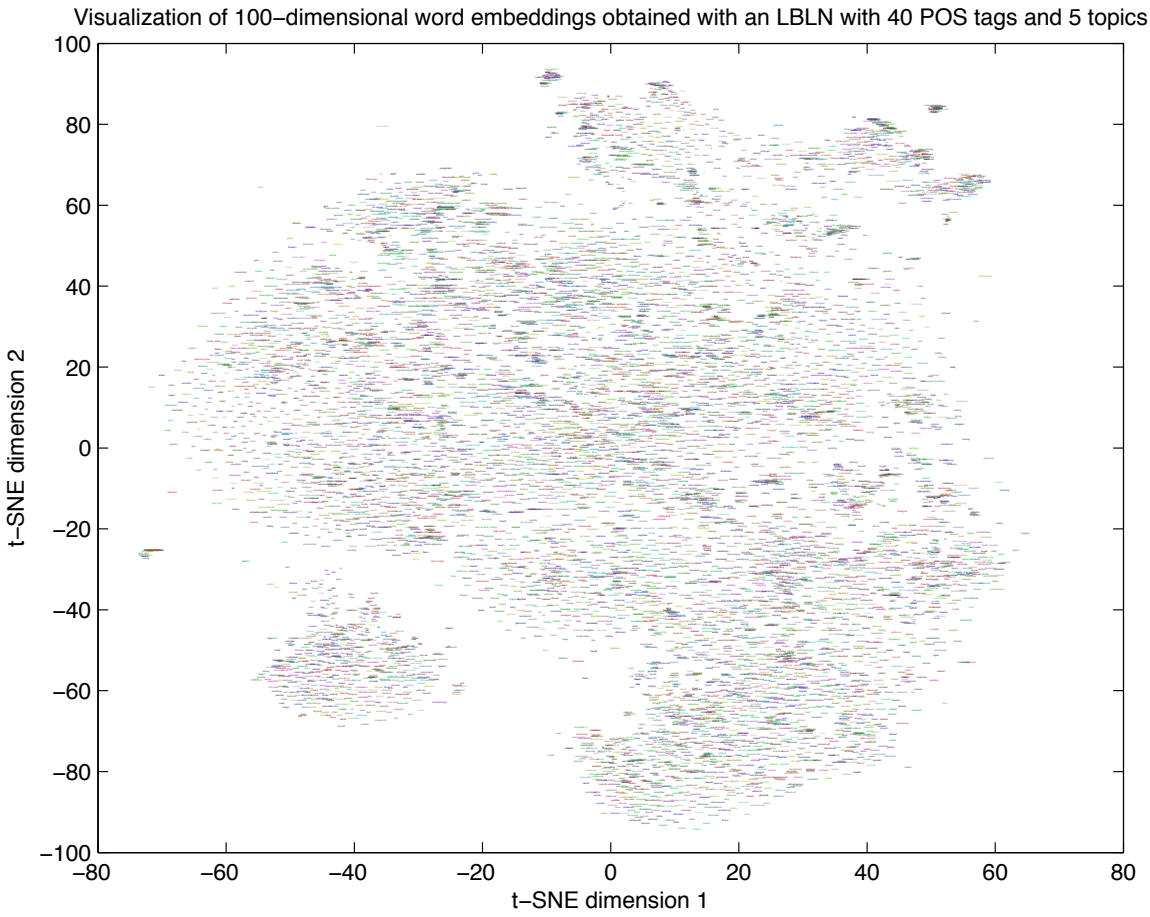

Figure 6.2: 2D representation of the word embedding, obtained by applying the t-SNE algorithm on the word embedding matrix $\mathbf{R}$ from our best LBLN architecture with POS tags and topic mixtures. Only 8983 words are shown out of the full 17965-word vocabulary. This figure requires is designed for the electronic version of the document, as it requires zooming.

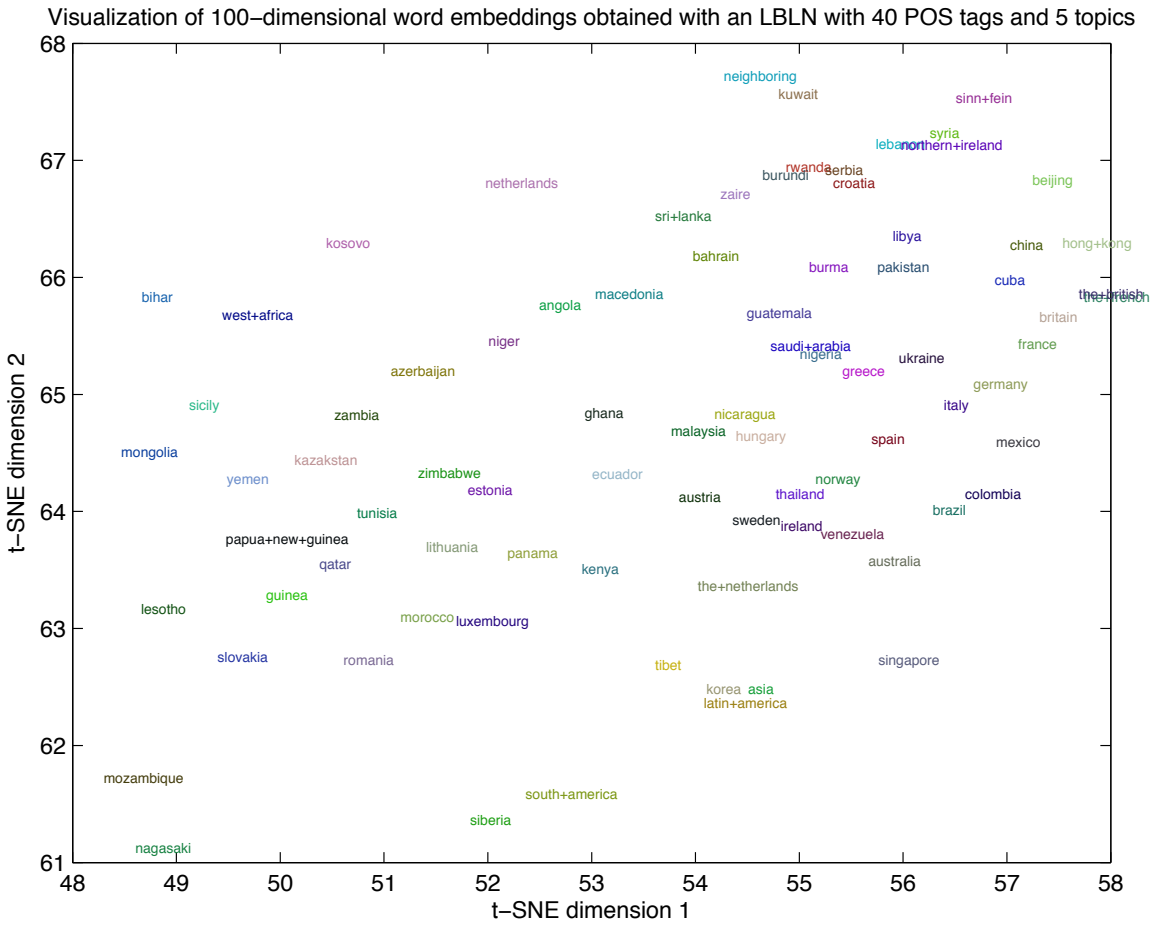

Figure 6.3: Detail of Figure 6.2 focusing on “country names”. Note that ”the+french” and ”the+british” seem to be on top of each other.

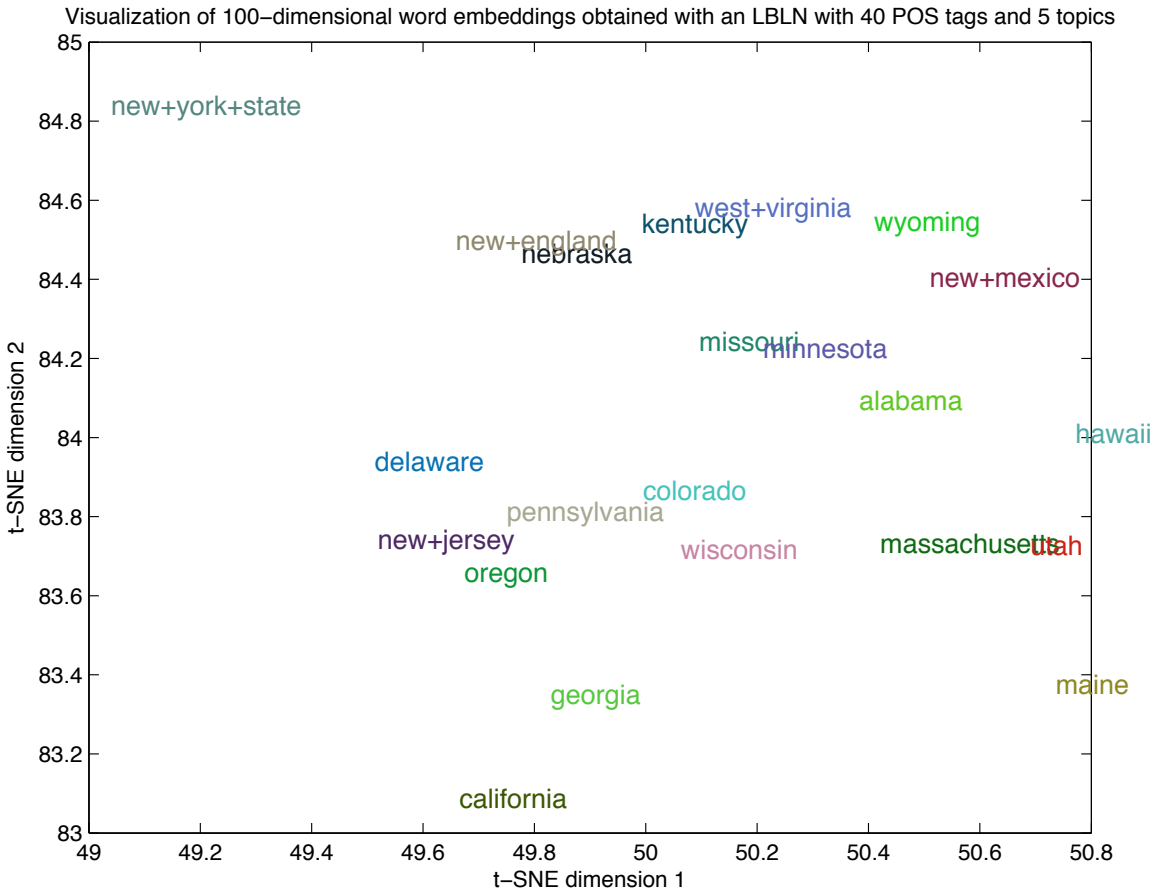

Figure 6.4: Detail of Figure 6.2 focusing on "US states".

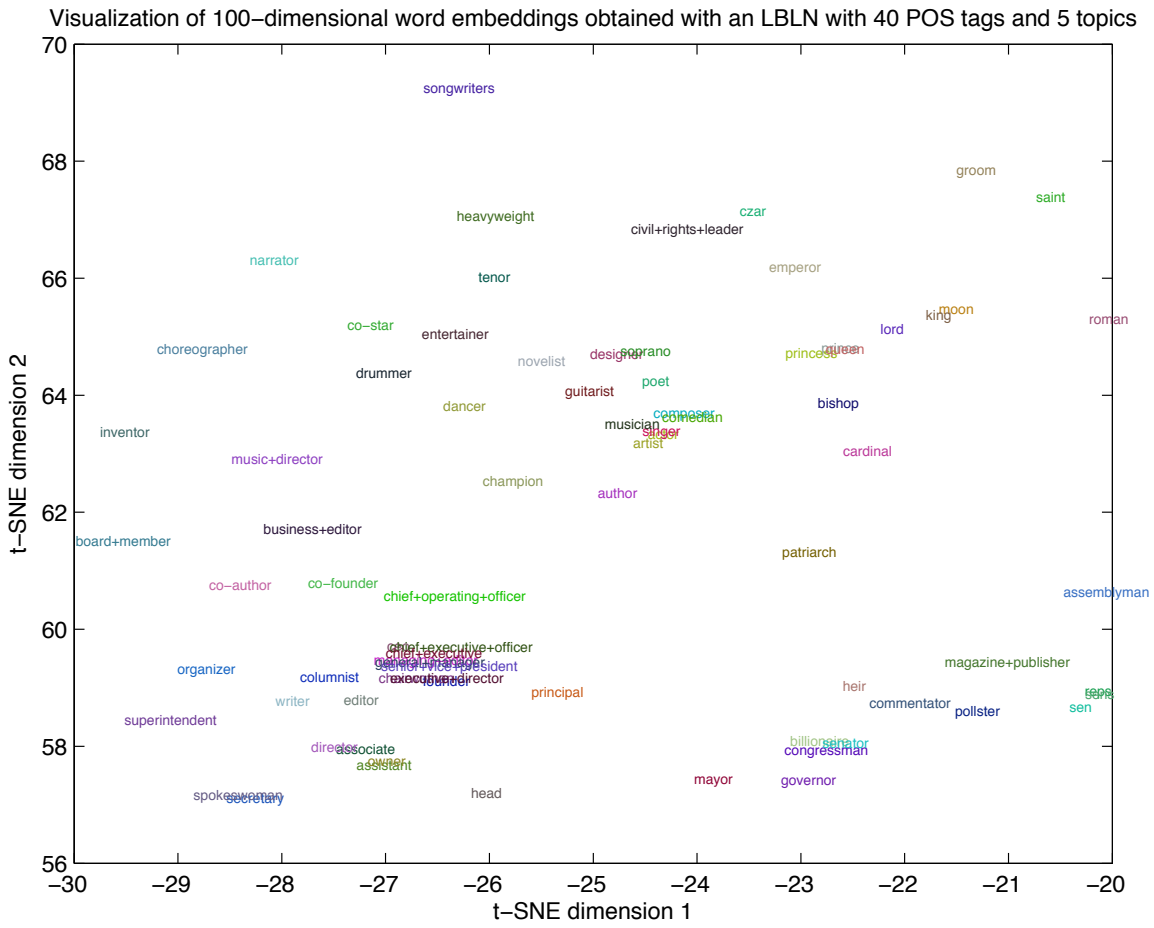

Figure 6.5: Detail of Figure 6.2 focusing on "occupations". Note how "ceo", "chief+executive+officer", "chief+executive", "general+manager", etc... are superimposed. This figure requires is designed for the electronic version of the document, as it requires zooming.

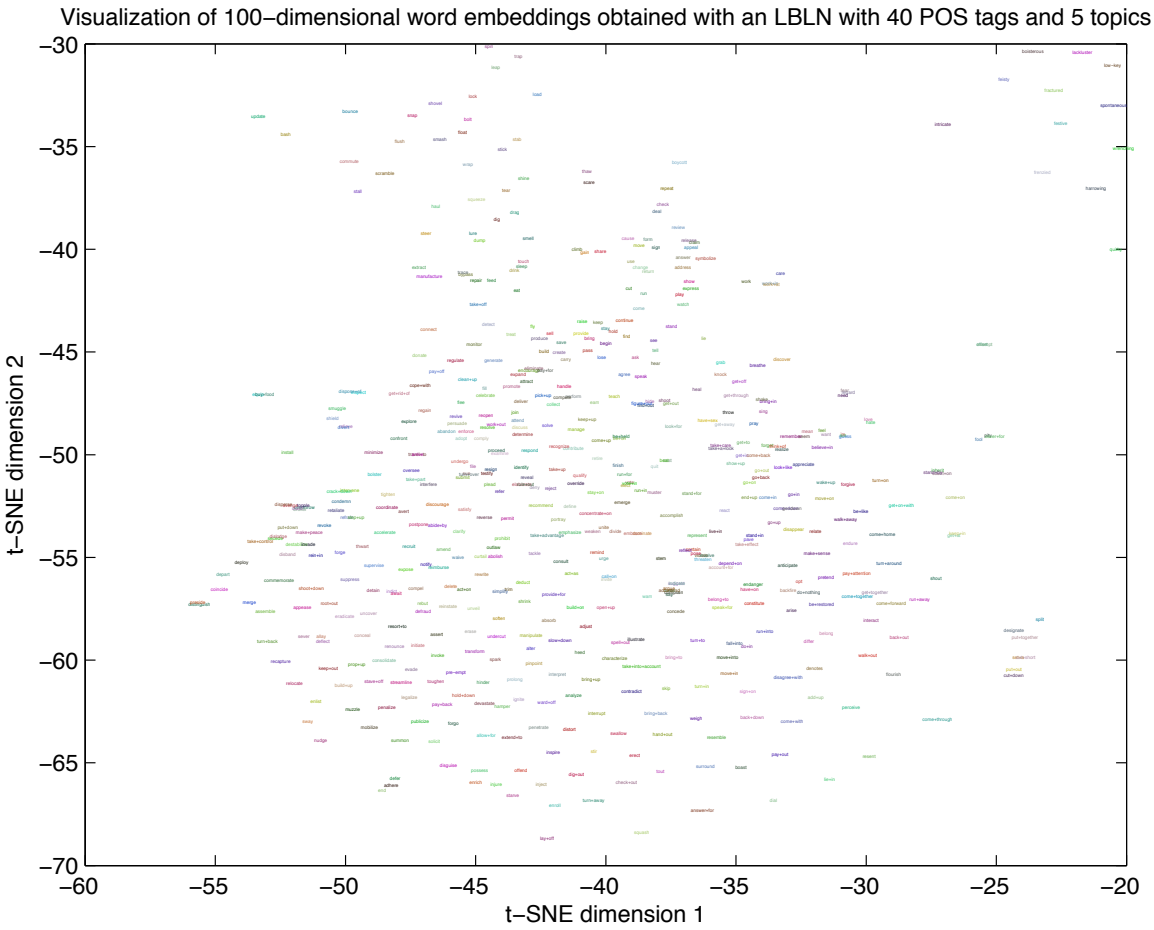

Figure 6.6: Detail of Figure 6.2 focusing on "verbs". This figure requires is designed for the electronic version of the document, as it requires zooming.

Chapter 7

Conclusion

> Parsifal - the kind of opera that starts at six o'clock and after it has been going three hours, you look at your watch and it says 6:20
>
> David Randolph, conductor

Dear Reader, thank you for navigating through this extended account of my doctoral work. It introduced a new and simple methodology to modeling time series and sequences, resorting to dynamics on hidden variable representations.

The major obstacle to overcome was the intractable problem of inferring latent representations of sequences with (non)linear dynamics. Although numerous approaches had been introduced in the past decade to solve that problem, consisting mostly of variational Bayes and sampling methods, I proposed a simple maximum a posteriori gradient-based inference enabled by a constant partition function, and a deterministic Expectation-Maximization learning procedure. I justified that these approximations were principled, and demonstrated the efficiency of my method on several real world problems and datasets, where I achieved state-of-the-art results.

There are multiple reasons that explain why DFGs work so well with a MAP ap-

proximation of latent variables, even though the distribution of the latent variables could theoretically be multimodal. These reasons differ from dataset to dataset. For instance, most of the dataset that I considered, with the exception of the gene regulation data, were relatively long, dispensing with the need to model uncertainty in the data, and thus well suited for energy-based methods. In the only case when the dataset was very short (mRNA micro-arrays), I used heavily regularized simple linear or nonlinear models. Secondly, I would always regularize the hidden representations to limit their information content. Thirdly, I would in some cases initialize the hidden representations in an unsupervised way, using Singular Value Decomposition, to further avoid suboptimal (local minima) solutions.

This multiple proof of principle demonstrated that a MAP inference was a valid simplification, whose benefits were multiple: thanks to DFGs, one could learn long sequences in linear time, handle high-dimensional hidden and observed variables, and most importantly, model highly nonlinear dynamics and observation functions. As I explained in Chapter 3, the computational complexity of DFGs is dominated by the E-step inference, and it is linear in the number T of training samples, linear in the number of observed variables and quadratic in the number of hidden variables. More precisely, if we note $|\mathbf{W}|$ the number of parameters of the model, the total computational complexity of one inference step over the full sequence is $O\left(T\,|\mathbf{W}|\right)$. The DFG algorithm is therefore comparable, in terms of running time, to Back-Propagation Through Time for Recurrent Neural Networks, but unlike the latter, it explicitly optimizes the hidden representations.

Further investigations are envisioned, regarding the inference of gene regulation networks and epileptic seizure prediction from EEG.

A word on the software implementation

The factor graph formulation makes our algorithm inherently modular and relatively easy to implement as software[1].

Each module needs only two functions to be defined, which we call *fprop* and *backprop*. The *fprop* function is used to forward-propagate the variables through the factor's function and to evaluate the energy of the factor; the *backprop* function is used to evaluate the derivatives of the loss of the factor with respect to both the function's parameters and the latent variables (if they serve as inputs to the function). For this reason, any function and energy/loss that are differentiable can be used. The loss function $\mathcal{L}$ consists in the sum of energies at each factor, plus regularization terms on the latent variables and on the parameters of the module.

One then needs to define an E-step relaxation function that performs iterated *fprop* and *backprop* on the latent variables until convergence, and several M-step functions, one per type of factor/module. Both the E-step and M-step can consist in simple gradient descents; the M-step can further benefit from other types of optimizations, such as stochastic gradient (Bottou, 2004), exact solution to ridge regression, or conjugate gradient (LeCun et al., 1998b).

Remaining portions of code deal with data pre-processing, early stopping strategies and bookkeeping the energies and statistics on latent variables and parameters.

Although we ultimately made four different implementations of our software for the four problems we handled, all the algorithms possessed the same properties enunciated above. Two implementations are currently being used by other researchers, respectively for the inference of gene regulation networks and for statistical language modeling. A third software release is planned, concerning the Dynamic Auto-

[1]Which we did in Lush (available at http://lush.sourceforge.net) and Matlab (by Mathworks).

Encoders, which could be applied not only to text but also other types of data, such as features derived from EEG or perhaps even musical notation ...

Bibliography

Abarbanel, H., Brown, R., Sidorowich, J. and Tsimring, L. (1993). The analysis of observed chaotic data in physical systems. *Reviews of Modern Physics* **65**.

Akaike, H. (1973). Information theory and an extension to the maximum likelihood principle. In *2nd International Symposium on Information Theory*.

Alvarez, M., Luengo, D. and Lawrence, N. (2009). Latent force models. In *ICML*.

Alvarez-Buylla, E., Benitez, M., Balleza-Davila, E., Chaos, A., Espinosa-Soto, C. and Padilla-Longoria, P. (2007). Gene regulatory network models for plant development. *Current Opinion in Plant Biology* **10**, 83–91.

Angus, J., Beal, M., Li, J., Rangel, C. and Wild, D. (2010). Inferring transcriptional networks using prior biological knowledge and constrained state-space models. In M. R. Neil Lawrence, Mark Girolami and G. Sanguinetti, eds., *Learning and Inference in Computational Systems Biology*. Cambridge, MA: MIT Press, pages 117–153.

Aristidou, A., Cameron, J. and Lasenby, J. (2008). Real-time estimation of missing markers in human motion capture. In *Proceedings of the 2nd International Conference on Bioinformatics and Biomedical Engineering ICBBE'08*.

Arnhold, J., Grassberger, P., Lehnertz, K. and Elger, C. (1999). A robust method for detecting interdependence: applications to intracranially recorded EEG. *Physica D* **134**, 419–430.

Aschenbrenner-Scheibe, R., Maiwald, T., Winterhalder, M., Voss, H. and Timmer, J. (2003). How well can epileptic seizures be predicted? An evaluation of a nonlinear method. *Brain* **126**, 2616–2626.

Bakker, R., Schouten, J., Giles, C., Takens, F. and van den Bleek, C. (2000). Learning chaotic attractors by neural networks. *Neural Computation* **12**, 2355–2383.

Baldi, P. and Rosen-Zvi, M. (2005). On the relationship between deterministic and probabilistic directed graphical models: From bayesian networks to recursive neural networks. *Neural Networks* **18**, 1080–1086.

Bangalore, S. (1997). *Complexity of Lexical Descriptions and its Relevance to Partial Parsing*. Ph.D. thesis, University of Pennsylvania, Philadelphia, PA.

Bangalore, S. and Joshi, A. (1999). Supertagging: An approach to almost parsing. *Computational Linguistics* **25**.

Barber, D. (2003). Dynamic bayesian networks with deterministic latent tables. In *NIPS'03: Advances in Neural Information Processing Systems*. Cambridge MA: MIT Press.

Barenco, M., Tomescu, D., Brewer, D., Callard, R., Stark, J. and Hubank, M. (2006). Ranked prediction of p53 targets using hidden variable dynamic modeling. *Genome Biology* **7**.

Beal, M., Falciani, F., Ghahramani, Z., Rangel, C. and Wild, D. (2005). A bayesian approach to reconstructing genetic regulatory networks with hidden factors. *Bioinformatics* **21**, 349–356.

Bengio, Y., Ducharme, R., Vincent, P. and Jauvin, C. (2003). A neural probabilistic language model. *Journal of Machine Learning Research* **3**, 1137–1155.

Bengio, Y. and Frasconi, P. (1995). An input/output HMM architecture. In G. Teusauro, D. Touretzky and T. Leen, eds., *Advances in Neural Information Processing Systems NIPS'94*. Cambridge, MA: Morgan Kaufmann, MIT Press.

Bengio, Y., Lamblin, P., Popovici, D. and Larochelle, H. (2006). Greedy layer-wise training of deep belief networks. In *NIPS*.

Bengio, Y., Simard, P. and Frasconi, P. (1994). Learning long-term dependencies with gradient descent is difficult. *IEEE Transactions on Neural Networks* **5**, 157–166.

Bishop, C. (2006). *Pattern recognition and machine learning*. New York, NY: Springer.

Blei, D. and Lafferty, J. (2006). Dynamic topic models. In *ICML*.

Blei, D. and McAulife, J. (2007). Supervised topic models. In *NIPS*.

Blei, D., Ng, A. and Jordan, M. (2003). Latent dirichlet allocation. *Journal of Machine Learning Research* **3**, 993–1022.

Blitzer, J., Weinberger, K., Saul, L. and Pereira, F. (2004). Hierarchical distributed representations for statistical language modeling. In *Advances in Neural Information Processing Systems*.

Bonneau, R., Facciotti, M., Reiss, D., Schmid, A., Pan, M., Kaur, A., Thorsson, V., Shannon, P., Johnson, M., Bare, J. and et al (2007). A predictive model for transcriptional control of physiology in a free living cell. *Cell* **131**, 1354–1365.

Bonneau, R., Reiss, D., Shannon, P., Facciotti, M., Hood, L., Baliga, N. and Thorsson, V. (2006). The inferelator: an algorithm for learning parsimonious regulatory networks from systems-biology data sets de novo. *Genome Biology* **7**.

Bottou, L. (2004). Stochastic learning. In U. v. L. O. Bousquet, ed., *Advanced Lectures on Machine Learning*. Berlin: Springer Verlag, pages 146–168.

Box, G. and Jenkins, G. (1976). *Time Series Analysis, Forecasting and Control*. Oakland, CA: Holden Day, 2nd edition edition.

Buntine, W. (2009). Estimating likelihoods for topic models. In Z.-H. Zhou and T. Washio, eds., *Advances in Machine Learning*, volume 5828 of *Lecture Notes in Computer Science*. Springer Berlin / Heidelberg, pages 51–64.

Casdagli, M. (1989). Nonlinear prediction of chaotic time series. *Physica D* **35**, 335–356.

Chen, S. F. and Goodman, J. (1996). An empirical study of smoothing techniques for language modeling. In *Proceedings of the Thirty-Fourth Annual Meeting of the Association for Computational Linguistics*. San Francisco: Morgan Kaufmann Publishers.

Chopra, S., Thampy, T., Leahy, J., Caplin, A. and LeCun, Y. (2007). Discovering the hidden structure of house prices with a non-parametric latent manifold model. In *Knowledge Discovery and Data Mining*.

Collobert, R. and Weston, J. (2008). A unified architecture for natural language processing: deep neural networks with multitask learning. In *ICML '08: Proceedings of the 25th international conference on Machine learning*. ISBN 978-1-60558-205-4.

Cortes, C. and Vapnik, V. (1995). Support vector networks. *Machine Learning* **20**, 273–97.

Cybenko, G. (1989). Approximation by superpositions of a sigmoidal function. *Mathematics of Control, Signals and Systems* **2**, 303–314.

Davis, J. and Goadrich, M. (2006). The relationship between precision-recall and roc curves. In *ICML*.

Debole, F. and Sebastiani, F. (2005). An analysis of the relative hardness of the Reuters-21578 subsets. *Journal of the American Society for Information Science and Technology* **56**, 584–596.

Deerwester, S., Dumais, S., Furnas, G., Landauer, T. and Harshman, R. (1990). Indexing by latent semantic analysis. *Journal of the American Society for Information Science* **41**, 391–407.

Dempster, A., Laird, N. and Rubin, D. (1977). Maximum likelihood from incomplete data via the EM algorithm. *Journal of the Royal Statistical Society B* **39**, 1–38.

Durrett, R. (1996). *Stochastic Calculus: A Practical Introduction*. Boca Raton, FL: CRC Press.

Efron, B., Hastie, T., Johnstone, I. and R., T. (2004). Least angle regression. *Annals of Statistics* **32**, 407–499.

Gao, P., Honkela, A., Rattray, M. and Lawrence, N. (2008). Gaussian process modeling of latent chemical species: applications to inferring transcription factor activities. *Bioinformatics* **24**, i70–i75.

Gehler, P., Holub, A. and Welling, M. (2006). The rate adapting poisson model for information retrieval and object recognition. In *ICML*.

Ghahramani, Z. (1998). *Learning Dynamic Bayesian Networks*. Lecture Notes in Artificial Intelligence. Berlin: Springer-Verlag, pages 168–197.

Ghahramani, Z. and Roweis, S. (1999). Learning nonlinear dynamical systems using an em algorithm. In *Advances in Neural Information Processing Systems NIPS'99*. Cambridge, MA: Morgan Kaufmann, MIT Press.

Gidofalvi, G. and Elkan, C. (2003). Using news articles to predict stock price movements. Technical report, Department of Computer Science and Engineering, University of California, San Diego.

Girard, A., Rasmussen, C., Candela, J. and Murray-Smith, R. (2003). Gaussian process priors with uncertain inputs - application to multiple-step ahead time series forecasting. In *Advances in Neural Information Processing Systems NIPS'03*. Cambridge, MA: MIT Press.

Goffin, V., Allauzen, C., Bocchieri, E., Hakkani-Tur, D., Ljolje, A., Parthasarathy, S., Rahim, M., Riccardi, G. and Saraclar, M. (2005). The AT&T WATSON Speech Recognizer. In *Proceedings of ICASSP*. Philadelphia, PA.

Griffiths, T. and Steyvers, M. (2004). Finding scientific topics. *PNAS* **10**, 5228–5235.

Griffiths, T., Steyvers, M., Blei, D. and Tenenbaum, J. (2005). Integrating topics and syntax. In *Advances in Neural Information Processing Systems*.

Gutierrez, R., Gifford, M., Poultney, C., Wang, R., Shasha, D., Coruzzi, G. and Crawford, N. (2007). Insights into the genomic nitrate response using genetics and the sungear software system. *Journal of Experimental Botanics* **58**, 2359–2367.

Herring, C. and Palmore, J. (1995). Random number generators are chaotic. *Communications of the ACM* **38**.

Hinton, G., Dayan, P., Frey, B. and Neal, R. (1995). The wake-sleep algorithm for unsupervised neural networks. *Science* **268**, 1158–1161.

Hinton, G., Osindero, S. and Teh, W.-H. (2006). A fast learning algorithm for deep belief nets. *Neural Computation* **18**, 1527–1554.

Hinton, G. and Salakhutdinov, R. (2006). Reducing the dimensionality of data with neural networks. *Science* **313**, 504–507.

Hirose, O., Yoshida, R., Imoto, S., Yamaguchi, R., Higuchi, T., Charnock-Jones, D., Print, C. and Miyano, S. (2008). Statistical inference of transcriptional module-based gene networks from time course gene expression profiles by using state space models. *Bioinformatics* **24**, 932–942.

Hochreiter, S. and Schmidhuber, J. (1995). Long short-term memory. *Neural Computation* **9**, 1735–1780.

Ilin, A., Valpola, H. and Oja, E. (2004). Nonlinear dynamical factor analysis for state change detection. *IEEE Transactions on Neural Networks* **15**, 559–575.

Jaeger, J. and Monk, N. (2010). Reverse engineering of gene regulatory networks. In M. R. Neil Lawrence, Mark Girolami and G. Sanguinetti, eds., *Learning and Inference in Computational Systems Biology*. Cambridge, MA: MIT Press, pages 9–35.

Jelinek, F. (2005). Some of my best friends are linguists. *Language Resources and Evaluation* **39**, 25–34. ISSN 1574-020X. 10.1007/s10579-005-2693-4.

Joachims, T. (1998). Text categorization with support vector machines: Learning with many relevant features. In *ECML*.

Joshi, A. K. (1987). An introduction to tree adjoining grammars. In A. Manaster-Ramer, ed., *Mathematics of Language*. Amsterdam: John Benjamins.

Kalman, R. E. (1960). A new approach to linear filtering and prediction problems. *Transaction of the ASME - Journal of Basic Engineering* , 35–45.

Katz, S. (1987). Estimation of probabilities from sparse data for the language moel component of a speech recognizer. *IEEE Transactions on Acoustics, Speech and Signal Processing* **ASSP-35**, 400–401.

Keshamouni, V., Jagtap, P., Michailidis, G., Strahler, J. and Kuick, R. (2009). Temporal quantitative proteomics by iTRAQ 2D-LC-MS/MS and corresponding mRNA expression analysis identify post-transcriptional modulation

of actin-cytoskeleton regulators during TGF-*beta*-induced epithelial-mesenchymal transition. *Journal of Proteome Research* **8**, 35–47.

Kim, M. and Pavlovic, V. (2007). Conditional state space models for discriminative motion estimation. In *IEEE International Conference on Computer Vision*.

Kohlmorgen, J., Muller, K.-R. and Pawelzik, K. (1994). Competing predictors segment and identify switching dynamics. In P. M. M. Marinaro, ed., *ICANN'94: Proceedings of the International Conference on Artificial Neural Networks*. London Berlin Heidelberg: Springer.

Kohlmorgen, J., Muller, K.-R. and Pawelzik, K. (1998). Analysis of drifting dynamics with neural network hidden markov models. In *NIPS'97: Advances in Neural Information Processing Systems*. Cambridge, MA: MIT Press.

Kolenda, T. and Kai Hansen, L. (2000). Independent components in text. In *Advances in Independent Component Analysis*.

Krogh, A., Thorbergsson, G. and Hertz, J. (1990). A cost function for internal representation. In *Advances in Neural Information Processing Systems*.

Krouk, G., Crawford, N., Coruzzi, G. and Tsay, Y. (2010). Nitrate signaling: adaptation to fluctuating environments. *Current Opinion in Plant Biology* .

Krouk, G., Mirowski, P., Yann, Y., Shasha, D. and Coruzzi, G. (Provisionally accepted for publication). High-resolution dynamics of transcriptome responses to no3- in arabidopsis roots: Molecular physiology and predictive modeling. *Genome Biology* .

Kschischang, F., Frey, B. and Loeliger, H.-A. (2001). Factor graphs and the sum-product algorithm. *IEEE Transactions on Information Theory* **47**, 498–519.

Kuo, J.-M. and Principe, J. (1994). Reconstructed dynamics and chaotic signal modeling. In *IEEE International Conference on Neural Networks*.

Lafferty, J., McCallum, A. and Pereira, F. (2001). Conditional random fields: Probabilistic models for segmenting and labeling sequence data. In *Proceedints of the International Conference on Machine Learning*. San Francisco, CA: Morgan Kaufmann.

Lahdesmaki, H., Shmulevich, I. and Yli-Harja, O. (2003). On learning gene regulatory networks under the boolean network model. *Machine Learning* **52**, 147–167.

Lang, K. and Hinton, G. (1988). The development of the time-delay neural network architecture for speech recognition. Technical Report CMU-CS-88-152, Carnegie-Mellon University.

Lawrence, N. (2004). Gaussian process latent variable models for visualisation of high dimensional data. In *Advances in Neural Information Processing Systems NIPS'04*. Cambridge, MA: MIT Press.

Lawrence, N. and Sanguinetti, G. (2007). Modelling trancriptional regulation using gaussian processes. In *NIPS*.

Le Van Quyen, M., Foucher, J., Lachaux, J.-P., Rodriguez, E., Lutz, A., Martinerie, J. and Varela, F. (2001). Comparison of hilbert transform and wavelet methods for the analysis of neuronal synchrony. *Journal of Neuroscience Methods* **11**, 83–98.

Le Van Quyen, M., Navarro, V., Martinerie, J., Baulac, M. and Varela, F. (2003). Toward a neurodynamical understanding of ictogenesis. *Epilepsia* **44/12**, 30–43.

LeCun, Y., Bottou, L., Bengio, Y. and Haffner, P. (1998a). Gradient-based learning applied to document recognition. *Proceedings of the IEEE* **86**, 2278–2324.

LeCun, Y., Bottou, L., Orr, G. and Muller, K. (1998b). Efficient backprop. In K. M. G. Orr, ed., *Neural Networks: Tricks of the trade*, Lecture Notes in Computer Science. Berlin/Heidelberg: Springer, pages 9–50.

LeCun, Y., Chopra, S., Hadsell, R. and Huang, F. (2006). A tutorial on energy-based learning. In *Predicting Structured Outputs*. MIT Press.

Lendasse, A., Oja, E. and Simula, O. (2004). Times series prediction competition: The cats benchmark. In *Proceedings of IEEE International Joint Conference on Neural Networks (IJCNN)*, volume 2.

Levin, E. (1993). Hidden control neural architecture modeling of nonlinear time-varying systems and its applications. *IEEE Transactions on Neural Networks* **4**, 109–116.

Liu, G. and McMillan, L. (2006). Estimation of missing markers in human motion capture. *The Visual Computer* **22**, 721–728.

Lorenz, E. (1963). Deterministic nonperiodic flow. *Journal of Atmospheric Sciences* **20**, 130–141.

Lozano, A., Abe, N., Liu, Y. and Rosset, S. (2009). Grouped graphical granger modeling for gene expression regulatory networks discovery. *Bioinformatics* **25**, 110–118.

MacKay, D. (2003). *Information Theory, Inference and Learning*. Cambridge, UK: Cambridge University Press.

Maiwald, T., Winterhalder, M., Aschenbrenner-Scheibe, R., Voss, H. and Schulze-Bonhage, A. (2004). Comparison of three nonlinear seizure prediction methods by means of the seizure prediction characteristic. *Physica D* **194**, 357–368.

Mallat, S. (1999). *A Wavelet Tour of Signal Processing*. San Diego, CA: Elsevier, Academic Press.

Mattera, D. and Haykin, S. (1999). Support vector machines for dynamic reconstruction of a chaotic system. In A. S. B. Scholkopf, C.J.C. Burges, ed., *Advances in Kernel Methods: Support Vector Learning*. Cambridge, MA: MIT Press, pages 212–239.

Mirowski, P., Chopra, S., Balakrishnan, S. and Bangalore, S. (2010a). Feature-rich continuous language models for speech recognition. In *Proceedings of the IEEE Workshop on Spoken Language Technology*.

Mirowski, P., Chopra, S., Balakrishnan, S. and Bangalore, S. (2010b). System and method for feature-rich continuous space language models. *US Patent Application* **AT&T Docket 2010-0851**.

Mirowski, P. and LeCun, Y. (2009). Dynamic factor graphs for time series modeling. In *European Conference on Machine Learning*.

Mirowski, P., Madhavan, D. and LeCun, Y. (2007). Time-delay neural networks and independent component analysis for eeg-based prediction of epileptic seizures propagation. In *AAAI*.

Mirowski, P., Madhavan, D., LeCun, Y. and Kuzniecky, R. (2008). Comparing svm and convolutional networks for epileptic seizure prediction from intracranial eeg. In *Proceedings of the IEEE Workshop on Machine Learning for Signal Processing*.

Mirowski, P., Madhavan, D., LeCun, Y. and Kuzniecky, R. (2009a). Classification of patterns of eeg synchronization for seizure prediction. *Clinical Neurophysiology* **120**, 1927–1940.

Mirowski, P., Madhavan, D., LeCun, Y. and Kuzniecky, R. (2009b). Method, system and computer-accessible medium for classification of at least one ictal state. *International Patent Publication* **WO 2009/149126 A2**.

Mirowski, P., Ranzato, M. and LeCun, Y. (2010c). Dynamic auto-encoders for semantic indexing. In *Proceedings of the NIPS Deep Learning and Unsupervised Learning Workshop*.

Mnih, A. and Hinton, G. (2007). Three new graphical models for statistical language modelling. In *24th International Conference on Machine Learning ICML*. ISBN 978-1-59593-793-3.

Mnih, A. and Hinton, G. (2008). A scalable hierarchical distributed language model. In *Advances in Neural Information Processing Systems NIPS*.

Mnih, A., Zhang, Y. and Hinton, G. (2009). Improving a statistical language model through non-linear prediction. *Neurocomputing* **72**, 1414 – 1418. ISSN 0925-2312.

Moon, K. and Pavlovic, V. (2008). 3D human motion tracking using dynamic probabilistic latent semantic analysis. In *Canadian Conference on Computer and Robot Vision CRV'08*.

Moon, T. (1996). The expectation-maximization algorithm. *IEEE Signal Processing Magazine* **13**, 47–60.

Morin, F. and Bengio, Y. (2005). Hierarchical probabilistic neural network language model. In *Advances in Neural Information Processing Systems NIPS*.

Mukherjee, S., Osuna, E. and Girosi, F. (1997). Nonlinear prediction of chaotic time series using support vector machines. In *Proceedings of IEEE Workshop on Neural Networks for Signal Processing NNSP'97*.

Muller, K., Smola, A., Ratsch, G., Scholkopf, B., Kohlmorgen, J. and Vapnik, V. (1999). Using support vector machines for time-series prediction. In A. J. S. B. Scholkopf, C. J. C. Burges, ed., *Advances in Kernel Methods: Support Vector Learning*. Cambridge, MA: MIT Press, pages 212–239.

Murphy, K. and Mian, S. (1999). Modelling gene expression data using dynamic bayesian networks. Technical report, Computer Science Division, University of California and Life Sciences Division, Lawrence Berkeley National Laboratory.

Neal, R. and Hinton, G. (1998). A view of the em algorithm that justifies incremental, sparse, and other variants. In M. Jordan, ed., *Learning in Graphical Models*. Cambridge, MA: MIT Press, pages 355–370.

Nelson, L. and Stear, E. (1976). The simultaneous on-line estimation of parameters and states in linear systems. *IEEE Transactions on Automatic Control* **21**, 94–98.

Olshausen, B. and Field, D. (1997). Sparse coding with an overcomplete basis set: a strategy employed by V1? *Vision Research* **37**, 3311–3325.

Pavlovic, V., Frey, B. and Huang, T. (1999). Time-series classification using mixed-state dynamic bayesian networks. In *Proceedings of the Conference on Computer Vision and Pattern Recognition CVPR'99*, volume 2. IEEE Computer Society.

Pruteanu-Malinici, I., Ren, L., Pailsey, J., Wang, E. and Carin, L. (2010). Hierarchical bayesian modeling of topics in time-stamped documents. *IEEE Transactions on Pattern Analysis and Machine Intelligence* **32**, 996–1011.

Puskorius, G. and Feldkamp, L. (1994). Neurocontrol of nonlinear dynamical systems with kalman filter trained recurrent networks. *IEEE Transactions on Neural Networks* **5**, 279–297.

Rabiner, L. (1989). A tutorial on hidden markov models and selected applications in speech recognition. *Proceedings of the IEEE* **77**, 257–286.

Rangel, C., Angus, J., Ghahramani, Z., Lioumi, M., Sotheran, E., Gaiba, A., Wild, D. and Falciani, F. (2004). Modeling t-cell activation using gene expression profiling and state-space models. *Bioinformatics* **20**, 1361–1372.

Ranzato, M. (2009). *Unsupervised Learning of Feature Hierarchies*. Ph.D. thesis, Courant Institute of Mathematical Sciences, New York University.

Ranzato, M., Boureau, Y. and LeCun, Y. (2007). Sparse feature learning for deep belief networks. In *NIPS*.

Ranzato, M. and Szummer, M. (2008). Semi-supervised learning of compact document representations with deep networks. In *ICML*.

Resnik, P. (1999). Semantic similarity in a taxonomy: An information-based measure and its application to problems of ambiguity in natural language. *Journal of Artificial Intelligence Research* **11**, 95–130.

Robertson, C., Geva, S. and Wolff, R. (2007). News aware volatility forecasting: Is the content of the news important? In *Sixth Australasian Data Mining Conference*.

Rohwer, R. (1989). The moving targets training algorithm. *Neural Networks* **412**, 100–109.

Rumelhart, D., Hinton, G. and Williams, R. (1986). Learning representations by back-propagating errors. *Nature* **323**, 533–536.

Salakhutdinov, R. and Hinton, G. (2007). Semantic hashing. In *ACM SIGIR Workshop on Information Retrieval and Applications of Graphical Models*.

Salakhutdinov, R. and Hinton, G. (2009). Replicated softmax. In *ICML*.

Sarikaya, R., Emami, A., Afify, M. and Ramabhadran, B. (2010). Continuous space language modeling technique. In *IEEE International Conference on Acoustics, Speech and Speech Processing ICASSP*.

Sarkka, S., Vehtari, A. and Lampinen, J. (2004). Time series prediction by kalman smoother with cross-validated noise density. In *Proceedings of IEEE International Joint Conference on Neural Networks (IJCNN)*, volume 2.

Schelter, B., Winterhalder, M., Maiwald, T., Brandt, A. and Schad, A. (2006a). Do false predictions of seizures depend on the state of vigilance? a report from two seizure-prediction methods and proposed remedies. *Epilepsia* **47**, 2058–2070.

Schelter, B., Winterhalder, M., Maiwald, T., Brandt, A. and Schad, A. (2006b). Testing statistical significance of multivariate time series analysis techniques for epileptic seizure prediction. *Chaos* **16**.

Schulze-Bonhage, A., Kurth, C., Carius, A., Steinhoff, B. and Mayer, T. (2006). Seizure anticipation by patients with focal and generalized epilepsy: a multicentre assessment of premonitory symptoms. *Epilepsy Research* **70**, 83–88.

Schwenk, H. (2010). Continuous-space language models for statistical machine translation. *The Prague Bulletin of Mathematical Linguistics* **93**, 137–146.

Schwenk, H. and Gauvain, J.-L. (2003). Using continuous space language models for conversational speech recognition. In *IEEE Workshop on Spontaneous Speech Processing and Recognition SSPR*.

Segal, E., Shapira, M., Regev, A., Pe'er, D., Botstein, D., Koller, D. and Friedman, N. (2003). Module networks: identifying regulatory modules and their condition-specific regulators from gene expression data. *Nature Genetics* **34**, 166–176.

Shimamura, T., Imoto, S., Yamaguchi, R., Fujita, A., Nagasaki, M. and Miyano, S. (2009). Recursive regularization for inferring gene networks from time-course gene expression profiles. *BMC Systems Biology* **3**.

Spellman, P., Sherlock, G., Zhang, M., Iyer, V., Anders, K., Eisen, M., Brown, P., Botstein, D. and Futcher, B. (1998). Comprehensive identification of cell cycle-regulated genes of the yeast saccharomyces cerevisiae by microarray hybridization. *Molecular Biology of the Cell* **9**, 3273–3297.

Stolcke, A. (2002). Srilm - an extensible language modeling toolkit. In *7th International Conference on Spoken Language Processing ICSLP*.

Strogatz, S. (1994). *Nonlinear Dynamics and Chaos. With Applications to Physics, Biology, Chemistry, and Engineering*. Studies in Nonlinearity. Westview Books, Perseus Books Publishing, Cambridge, MA.

Sutskever, I. and Hinton, G. (2006). Learning multilevel distributed representations for high-dimensional sequences. In *NIPS'06: Advances in Neural Information Processing Systems*. Cambridge, MA: Morgan Kaufmann, MIT Press.

Takens, F. (1981). *Detecting strange attractors in turbulence*, volume 898 of *Lecture Notes in Mathematics*. Warwick, UK: Springer, pages 336–381.

Taleb, N. (2007). *The Black Swan: The Impact of the Highly Improbable*. New York, NY: Random House.

Taylor, G., Hinton, G. and Roweis, S. (2006). Modeling human motion using binary latent variables. In *NIPS'06: Advances in Neural Information Processing Systems*. Cambridge, MA: Morgan Kaufmann, MIT Press.

Tibshirani, R. (1996). Regression shrinkage and selection via the lasso. *Journal of the Royal Statistics Society B* **58**, 267–288.

Tsay, R. (2005). *Analysis of Financial Time Series*. Wiley Series in Probability and Statistics. Hoboken, NJ: John Wiley and Sons, second edition edition.

Van der Maaten, L. and Hinton, G. (2008). Visualizing data using t-SNE. *JMLR* **9**.

Wahde, M. and Hertz, J. (2001). Modeling genetic regulatory dynamic in neural development. *Journal of Computational Biology* **8**, 429–442.

Waibel, A., Hanazawa, T., Hinton, G., Shikano, K. and Lang, K. (1989). Phoneme recognition using time-delay neural networks. *IEEE Transactions in Acoustics, Speech, Signal Processing* **37**, 328–339.

Wan, E. (1993). Time series prediction by using a connectionist network with internal delay lines. In N. A. G. A. S. Weigend, ed., *Time Series Prediction: Forecasting the Future and Understanding the Past*. Reading, MA: Addison-Wesley, pages 195–217.

Wan, E. and Nelson, A. (1996). Dual kalman filtering methods for nonlinear prediction, estimation, and smoothing. In *Advances in Neural Information Processing Systems*, volume 9. Cambridge, MA: Morgan Kaufmann, MIT Press.

Wan, E. and Van Der Merwe, R. (2000). The unscented kalman filter for nonlinear estimation. In *Proceedings of the IEEE 2000 Symposium on Adaptive Systems for Signal Processing, Communications, and Control AS-SPCC*.

Wang, J., Fleet, D. and Hertzmann, A. (2006a). Gaussian process dynamical models. In *Advances in Neural Information Processing Systems NIPS'06*. Cambridge, MA: MIT Press.

Wang, R., Guegler, K., LaBrie, S. and Crawford, N. (2000). Genomic analysis of a nutrient response in Arabidopsis reveals diverse expression patterns and novel metabolic and potential regulatory genes induced by nitrate. *Plant Cell* **12**, 1491–1510.

Wang, X. and McCallum, A. (2006). Topics over time: A non-markov continuous-time model of topical trends. In *KDD*.

Wang, Y., Joshi, T., Zhang, X.-S., Xu, D. and Chen, L. (2006b). Inferring gene regulatory networks from multiple microarray datasets. *Bioinformatics* **22**, 2413–2420.

Weigend, A. and Gershenfeld, N. (1994). *Time series prediction: Forecasting the future and understanding the past*. Reading, MA: Addison-Wesley.

Wierstra, D., Gomez, F. and Schmidhuber, J. (2005). Modeling systems with internal state using evolino. In *Proceedings of the 2005 Conference on Genetic and Evolutionary Computation*.

Williams, C. and Rasmussen, C. (1996). Gaussian processes for regression. In *Advances in Neural Information Processing Systems NIPS'96*. Cambridge, MA: MIT Press.

Williams, R. and Zipser, D. (1995). *Gradient-Based Learning Algorithms for Recurrent Networks and Their Computational Complexity*. Lawrence Erlbaum Associates, pages 433–486.

Yamaguchi, R., Imoto, S. and Satoru, M. (2010). Network-based predictions and simulations by biological state space models for drug mode of action. *Journal of Computer Science and Technology* **25**, 131–153.

Yamaguchi, R., Yoshida, R. and Imoto, S. (2007). Finding module-based gene networks with state-space models. *IEEE Signal Processing Magazine* **37**.

Yang, D. and Zhang, Q. (2000). Drift independent volatility estimation based on high, low, open and close prices. *Journal of Business* **73**, 477–491.

Zhang, Y., Hatch, K., Bacon, J. and Wernisch, L. (2010). An integrated machine learning approach for predicting dosr-regulated genes in mycobacterium tuberculosis. *BMC Systems Biology* **4**.

Zou, H. and Hastie, T. (2005). Regularization and variable selection via the elastic net. *Journal of Royal Statistical Society B* **67**, 301–320.